Polyelectrolyte Coatings with Internal Hierarchy

DISSERTATION

zur Erlangung des akademischen Grades eines Doktors der Naturwissenschaften (Dr. rer. nat.) im Fach Chemie der Fakultät für Biologie, Chemie und Geowissenschaften der Universität Bayreuth

vorgelegt von

Julia Gensel

geboren in Charkow/Ukraine

Bayreuth, 2012

Die vorliegende Arbeit wurde in der Zeit von November 2008 bis März 2012 am Lehrstuhl Physikalische Chemie II der Universität Bayreuth in der Arbeitsgruppe von Herrn Prof. Dr. Andreas Fery angefertigt.

Vollständiger Abdruck der von der Fakultät für Biologie, Chemie und Geowissenschaften der Universität Bayreuth genehmigten Dissertation zur Erlangung des akademischen Grades eines Doktors der Naturwissenschaften (Dr. rer. nat.).

Amtierender Dekan: Prof. Dr. Beate Lohnert

Tag des Einreichens der Dissertation: 08. März 2012

Tag des wissenschaftlichen Kolloquiums: 16. Oktober 2012

Prüfungsausschuss:

Prof. Dr. Andreas Fery (Erstgutachter)
Prof. Dr. Georg Papastavrou (Zweitgutachter)
Prof. Dr. Felix Schacher (Drittgutachter)
Prof. Dr. Axel H. E. Müller
Prof. Dr. Birgit Weber (Vorsitz)

Das Leben bildet eine Oberfläche,
die so tut, als ob sie so sein müsste, wie sie ist,
aber unter ihrer Haut treiben und drängen die Dinge.

Robert Musil, in „Der Mann ohne Eigenschaften"

Meiner Familie

Table of Contents

Summary

The results presented in this thesis are focused on the surface modification by polyelectrolytes and polyelectrolyte copolymers. The internal structural hierarchy originate thereby from the self-assembly processes at different length scales. To generate different levels of hierarchy, the coatings were constructed by using either the layer-by-layer (LbL) deposition method (lateral chemical structure), the adsorption of supramolecular aggregates (lateral topographycal structure), or the combination of both. Using these techniques, one can control the properties of the coatings by varying the chemical structure of the polyelectrolytes, for instance, their charge density, thus providing a convenient way for their functionalization and the ability to tune properties of the surface. Therefore, we were working with systems which have variable charge densities. With this approach, we were able to produce thin and ultrathin nanostructured films with tunable properties and functionality.

The objective of the thesis can be divided into two main parts.

In the first part, construction of passive coatings by the layer-by-layer assembly of strong polyelectrolytes with tunable charge density is presented. The key point thereby was understanding of polyelectrolyte multilayer assemblies depending on the chemical structure of the LbL components. Here, we studied the buildup and cross-linking of the film prepared by spray coating of novel polyanions with variable charge density (21 -100%) and cross-linkable cationic polyelectrolyte. This opens the possibility to tune both ionic and covalent cross-linking. The polyelectrolytes were synthesized by Patrick Ott in the group of Prof. Dr. André Laschewsky (Institute of Chemistry at the University of Potsdam).

We have found that for all ionic strengths studied, the charge density of polyanion in the „strong screening zone" (high charge density) only slightly affects the buildup behavior. This can be attributed to the Manning counterion condensation. Indeed, some of the charges on the polymer backbone are effectively neutralized by the counterions if the length between two charged groups is smaller than the Bjerrum length resulting in a constant effective distance between charges. However, in the case of low charged polyanions, the counterion condensation is suppressed and the effective charge density is equal to the linear charge density leading to much thicker films with higher roughness.

Further, the system allows cross-linking of the films by inter- and intramolecular cross-link formation between polycationic moieties without affecting the charge density of the charge diluted part. The cross-linked groups are strong chromophores and show a characteristic absorption wavelength. Thus, the system gives perspectives for quantifying cross-linking kinetics and cross-link densities by using spectroscopic characterization methods. Due to the additional covalent cross-linking, films show increased stability against conditions where non-cross-linked films are not stable.

Since the charge density of strong polyelectrolytes is fixed, the resulting coatings are of passive nature, *e.g.* their properties are adjusted by the deposition conditions and the nature of polymers used. For weak polyelectrolytes, the charge density is regulated by the solution pH. Therefore, these types of polyelectrolytes are attractive for construction of active coatings with stimuli-responsive properties.

In the second part, active surface construction by polyelectrolyte copolymer is demonstrated. We used an ABC triblock terpolymer consisting of a hydrophobic polybutadiene (B) block, a pH-sensitive poly(methacrylic acid) (MAA) middle block, and a permanently charged block of quarternized poly(2-(dimethylamino)ethyl methacrylate) (Dq). The polymers were synthesized in the group of Prof. Dr. Axel H. E. Müller by Eva Betthausen (Department of Macromolecular Chemistry II at the University of Bayreuth). In water, the polymer chains self-assemble to micelles with a well defined structure and integrated pH-responsive properties.

We studied the adsorption and the pH-responsive behavior of micelles on silica. We found that the adsorption of positively charged micelles results in a monolayer of micelles with a maximum coverage of 54% according to the Random Sequential Adsorption model.

Further, we showed that the micellar morphology and charge density of the corona can be controlled by pH at the solid-liquid interface of the adsorbed micelles. This behavior is related to the degree of dissociation of the weak polyacid block and is completely reversible on short time scale. On the contrary, the long-term treatment under acidic conditions causes irreversible changes in the morphology of adsorbed micelles, which indicate an "opening" of the hydrophobic cores. The two types of conformational response to pH-trigger were found to be coupled with the mobility of the B core, since the covalent crosslinking of the core

prevents slow irreversible changes. Hence, only one relaxation dynamic was found for the cross-linked system.

Building up on these results, we investigated the interactions of cells with surfaces which were modified by a layer of the pH-responsive micelles. Here, in collaboration with Dr. Daria V. Andreeva from the department of Physical Chemistry II at the University of Bayreuth and Dr. Katja V. Skorb from the Max Planck Institute of Colloids and Interfaces in Golm, we demonstrated a nice way of controlled self-regulated bacteria release. The special feature of the system is that the release of bacteria occurs without receiving energy from an external source. Bacteria themselves trigger the switching in properties of the micellar monolayer by changing pH due to their metabolic activity. Thereby, bacteria decrease their own adhesion on the underlying surface.

Using the layer-by-layer approach, the polyelectrolyte block copolymer micelles were included within multilayer films. Thereby, the cationic micelles were electrostatically self-assembled in an alternating manner using poly(sodium 4-styrenesulfonate) as anionic counterpart. With this concept, we achieved the way to construct nanoporous films with novel internal double-end-tethered brush-like structures. The solution pH strongly influences the ionization degree of the double-end-tethered MAA brush. Therefore, the films' swelling degree with up to 1200%, pore closing/opening, as well as the mechanical properties are reversibly tunable by the surrounding medium. Moreover, the equilibrium swelling degrees are controlled by the porosity of the assemblies, which in turn is tunable by the number of deposition steps. The novelty of the designed system comes from the fact that the stimulus-responsive block is not involved into the complexation within the multilayer film. The disadvanteges of the classical multilayer approach to produce stimuli-responsive coatings such as loss of responsiveness or destruction by the trigger are therefore avoided.

In summary, various examples of coatings based on polyelectrolytes are presented in this work. The coatings possess internal hierarchy on different levels from lateral chemical structure (layer-by-layer assembled films) to lateral topographical structure (surface immobilized block copolymer micelles and the layer-by-layer assembly of micelles).

These coatings can be stimulus-responsive and functional. The most prominent examples presented here are the self-regulated bacteria adhesion and the highly swellable multilayers with reversible pH-response, which are potentially interesting as nano-actuators.

Zusammenfassung

Der Schwerpunkt dieser Arbeit lag auf der Oberflächenmodifizierung durch Polyelektrolyte und Polyelektrolytcopolymere. Die interne strukturelle Hierarchie entsteht dabei durch die Selbstorganisation auf unterschiedlichen Längenskalen. Um unterschiedliche Hierarchieebenen zu erzeugen, erfolgte die Beschichtung von Oberflächen entweder durch die Layer-by-Layer-Methode (LbL) (lateral-chemische Struktur), durch die Adsorption supramolekularer Aggregate (lateral-topographische Struktur) oder durch Kombination beider Methoden. Die Verwendung dieser Methoden ermöglicht die Kontrolle der Oberflächeneigenschaften, wie z. B. Ladungsdichte, durch Änderung der chemischen Struktur des Polyelektrolyts und liefert damit eine bequeme Art und Weise, die Oberfläche zu funktionalisieren und deren Eigenschaften zu steuern. Aus diesem Grund haben wir mit Systemen gearbeitet, deren Ladungsdichten variabel sind. Ausgehend von diesem Ansatz ist es uns gelungen, dünne und ultradünne nanostrukturierte Filme mit steuerbaren Eigenschaften und Funktionalität herzustellen.

Das Ziel dieser Arbeit kann in zwei Hauptteile gegliedert werden.

Im ersten Teil wird der Aufbau passiver Beschichtungen präsentiert, die durch LbL-Aufbau starker Polyelektrolyte mit steuerbarer Ladungsdichte hergestellt wurden. Die Betonung lag dabei auf dem Verständnis des Multilagenaufbaus in Abhängigkeit der chemischen Struktur der LbL-Komponenten. Dabei wurden der Aufbau und die chemische Quervernetzung der Filme untersucht, welche durch Sprühmethode neuartiger Polyanione mit variablen Ladungsdichten (21-100%) und vernetzbaren kationischen Polyelektrolyten hergestellt wurden. Dies ermöglicht die Steuerung sowohl der ionischen, als auch der kovalenten Vernetzungsdichte. Die Polyelektrolyte wurden von Patrick Ott aus der Gruppe von Prof. Dr. André Laschewsky (Institut für Chemie an der Universität Potsdam) synthetisiert.

Wir fanden heraus, dass die Ladungsdichte von Polyanionen im Bereich der hohen Ladungsdichte für alle untersuchten Ionenstärken nur einen geringen Einfluss auf das Aufbauverhalten hat. Dies kann auf die Manning-Gegenionenkondensation zurückgeführt werden. Tatsächlich werden einige Ladungen des Polymerrückgrats effektiv durch die Gegenionen neutralisiert, sofern der Abstand zwischen zwei geladenen Gruppen kleiner ist als die Bjerrum-Länge, was in einem konstanten effektiven Abstand zwischen den Ladungen

resultiert. Im Fall von weniger geladenen Polyanionen wird dagegen die Gegenionenkondensation unterdrückt und die effektive Ladungsdichte ist gleich der linearen Ladungsdichte, was zu deutlich dickeren Filmen mit einer höheren Rauigkeit führt.

Des Weiteren erlaubt das System die chemische Quervernetzung des Films durch inter- und intramolekulare Vernetzung zwischen polykationischen Einheiten, ohne dabei die Ladungsdichte des ladungsverdünnten Teils zu beeinflussen. Die vernetzten Gruppen sind starke Chromophore und weisen eine charakteristische Absorptionswellenlänge auf. Somit bietet das System eine Möglichkeit der quantitativen Bestimmung der Vernetzungskinetik sowie der Vernetzungsdichte mit Hilfe spektroskopischer Charakteresierungsmethoden. Aufgrund zusätzlicher kovalenter Vernetzung, weisen die Filme eine erhöhte Stabilität unter Bedingungen auf, unter wlchen nicht vernetzte Filme instabil sind.

Da die Ladungsdichte starker Polyelektrolyte konstant ist, sind die resultierenden Beschichtungen von passiver Natur, d. h., dass ihre Eigenschaften durch die Beschichtungs-bedingungen und die Art des verwendeten Polymers bestimmt sind. Bei schwachen Polyelektrolyten wird die Ladungsdichte durch den pH-Wert der Lösung geregelt. Aus diesem Grund ist dieser Polyelektrolyttyp von besonderem Interesse für den Aufbau aktiver Beschichtungen mit stimuli-responsiven Eigenschaften.

Im zweiten Teil der Arbeit wird der Aufbau aktiver Oberflächen durch Polyelektrolytcopolymere vorgestellt. Es wurde ein ABC-Triblockterpolymer, bestehend aus einem hydrophoben Polybutadienblock (B), einem pH-sensitiven Polymethacrylsäure-Mittelblock (MAA) und einem permanent geladenen Block aus quarternisiertem Poly(2-dimethylamino)ethylmethacrylat) (Dq), verwendet. Die Polymere wurden von Eva Betthausen aus der Gruppe von Prof. Dr. Axel Müller (Lehrstuhl Macromolekulare Chemie II an der Universität Bayreuth) synthetisiert. In wässriger Lösung lagern sich die Polymerketten durch Selbstorganisation zu Mizellen mit genau definierter Struktur und integrierten pH-responsiven Eigenschaften an.

Es wurde das Adsorptions- und das pH-responsive Verhalten der Mizellen auf Siliziumwafern untersucht. Dabei wurde festgestellt, dass die Adsorption positiv geladener Mizellen zu einer Monolage mit einer maximalen Belegungsdichte von 54% entsprechend dem *Random Sequential Adsorption* Modell führt.

Ferner wurde gezeigt, dass sich die mizellare Morphologie und die Ladungsdichte der Korona durch pH-Änderungen an der fest-flüssig Grenzfläche der adsorbierten Mizellen kontrollieren lässt. Dieses Verhalten steht im Zusammenhang mit dem Dissoziationsgrad des

schwachen Polysäureblocks und ist vollständig reversibel auf einer kurzen Zeitskala. Im Gegensatz dazu führt die langzeitige Behandlung unter sauren Bedingungen zu irreversiblen Änderungen der Morphologie adsorbierter Mizellen, die auf das „Öffnen" der hydrophoben Kerne andeutet. Zwei Arten der Konformationsänderung ausgelöst durch den pH-Wechsel sind mit der Mobilität des B-Kerns gekoppelt, da dessen kovalente Vernetzung langsame irreversible Änderungen verhindert. Deshalb wurde bei dem vernetzten System nur eine Relaxationsdynamik beobachtet.

Ausgehend von diesen Ergebnissen wurden die Wechselwirkungen von Zellen mit Oberflächen, welche mit einer Lage pH-responsiver Mizellen modifiziert waren, untersucht. Dabei wurde in Kooperation mit Dr. Daria V. Andreeva (Lehrstuhl Physikalische Chemie II an der Universität Bayreuth) und Dr. Katja V. Skorb (Max Planck Institut für Kolloide und Grenzflächen in Golm) eine einfache Art der kontrollierten, selbstregulierenden Freisetzung der Bakterien demonstriert. Ein besonderes Merkmal dieses Systems ist, dass die Freisetzung der Bakterien ohne Energiezufuhr von außen erfolgt. Die Bakterien lösen selbst das Umschalten der Eigenschaften der mizellaren Monolage aus, indem sie durch ihren Metabolism den pH-Wert der Umgebung ändern. Dabei erniedrigen sie die eigene Adhäsion an die darunter liegende Oberfläche.

Unter Verwendung der LbL-Methode wurden die Polyelektrolytcopolymer-Mizellen in Multilagenfilme eingebaut. Dabei wurden die kationischen Mizellen alternierend mit anionischem Natrium-Polystyrolsulfonat elektrostatisch angeordnet. Mit diesem Konzept wurden nanoporöse Filme mit neuartigen internen *double-end-tethered* bürstenartigen Strukturen hergestellt. Der Ionisierungsgrad der MAA-Bürsten wird dabei stark durch den pH-Wert der Lösung beeinflusst. Aus diesem Grund lassen sich der Quellungsgrad von bis zu 1200%, das Öffnen/Schließen der Poren, sowie die mechanischen Eigenschaften reversibel durch das sie umgebende Medium steuern. Außerdem werden die Gleichgewichtsquellungs-grade durch die Porosität der Filme, und diese wiederum durch die Anzahl der aufgebrachten Schichten kontrolliert. Das Interressante an dem neu entwickelten System ist, dass der responsive Block nicht an der Komplexbildung innerhalb der Multilagen beteiligt ist. So können die Nachteile des klassischen Einbaus von responsiven Einheiten in die LbL-Filme (wie Response-Verlust oder Auflösung durch den Auslöser) umgegangen werden.

Zusammenfassend werden in dieser Arbeit unterschiedliche Beispiele für Beschichtungen gezeigt, die auf der Polyelektrolytadsorption beruhen. Die untersuchten Filme weisen

unterschiedliche Ebenen der internen Hierarchie auf, von lateral-chemischen Struktur (LbL-Filme) bis hin zu lateral-topographischen Strukturen (adsorbierte Blockcopolymer Mizellen und LbL-Filme von Mizellen).

Diese Beschichtungen können stimuli-responsive und funktionale Eigenschaften zeigen. Die wichtigsten in dieser Arbeit gezeigten Beispiele dafür sind die selbstregulierende Bakterienadhäsion und die hoch quellfähigen Multischichten mit pH-sensitiven reversiblen Eigenschaften. Die Letzteren haben ein großes Potential für die Entwicklung von Nanoaktuatoren.

List of Publications

1. **"Micro-structure – Macro-response" relationship in swollen block copolymer films.** Gensel, J.; Liedel, C.; Schoberth, H. G.; Tsarkova, L., *Soft Matter*, **5**, 2534-2537 (2009)

2. **Cross-linkable polyelectrolyte multilayer films of tailored charge density.** Ott, P.; Gensel, J.; Roesler, S.; Trenkenschuh, K.; Andreeva D. V.; Laschewsky, A.; Fery, A., *Chemistry of Materials*, **22**, 3323-3331 (2010)

3. **Free-standing membranes via covalent cross-linking of polyelectrolyte multilayers with complementary reactivity**. Ott, P.; Trenkenschuh, K.; Gensel, J., Fery, A.; Laschewsky, A., *Langmuir*, **26**(23), 18182-18188 (2010)

4. **Surface immobilized block copolymer micelles with switchable accessibility of hydrophobic pockets**. Gensel, J.; Betthausen, E.; Hasenöhrl, C.; Trenkenschuh, K.; Hund, M.; Boulmedais, F.; Schaaf, P.; Müller, A. H. E.; Fery A., *Soft Matter,* **7**, 11144-11153 (2011)

5. **Tuning of the elastic modulus of polyelectrolyte multilayer films built up from polyanions mixture**. Trenkenschuh, K.; Erath, J.; Kuznetsov, V.; Gensel, J.; Boulmedais, F.; Schaaf, P.; Papastavrou, G.; Fery, A., *Macromolecules,* **44**(22), 8954-8961 (2011)

6. **Cavitation engineered 3-D sponge networks and their application in active surface construction**. Gensel, J.*,* Borke T., Pazos Perez, N., Fery, A.*,* Müller, A. H. E., Betthausen, E., Andreeva, D. V.*,* Möhwald, H.*,* Skorb, E. V., *Advanced Materials,* **24**(7), 985-989 (2012)

7. **Reversible swelling transitions in stimuli-responsive layer-by-layer coatings containing block copolymer micelles**. Gensel, J.*,* Dewald, I., Erath, J., Betthausen, E., Müller, A. H. E.; Fery, A., *Chemical Science* DOI: 10.1039/C2SC20836A (2012)

List of Abbreviations and Symbols

α	degree of dissociation
α'	degree of neutralization
AFM	Atomic Force Microscopy
B	polybutadiene
$c(H^+)$	molar concentration of H^+ ions
cmc	critical micelle concentration
$c(PE)$	molar concentration of polyelectrolyte
c_s	concentration of salt ions
CP	colloidal probe
DLS	dynamic light scattering
D_s	diffusion coefficient
δ^{-1}	grafting density
e	elementary charge
I	ionic strength
IPEC	interpolyelectrolyte complex
κ^{-1}	Debye length
K_a	dissociation constant
$k_B T$	thermal energy
l_B	Bjerrum length
LbL	layer-by-layer
LCST	lower critical solution temperature
MAA	poly(methacrylic acid)
µCP	microcontact printing
n	refractive index
p	packing parameter
P	porosity
pK_a	acidity constant
p$K_{a, apparent}$	apparent acidity constant
PAA	poly(acrylic acid)

9

PDI	polydispersity index
PNIPAM	poly(N-isopropylacrylamide)
R_c	core radius
R_m	radius of the micelle
PSS	poly(sodium 4-styrenesulfonate)
RSA	Random Sequential Adsorption
SEM	Scanning Electron Microscopy
t	time
TEM	Transmission Electron Microscopy
$\theta(\infty)$	jamming limit
QCM	Quartz Crystal Microbalance
UV-vis	Ultraviolet-visible Spectroscopy
χ	Flory-Huggins interaction parameter
ζ	Zeta potential
$4\pi\varepsilon\varepsilon_0$	relative permittivity

1 Introduction

Surfaces can be found everywhere in our daily life.

Various material properties such as wettability, adhesion, texture, color, friction, lubrication *etc.* are regulated by the surface. Since the control over surface and interface properties is of particular importance in current material science, one would like to engineer and design functional surface coatings depending on their purpose.

This raises the question of how to precisely control the surface properties and to produce tailored surfaces?

In the course of ever-smaller scales for functional products and devices, surface modification by polymers with integrated functional properties opens a great potential. The choice for this field is initiated by the breakthrough of the layer-by-layer deposition technique[1] to produce self-assembled multilayer films by a sequential adsorption of oppositely charged polyelectrolytes. Besides this, the increased level of synthetic progress provides many advances in the field of polyelectrolyte block copolymers which undergo spontaneous self-assembly resulting in well-defined structures with tunable composition, morphology, and size on the nano-scale.

Coatings based on one of the mentioned approaches, or the combination of both, are in the focus of many applications as well as for the fundamental stand of surface engineering.

Further interest in such self-assembled systems arises from the precise control over the film composition, providing the ability to tune properties of the surface. Charge density of polyelectrolytes plays thereby a major role. In case of strong polyelectrolytes, the properties of the resulting coatings are adjusted by the deposition conditions and the nature of polymers used since their charge density is fixed. For weak polyelectrolytes, the charge density is regulated by the solution pH. Therefore, coatings by weak polyelectrolytes can be of active nature.

Due to the ease of fabrication and use combined with a good stability and durability in water, both adsorbed self-assembled polymer nanoparticles and layer-by-layer films have been investigated with respect to diverse applications, *e.g.* for controlling wetting properties[2] or interactions with proteins,[3] as anti-corrosion coatings,[4] osmotic pressure sensors[5] *etc.* A

topic of more recent interest includes the design of coatings for controlled interactions with complex biological systems such as cells.[6, 7]

In this respect, systems based on stimuli-responsive materials are very interesting because they can switch their properties in response to external stimuli such as temperature, pH, ionic strength, or light. However, the classical multilayer approach to produce stimuli-responsive coatings often results in either a loss of responsiveness or even worse, the destruction of the film by a trigger. Therefore, it would be beneficial if effective separation of functional compartments could be achieved. Among several methods for the engineering of such coatings, hierarchically organized self-assembled systems are inspired by nature. The best example is perhaps the human being representing different levels of the biological hierarchy starting from molecules such as DNA through organelles, cells to tissue and organs, and finally to a complex organism. At the same time, these components are multifunctional and stimuli-responsive.

The central point of this thesis is the systematic investigation of correlations between molecular scale architecture and properties of thin and ultrathin polyelectrolyte coatings, with emphasis on internal hierarchy and functionality. For this approach, we will focus on systems with variable charge densities as one of the major factors for controlling properties and functionality of polyelectrolyte coatings. In the first part of the thesis, the construction of layer-by-layer films of strong polyelectrolyte copolymers will be demonstrated. The second part of the work will deal with the surface modification by self-assembled triblock terpolymer micelles with a pH-sensitive weak polyelectrolyte block. In other words, the work will demonstrate ways to produce tailored surfaces by thin films with different levels of internal hierarchy including fundamental aspects and applications.

1. G. Decher, *Science*, 1997, **277**, 1232-1237.

2. W. Niemiec, S. Zapotoczny, K. Szczubialka, A. Laschewsky and M. Nowakowska, *Langmuir*, 2010, **26**, 11915-11920.

3. D. S. Salloum and J. B. Schlenoff, *Biomacromolecules*, 2004, **5**, 1089-1096.

4. D. V. Andreeva, D. Fix, H. Möhwald and D. G. Shchukin, *Advanced Materials*, 2008, **20**, 2789-2794.

5. M. Nolte, I. Dönch and A. Fery, *ChemPhysChem*, 2006, **7**, 1985-1989.

6. J. D. Mendelsohn, S. Y. Yang, J. Hiller, A. I. Hochbaum and M. F. Rubner, *Biomacromolecules*, 2003, **4**, 96-106.

7. S. Schmidt, M. Zeiser, T. Hellweg, C. Duschl, A. Fery and H. Möhwald, *Advanced Functional Materials*, 2010, **20**, 3235-3243.

2 Theory / Status of the Field

This chapter gives an overview over the theoretical basics and status of the field necessary for the understanding of this work. First, the field of polyelectrolytes in solution including linear homopolyelectrolytes, polyelectrolyte random and block copolymers, and polyelectrolyte brushes is introduced. Then, methods to produce thin films by polyelectrolyte adsorption are reviewed, with a special emphasis on the layer-by-layer technique and adsorption of colloidal particles. In addition, a general overview of the field of stimuli-responsive coatings is discussed. Finally, the objectives of the thesis are presented.

2.1 Polyelectrolytes in Solution

2.1.1 Classification of Polyelectrolytes

Polyelectrolytes are water-soluble polymers containing ionizable groups.[1] After their dissociation in water, polyelectrolytes carry either positive charges (polycations) or negative charges (polyanions) according to their monomeric units. The electroneutrality of the system is achieved by counterion condensation.

Polyelectrolytes can be natural or synthetic. A distinction is made between strong (quenched) and weak (annealed) polyelectrolytes. In the case of strong homopolyelectrolytes, the ionization degree is independent from the solution pH and therefore the charge density is permanently high. On the contrast, the ionization behavior of weak polyelectrolytes can be varied by pH.

2.1.2 Tuning the Charge Density of Polyelectrolytes

Weak Polyelectrolytes

The charge density of a weak polyelectrolyte is described by its degree of dissociation α.

For weak acids with dissociation constant K_a, the dependence of the neutralization degree α' on the pH value is explained by the Henderson-Hasselbalch equation

$$pK_a = pH + \log \frac{1-\alpha'}{\alpha'} \qquad (2.1)$$

However, for a weak polyacid in an aqueous medium, due to electrostatic contribution of previously formed charges, an additional work ΔG_{el} is needed to separate a proton from an acid group to infinite distance.[1-3] The resulting pK_a is therefore dependent on the actual dissociation degree α and only an apparent $pK_{a,apparent}$ value. α can be calculated from the neutralization degree α', molar concentration of H^+ ions $c(H^+)$, and molar concentration of polyelectrolyte $c(PE)$ according to the equation

$$\alpha = \alpha' + \frac{c(H^+)}{c(PE)} \qquad (2.2)$$

Taking the additional work into account, equation (2.1) can be expressed as following [2]

$$pH = pK_{a,apparent} - \log \frac{1-\alpha}{\alpha} = pK_a^0 - \log \frac{1-\alpha}{\alpha} + 0.4343 \frac{\Delta G_{el}}{RT} \qquad (2.3)$$

where K_a^0 is the intrinsic dissociation constant.

Finally, to show the dependence between the experimentally observed $pK_{a,apparent}$ and the intrinsic pK_a^0, equation (2.3) can be rewritten as follows

$$pK_{a,apparent} = pK_a^0 + 0.4343 \frac{\Delta G_{el}}{RT} \qquad (2.4)$$

The effective pK_a value of weak polyelectrolytes strongly depends on the local environment. For example, the apparent pK_a values of weak polyacids and polybases are shifted by ~1−4 pH units to the acidic or alkaline region, respectively, when they are incorporated into the multilayer film.[4-8] These results indicate that if the weak polyelectrolyte is a component of an interpolyelectrolyte complex, the polyacid becomes a stronger acid and the polybase a stronger base in comparison to their behavior in dilute solution.

An opposite effect is observed if weak polyelectrolyte chains are densely grafted to a planar[9-11] or curved surface resulting in polyelectrolyte brushes, or if chains are bound to a branching point (star-shaped polyelectrolytes).[12] In this case, the pK_a shifts to higher pH

values are found for polyacids as a result of the Coulombic repulsion of neighboring charges. Obviously, the pK_a shifts of polyelectrolyte brushes and stars become more pronounced with increasing grafting density.[11, 12]

Random Copolymers - Charge Density

An alternative elegant approach to design polyelectrolytes with variable charge density which is independent on the pH is the use of strong polyelectrolytes with fixed charge density by "intramolecular dilution". There are two ways for the design of charge diluted polyelectrolytes: either by fixing the distance between neighboring charged groups by complex constitutional repeat units,[13-17] or by reducing the charge of the polyelectrolyte chain through the incorporation of uncharged spacer groups separating the charged moieties.[18-22] The former strategy has the advantage of providing random copolymers with regular, well defined charge densities. However, care must be taken when choosing the non-ionic moieties: on the one hand these groups should have a hydrophilic character to avoid strong hydrophobic interactions and complications.[13, 14, 16, 17] On the other hand, the use of comonomer systems with reactivity ratios close to 1 is required in order to provide defined, truly random copolymers under so-called azeotropic conditions. Otherwise broad mixtures of copolymers with strongly differing charge contents are obtained.

2.1.3 Conformations of Polyelectrolytes in Solution

If a polyelectrolyte is dissolved in aqueous solution, the charges of dissociated groups on a chain interact among each other due to electrostatic repulsion. One important parameter is the linear charge density (Fig. 2.1), which describes the number of charged groups along the polyelectrolyte chain per unit length.

The Bjerrum length l_B is the distance at which the repulsive interaction between two elementary charges in a medium with a relative permittivity $4\pi\varepsilon\varepsilon_0$ is equal to the thermal energy $k_B T$.[1, 23, 24] l_B can be expressed as following

$$l_B = \frac{e^2}{4\pi\varepsilon\varepsilon_0 k_B T} \qquad (2.5)$$

where e is the elementary charge, k_B is the Boltzmann constant, and T is the absolute temperature.

Hence, l_B describes the distance below which the Coulomb interactions are predominant over the thermal fluctuations. The Bjerrum length in water at room temperature is ~ 7 Å.[1] If the distance between two charged groups is smaller than the Bjerrum length, some of the charges on the polymer backbone are effectively neutralized by the counterions with respect to Manning counterion condensation (Fig. 2.1).[25] This is so called „strong screening zone" where the effective distance between charges is constant due to counterion condensation.
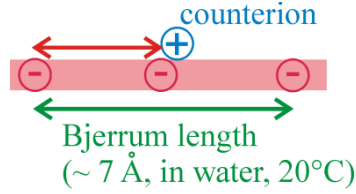

Fig. 2.1: Illustration of the counterion condensation.

In polyelectrolyte solution containing salt, the electrostatic interactions are screened by electrolyte ions. The effective electrostatic interaction between two charges which are separated by a distance r can be described with the Debye-Hückel potential[23]

$$\phi(r) = \frac{l_B}{r} e^{-\kappa r} \qquad (2.6)$$

The exponential decay is characterized by the Debye screening length κ^{-1}

$$\kappa^2 = 4\pi \, l_B \sum_s c_s q_s^2 \qquad (2.7)$$

which is related to the concentration c_s of salt ions s with a valence q_s.[23, 24] Thus, the conformation of polyelectrolytes is strongly dependent on the ionic strength of the surrounding solution. Fig. 2.2 schematically shows the effect of ionic strength on the conformation of a polyelectrolyte molecule.

In a dilute salt-free solution, the Debye screening length is high. Thus, unscreened Coulomb repulsion of charges along the chain leads to an extended conformation.[1, 24] With increasing ionic strength of the solution, the charges on the chain are screened by salt ions resulting in a more coiled form (Fig. 2.2).
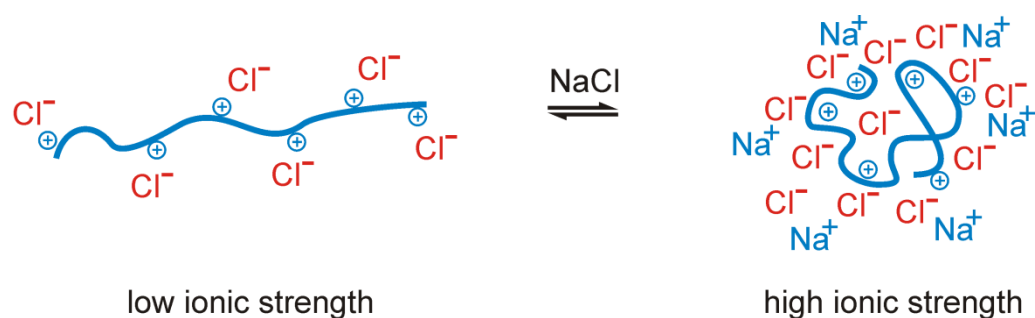
Fig. 2.2: The conformation of a polyelectrolyte chain in aqueous solution without added electrolytes (left) and with high ionic strength (right).

2.1.4   Interpolyelectrolyte Complexes (IPECs)

The simple mixing of aqueous solutions of oppositely charged polyelectrolytes results in interpolyelectrolyte complex (IPEC) formation through the cooperative electrostatic interactions of polycations and polyanions.[1, 26] The driving force for the interpolyelectrolyte coupling is the entropy gain through the release of counter ions. The resulting IPECs can be either insoluble but swellable in water or water-soluble. Insoluble co-assemblies are often formed if the IPECs have a 1:1 stoichiometry of charged groups (Fig. 2.3a, b). The ladder model and the "scrambled egg" model are the two limiting models of the 1:1 IPEC structure. If one of the IPEC components has an excess of charged fragments (host polyelectrolyte) compared to the other polyion of opposite charge (guest), non-stoichiometric structures will be generated.[26-28] Fig. 2.3c demonstrates the structure of water-soluble IPECs enabled by the uncomplexed parts of the host polyelectrolyte.

By increasing the ionic strength of the solution, IPECs dissociate into the starting components because of the screening of the polyelectrolyte charges by the electrolytes.[26, 28] In the case of weak polyelectrolytes, the dissociation of the IPEC can occur because of decreasing the ionization degree through changes in pH.
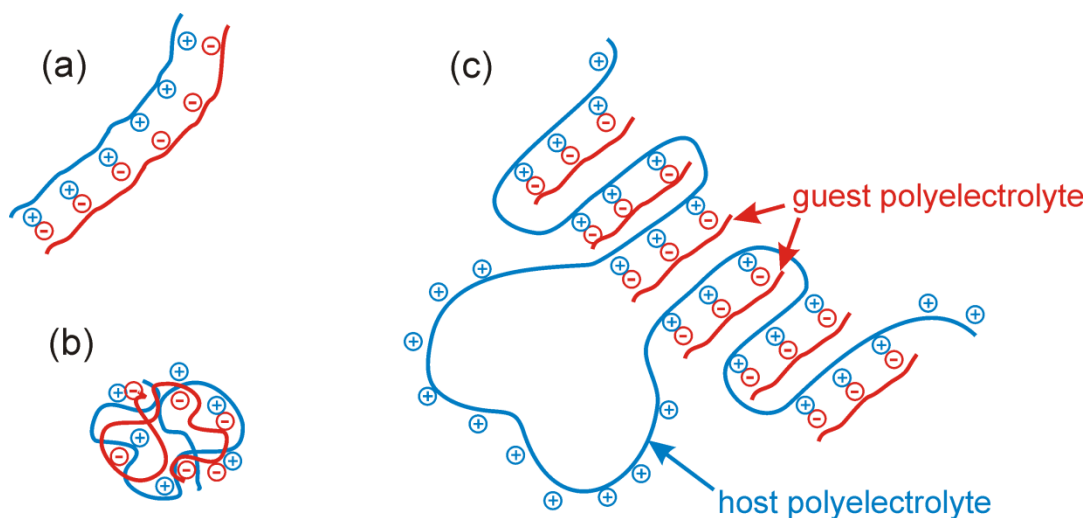
Fig. 2.3: The schematic representation of stoichiometric insoluble IPECs: Ladder model (a), and "scrambled egg" model (b) (reproduced from Ref. [1]), and non-stoichiometric IPEC structure (c) (reproduced from Ref. [27]).

2.1.5 Self-Assembly of Polyelectrolyte Block Copolymers in Aqueous Solution

Block copolymers are macromolecules where two or more homopolymer blocks with different chemical and physical properties are covalently linked to each other. Due to the incompatibility of the two polymer blocks combined with their covalent connectivity, block copolymers are able to self-assemble to form periodic structures in bulk and in solution.[29] The microphase separation in bulk leads to a variety of morphologies including lamellae, hexagonal-packed cylinders, gyroids, and body-centred cubic spheres.[30]

Block copolymers with at least one polyelectrolyte block are often referred to polyelectrolyte block copolymers.[31-33] When polyelectrolyte diblock copolymers are dissolved in water, which is a good solvent for charged block, at concentrations above critical micelle concentration (cmc), the chains of insoluble block will associate to form micellar aggregates with hydrophobic cores and charged corona (Fig. 2.4). The most typical micellar structures obtained for linear AB diblock copolymers are spherical or cylindrical micelles and vesicles.
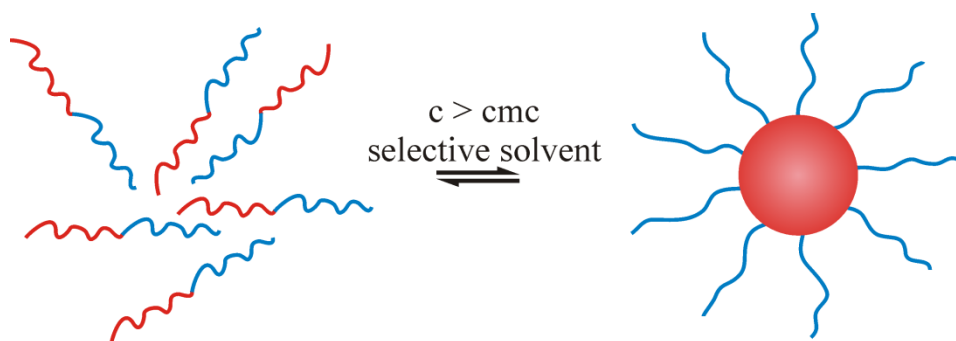
$$c > cmc$$
$$\text{selective solvent}$$

Fig. 2.4: Micelle formation of a diblock copolymer by a self-assembly in a selective solvent.

Two limiting structures can be distinguished, depending on the relative block length of the hydrophobic and polyelectrolyte blocks (see Fig. 2.5).[32] If the hydrophobic block is longer than the charged block, "crew-sut" micelles with a large core and short corona are formed (Fig. 2.5a). In the reverse case, "star-like" micelles are observed (Fig. 2.5b). Parameters which characterize the resulting micellar structure are the core radius R_c, the overall radius of the micelle R_m, the distance b between two neighboring blocks at the core/corona interface, and the aggregation number.[31] The size of micelles is controlled by the degree of polymerization of the blocks and the Flory-Huggins interaction parameter χ.[31] Therefore, the structure strongly depends on both, molecular parameters and parameters of the solution.[31]
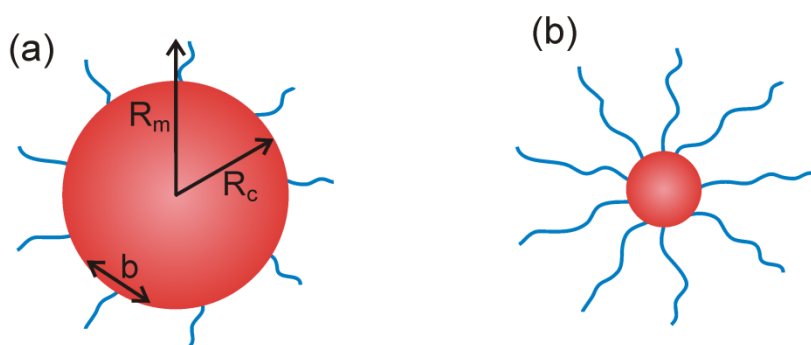

Fig. 2.5: Schematic representation of a "crew-cut" (a) and a "star-like" (b) micelle. Reproduced from Ref. [32].

Additionally to the above described factors, the micellization behavior of block copolymers can be described using the geometrical treatment (packing parameter), which was initially developed for low molecular weight surfactants.[34]

The packing parameter p is characterized by the volume of the hydrophobic group v, the area b^2 occupied by one chain, and the length l_c of the hydrophobic block (Fig. 2.6a) according to

$$p = \frac{v}{b^2 l_c} \tag{2.8}$$

Depending on the value of the packing parameter, the type of the final micellar structure can be predicted (see Fig. 2.6b).
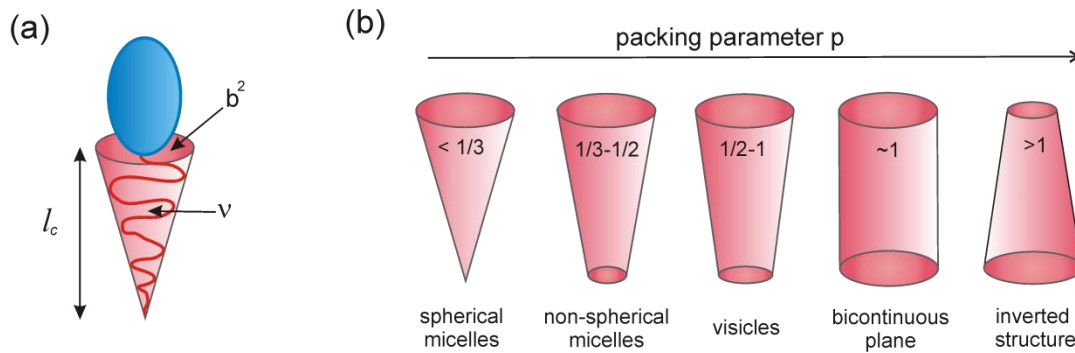

Fig. 2.6: Scematic representation of the values contributing to the packing parameter (a), and the final micellar structure predicted by the packing parameter (b). Reproduced from Ref. [34, 35].

Commonly, the properties of the polyelectrolyte corona are strongly influenced by following parameters: pH, ionic strength, and polar interactions.[32, 39] Moreover, at high segment concentration micelles can be described as spherical polyelectrolyte brushes (see chapter 2.2.4).[31, 40]

The dynamic equilibrium between unimers in the micelle depends on the glass transition temperature of the core-forming block. If the core-forming block of micelles is glassy (high glass transition temperature), the solubility of directly dissolved in water block copolymer is generally low.[41] Thus, the polymer has to be dialyzed from organic solvent against water to obtain micellar structure in aqueous solutions.[31, 39] In this case, so called "frozen" aggregates are observed, whose chains are kinetically trapped; thus no exchange of polymers between aggregates occurs on the time scale of experiment.[42] In other words, the structure of "frozen" aggregates depends rather on the preparation method than on environmental changes. On the contrary, micelles with low glass transition temperature core-forming block (*e.g.*

polybutadiene) are dynamic structures and show responsiveness to environmental changes by unimer exchange.[35, 43, 44]

If ABC block terpolymers are used, the micellar assemblies are becoming more complex.[36,37] The introduction of a third block results in morphologies with a structured core or shell, such as core-shell-corona micelles, micelles with a mixed corona as well as Janus micelles[38] (Fig. 2.7).
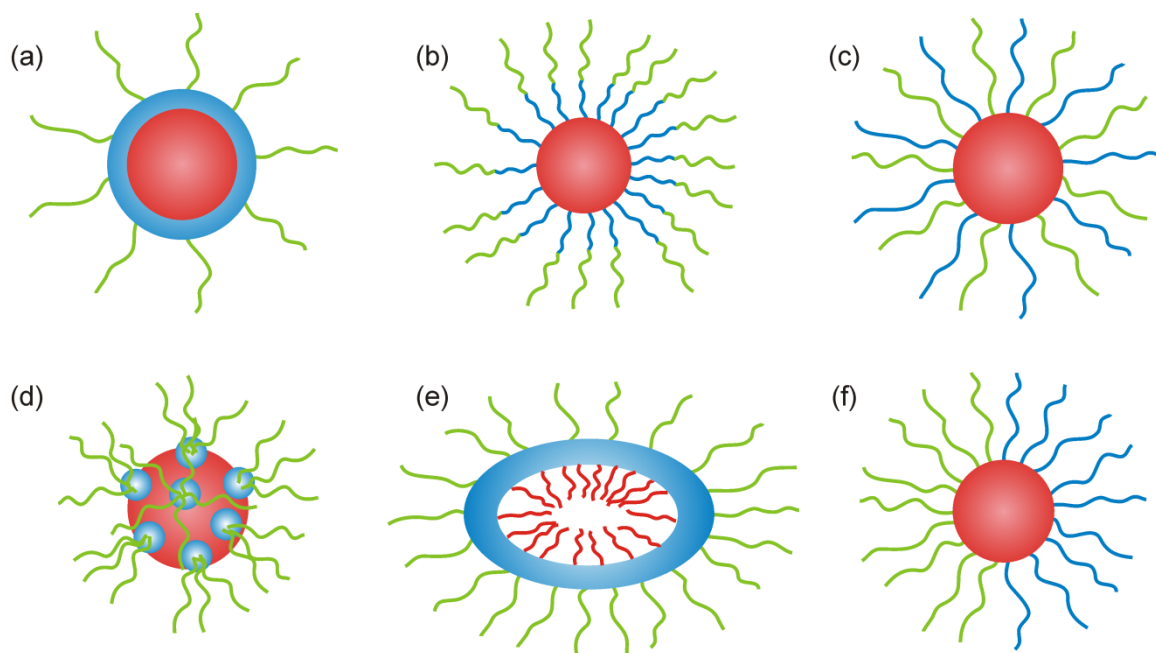

Fig. 2.7: Morphologies of ABC block terpolymers: core-shell-corona micelles (a, b), micelles with mixed corona (c), micelles with patchy corona (d), vesicles (e), and Janus micelles (d). Reproduced from Ref. [36].

ABC triblock terpolymer micelles, having a cationic, an anionic, and a hydrophobic block can form intramicellar IPECs (*im*-IPECs) without extrinsic crosslinking agents. Such so-called "self-locked" micelles[45] exhibit a micellar structure with an *im*-IPEC shell collapsed onto hydrophobic core. If one of the charged blocks has a higher degree of polymerization, the uncomplexed parts of this block are forming a charged corona.[45-48] The IPEC-shell can be reversibly disassembled by changes of the ionic strength or/and pH (weak polyelectrolytes) of the solution.[26, 28]

2.2 Thin Films via Self-Assembly of Polyelectrolytes and Polyelectrolyte Block Copolymers

2.2.1 Polyelectrolyte Adsorption

The adsorption of polyelectrolytes at surfaces provides a basis for surface modification.

Generally, polyelectrolytes are adsorbing onto oppositely charged surfaces. Usually their conformation is flat and the adsorbed amount increases with increasing ionic strength of the solution.[49-51]

The conformation of adsorbed polyelectrolytes as well as polymers in general on the surface can be described by the loop-train-tail model.[49] Fig. 2.8 shows the schematic illustration of an adsorbed polyelectrolyte molecule with segments in loops, trains and tails.
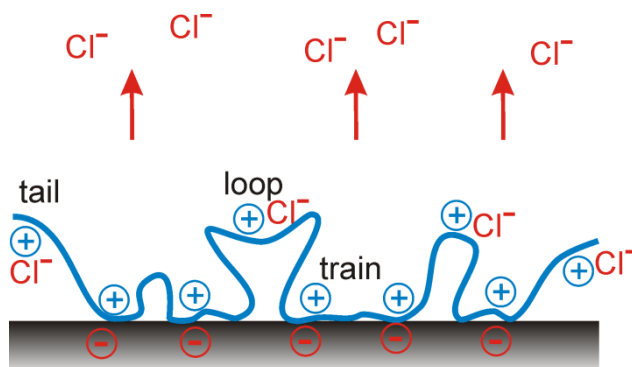

Fig. 2.8: Loop-train-tail model of adsorbed polyelectrolyte chain and release of counterions upon adsorption. Reproduced from Ref. [49].

The adsorption of polyelectrolytes can result in an inversion of the surface charge.[52] For the adsorption process, both entropic[53, 54] (release of counterions and hydration water, Fig. 2.8) and enthalpic[51] (Coulomb repulsion between charged units and electrostatic attraction between the surface and the polyelectrolyte chain) factors play an important role.

At low ionic strength of the solution, polyelectrolyte chains exhibit more stretched conformation resulting from electrostatic repulsion between charged units. In this case, the adsorbed layers are very thin indicating that the chain segments adsorb preferably as trains. At high ionic strength of the solution, the repulsion between the charges along the chain is

screened. For this reason, the adsorbed chain can adopt more conformations with tails and loops resulting in thicker layers.[51]

Similarly, for a weak polyelectrolyte or a strong polyelectrolyte with variable charge density, the conformation of adsorbed chain is quite relevant to its charge density.[50]

2.2.2 Polyelectrolyte Multilayers

Polyelectrolyte multilayers can be fabricated by the layer-by-layer (LbL) deposition technique.[55-60] LbL technique is an attractive and fast tool in the formation of thin nanostructured films with tunable properties and functionality. The method involves sequential alternating physisorption of oppositely charged polyelectrolytes. Fig. 2.9 schematically illustrates the electrostatic LbL self-assembly process. Typically, LbL adsorption is performed by the dip coating method sketched in Fig. 2.9a: first, a charge substrate is dipped into a solution of oppositely charged polyelectrolyte. Then, after a rinsing step, in which the residual polyelectrolyte chains are washed away, the substrate is dipped into the next solution with opposite charge. These steps can be repeated until the desired number of layers, which determine the thickness of the film.
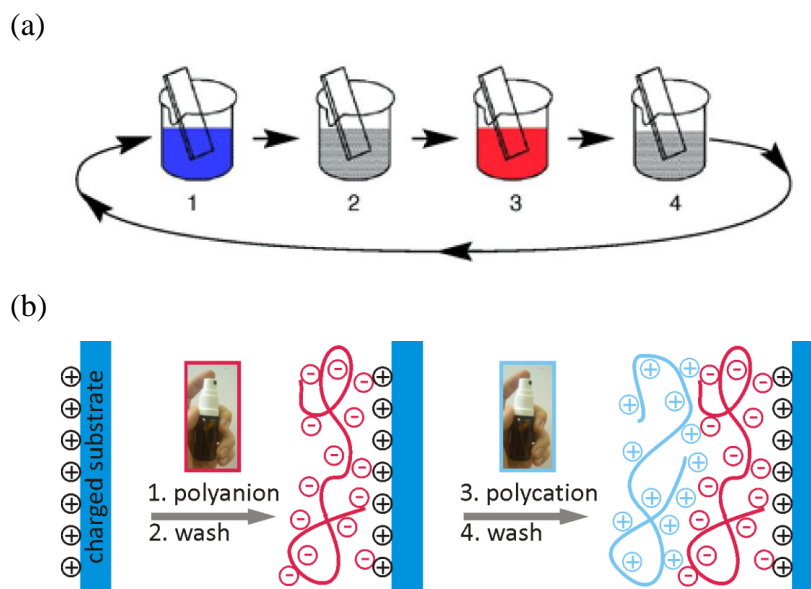

Fig. 2.9: Schematic representation of the layer-by-layer deposition technique by dip (a) and spray coating (b).[58]

Alternatively, the films can be assembled by spray (Fig. 2.9b) or spin coating following the same procedure. Both methods have the advantage of small amounts of polyelectrolyte solutions needed for the coverage of large surface areas.[60] Spray deposition is known to simplify and speed up the LbL deposition process as compared to conventional dip coating.[62, 63] Furthermore, this method can easily be automated and is suitable for the large-scale surface coatings, which is important for many industrial applications. Spin-coating deposition enables the formation of very homogeneous films with much smoother surfaces than the dip-coated films.[64, 65]

The driving force for the LbL deposition is the release of counterions and hydration water upon adsorption, thus increasing the entropy of the system.[53, 54] Subsequent adsorption of oppositely charged polyelectrolytes leads thereby to charge overcompensation (*cf.* Fig. 2.10), so that the sign of the surface charge is reversed after each deposition layer.[59, 66-68] Therefore, the thickness of the film and the resulting charge can be adjusted by the number of deposition steps.

Besides the number of layers, the precise structure of the coatings depends on various parameters such as chemical structure of the polyelectrolytes, for instance their architecture and charge density, and the conditions of adsorption process.[59, 60] The ionic strength of polyelectrolyte solutions is an important factor for the multilayer formation. The increasing salt concentration leads to thicker layers due to a more coiled conformation as a result of screening of repulsive interactions within the chain.[56, 69, 70] However, at very high ionic strength, the adsorption can be blocked due to the high screening effect or desorption of the polymers during the deposition process.[18, 71]

If deposition is performed from pure aqueous solutions of strong polyelectrolytes without salt addition, very thin layers are often observed.[15, 59, 72, 73] This observation may be attributed to the lack of charge overcompensation due to a more linear conformation of the polyelectrolytes.
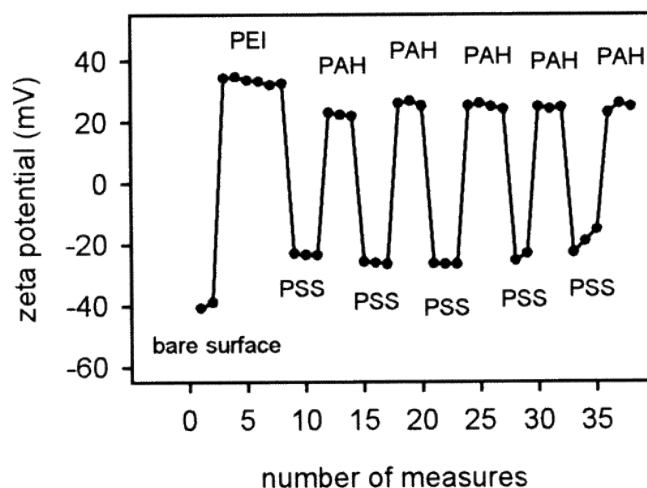
Fig. 2.10: ζ potential measurements showing charge reversal during the anionic poly(sodium 4-styrenesulfonate) PSS/ cationic polyallylamine hydrochloride (PAH) multilayer formation.[68]

For weak polyelectrolytes, the deposition pH plays an important role in the multilayer assembly. By controlling pH, it is possible to control their charge density and therefore the thickness and composition of the resulting films.[7]

Mostly, linear polyelectrolytes are used for the multilayer formation, but also inorganic nanoparticles,[74, 75] block copolymer micelles,[76-82] proteins[83, 84] *etc*. can be incorporated as well.

2.2.3 Coatings via Colloidal Particles

In contrast to the adsorption of linear homopolyelectrolytes, which leads to the formation of laterally homogeneous surfaces, the adsorption of colloidal particles can generally result in laterally structured surfaces.[85-91] As the particle size is typically in the range of 10-100 nm, two-dimensional patterning is possible on the nano-scale, which is difficult to obtain by other methods such as photolithography or micro-contact printing (μCP)[92-94] and selective deposition of polymeric material to pre-patterned surfaces.[95-97]

Adsorption of Micelles in Monolayers

In the special case of self-assembled micellar systems in selective solvents, the adsorption from solutions may occur from both the free chains and the micelles as predicted by theoretical studies.[98] Block copolymers can be adsorbed in a brush-like conformation with an

anchor block covering the substrate and a second block extending into the solution.[99] Other theoretical and experimental studies show that at concentrations above cmc, the adsorption of entire micelles dominates.[98, 100-102]

For polyelectrolyte copolymer micelles, the adsorption of coronal chains onto the oppositely charged surface inhibits the rearrangement of attached micelles. The adsorption of colloidal particles is typically irreversible.[86] Due to the electrostatic repulsion between micelles in solution and already adsorbed micelles and the surface exclusion effect, a semi-ordered monolayer of micelles is formed.[87, 88, 103-105] Under certain conditions, formation of hexagonally ordered micellar monolayer is possible if micelles are mobile after the attachment.[106]

Like in the case of linear polyelectrolytes, entropic effects such as the release of counter ions and hydration waters drives the adsorption of colloidal particles with charged corona.

Models of Colloidal Particle Adsorption

The most known Langmuir adsorption model describes the reversible adsorption of molecules. Since the adsorption of colloidal particles is typically irreversible, this model is inappropriate for their kinetic study. Instead, the theoretical model of random sequential adsorption (RSA) of monodisperse hard spheres can be applied.[107, 108] The RSA model describes a process, in which particles are sequentially and irreversibly adsorbed on a surface at random positions, thereby, the particles cannot overlap on the surface. The adsorption behavior of charged colloidal particles depends on the electrostatic interactions between particles and surface, which are strongly influenced by solution conditions such as ionic strength.[109, 110]

Simple RSA model is applicable only if adsorbed and adsorbing particles do not interact. In the case of particles with charged corona, long-range repulsions limit the extend of adsorption. For interacting spherical particles (soft spheres), the original model was extended to explain the interparticle interactions.[85] However, the addition of low molecular weight electrolyte can significantly reduce long-range forces between particles.[86] Thus, if the ionic strength is high, the adsorption behavior can be described by RSA of hard-spheres with an effective radius.

The RSA behaviour can be represented by two possible states (Fig. 2.11): the initial adsorption, when the surface coverage is low, and adsorption which is close to the saturation.
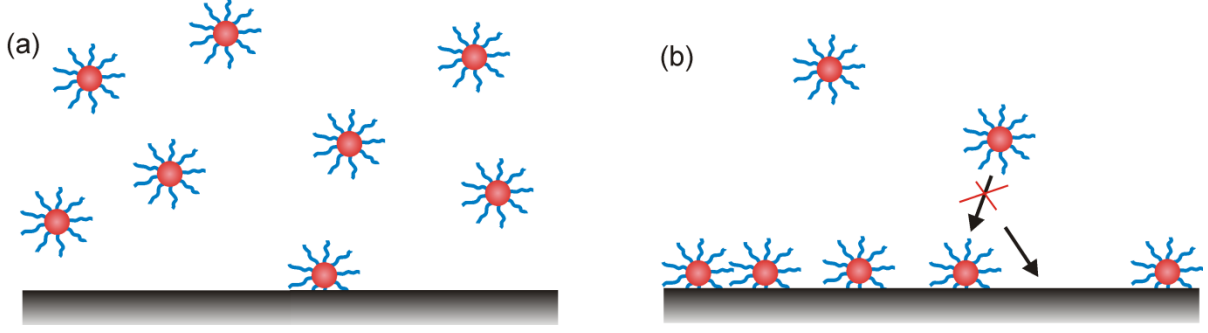
Fig. 2.11: Sketch of two RSA states of particles: diffusion-limited (a) and surface-exclusion-limited adsorption (b).

At the initial adsorption state (Fig. 2.11a), particles that are transported to the surface are not influenced by already adsorbed micelles. Therefore, the initial adsorption process should be limited by diffusion. Thus, the number of adsorbed micelles per unit area $n_s(t)$ is proportional to the square root of the adsorption time t according to the equation[111]

$$n_s(t) = 2n_b \sqrt{\frac{D_s t}{\pi}} \tag{2.9}$$

where n_b is the number of particles in the bulk solution, and D_s the diffusion coefficient of micelles to the silica surface.

At longer adsorption times, the surface coverage becomes saturated (Fig. 2.11). The surface exclusion effects[112] lead to asymptotical characteristics of particle adsorption. The surface coverage approaches a jamming limit $\theta(\infty)$ according to the relationship[107]

$$\theta(\infty) - \theta(t) \propto t^{-1/2} \tag{2.10}$$

The theoretical jamming limit for the adsorption of monodisperse hard spheres was found to be $\theta(\infty) = 0.547$.[113, 114]

By measuring particle adsorption for example with *ex situ* or *in situ* atomic force microscopy, information about the kinetics and the behaviour of adsorption can be observed using a method of counting particles adsorbed with cumulative time.[86]

2.2.4 Responsive Coatings

Compared to passive coatings, responsive or smart coatings can offer additional options. They can respond to external physical or chemical signal by switching of their physico-

chemical properties such as wettability,[115] permeability, optical properties, adhesion, and mechanical properties (Fig. 2.12).

Common external stimuli that induce reversible or irreversible changes are temperature, pH, ionic strength of the solution, or light. This special feature is of extreme importance for emerging and existent applications, *e.g.* for microfluidic devices, drug delivery, cell tissue engineering, for sensing, or actuation. Recent results in the field of responsive coating construction and applications can be found in reviews.[116-124]
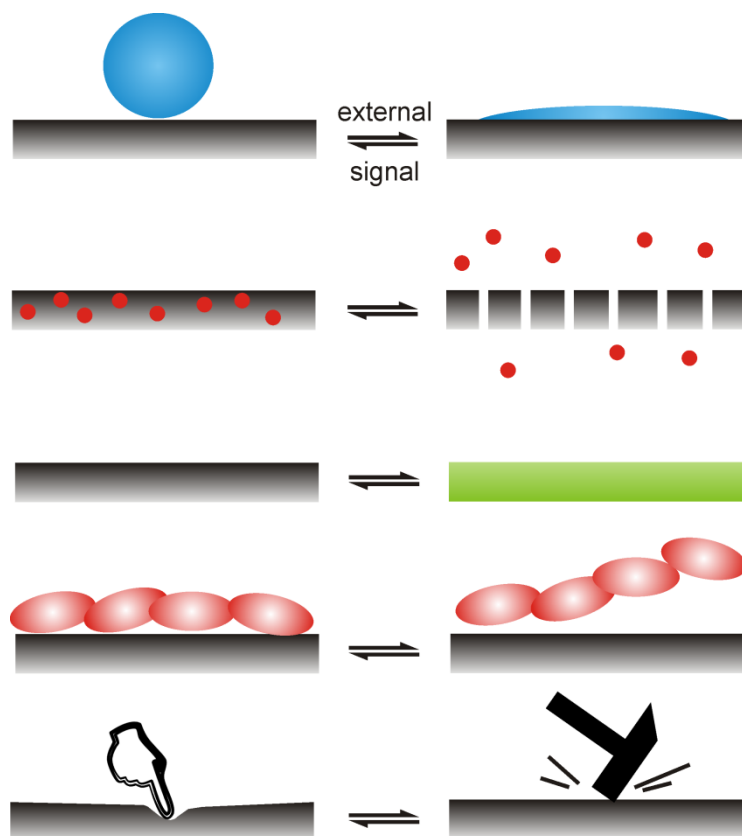

Fig. 2.12: Responsive coatings switching their wettability, permeability, optical properties, adhesion, and mechanical properties in response to an external signal.

An effective and simple way to construct responsive coatings is the adsorption of stimuli-responsive polymers or particles on a solid support (Fig. 2.13). Examples of systems, which may serve as responsive coatings, are single or mixed polymer brushes on planar [125-129] or curved [40] surfaces. Alternatively, thin films of polymer networks can be used as smart coatings. These, in most cases stimuli-responsive hydrogel-like films, can uptake large amounts of water. The swelling state, which can be controlled by external stimuli, defines thereby its permeability, adhesion and elastic modulus. Such a modulation of mechanical

properties of the coatings is important, for example, to control cell adhesion.[130]Another elegant approach of designing smart surfaces is the adsorption of stimuli-responsive block copolymer micelles [103, 104, 106, 131, 132] or by sequential adsorption of oppositely charged polyelectrolytes resulting in multilayer films.[117, 133] Other possibilities for smart coating construction are thin films of block copolymers and membranes.[123]
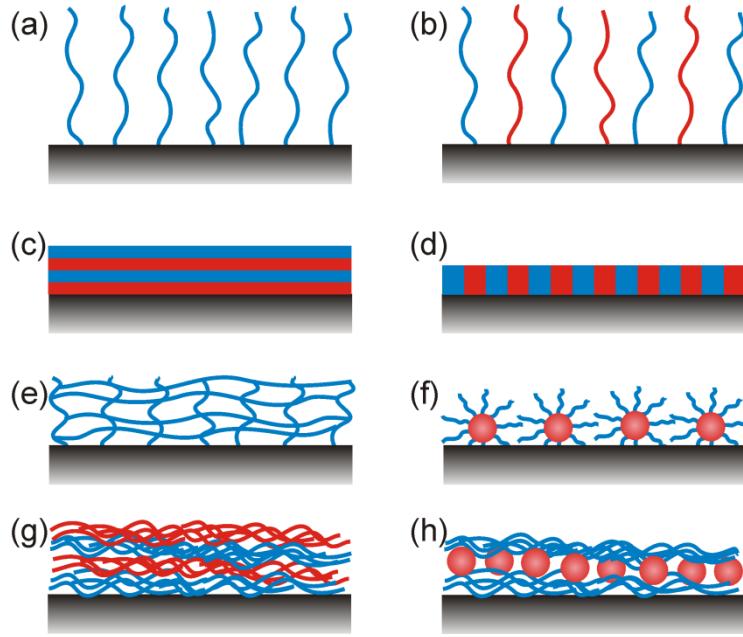

Fig. 2.13: Schematics of general designs of stimuli-responsive thin films: homopolymer (a) and mixed polymer brushes (b), block-copolymer films (c, d), crosslinked films (e), films from functional particles (f), layer-by-layer (LbL) films (g) and LbL films with incorporated functional nanoparticles (h). Reproduced from Ref. [123].

Polyelectrolyte Brushes

If polyelectrolyte chains are densely grafted (grafting density δ < random coil radius) to a planar surface, they represent a polyelectrolyte brushes.[125, 134] The chains can also be grafted to a spherical substrate or to the backbone of a polymer chain resulting in a spherical polyelectrolyte brush[40] or a cylindrical molecular brush,[135, 136] respectively.

In polymer brushes, the grafting density is sufficiently high, *i.e.* the brush height L is much larger than the distance δ between two end-grafted chains (Fig. 2.14). In the reverse case, the mushroom regime is obtained.
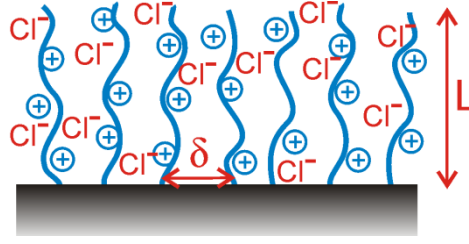
Fig. 2.14: Polyelectrolyte brush in the osmotic brush regime.

In the case of highly charged polyelectrolytes in salt-free aqueous solutions (osmotic brush regime, Fig. 2.14), the major fraction of the counterions is confined within the brush.[127, 137, 138] Due to the high osmotic pressure of trapped counterions, the polyelectrolyte chains adopt a stretched conformation. In the osmotic brush regime, the brush height L doesn't depend on the salt concentration c_s and on the grafting density.[137, 138] However, if the external ionic strength reaches the level of internal ionic strength inside the brush, the height of the brush decreases due to the additional screening of Coulomb repulsion according to $L \sim c_s^{-1/3}$ scaling law (salted brush regime).[31, 134]

Hence, by variation of the ionic strength of the solution, it is possible to control the osmotic pressure and therefore expansion of the brush layer.

Weak polyelectrolyte brushes demonstrate, in addition, responsive behavior to pH.[139] In these systems, the dissociation degree is a function of the grafting density and the ionic strength.[11, 140]

Monolayer of Block Copolymer Micelles

The adsorption of stimuli-responsive block copolymer micelles onto solid substrates provides an opportunity to design stimuli-responsive surfaces with nano-patterned structure.

Stimuli-responsive block copolymer micelles adsorbed at the solid-liquid interface can reversibly or irreversibly change their morphology and composition. This responsive behavior can be controlled by the ionization degree of the weak polyelectrolyte blocks such as poly(acrylic acid) (PAA), or by ionic strength if one of the blocks is a strong polyelectrolyte. Further, increasing the ionic strength of the solution would lead to the dissociation of IPECs into its components.[26, 28] Therefore, monolayers of IPEC-containing block copolymer micelles can switch their structure and charge density.[48] Further, temperature-responsive block copolymer micelles can be used to develop temperature-sensitive coatings. For example, poly(*N*-isopropylacrylamide) (PNIPAM) or its derivates exhibits a lower critical solution

temperature (LCST) *i.e.* temperature above which the block becomes insoluble in water. At temperatures below the LCST, the block is soluble in aqueous solutions due to hydrogen bonding with water molecules.

Webber *et al.* have studied the stimuli-responsive behavior of adsorbed micelles with pH-sensitive cores. By changing pH, the original micelle-like morphology of the adsorbed block copolymer micelles disappeared to produce brush-like structure.[104] This reversible change resulted due to the protonation of the weak polyelectrolyte chains in the core. In contrast, the analogous pH change of micellar solutions resulted in dissociation into unimers.[141] Therefore, the immobilization of micelles can prevent their dissociation or aggregation due to the large number of polymer-surface interactions.[104]

However, the long-term treatment of micelles under certain conditions frequently causes irreversible changes in the morphology of adsorbed micelles.[103, 106, 142, 143] The instability of adsorbed micelles is especially pronounced for dynamic structures, which can exchange unimers due to the low glass transition temperature of core-forming block.

The dynamic structures can be "frozen" by chemical cross-linking of the hydrophobic cores.[144] Another facile way of stabilization against environmental influences for otherwise instable surface-attached micelles is using a top layer of polyelectrolyte as a cover.[143]

Layer-by-Layer Stimuli Responsive Films

The approach of producing smart LbL films demands the use of responsive components for their construction.[117] One way is to introduce thermoresponsive polymers such as PNIPAM into the multilayer assemblies. Although PNIPAM homopolymer can be incorporated into the multilayers by hydrogen bonding *e.g.* with PAA, these systems are unstable at certain pH values.[145] Therefore, ionically modified PNIPAM copolymers were introduced for multilayer construction.[146, 147]

LbL assemblies containing at least one weak polyelectrolyte can be responsive to pH variations induced by a change in the charge density. Charge density of complexed polyelectrolytes affects their interactions, that result in the swelling or shrinking of the films.[133] Although these films are highly swellable, they are often unstable with respect to pH variations.[148] The stability can be significantly increased *via* chemical cross-linking of assembled layers.[149] However, LbL-derived stimuli-responsive systems which structures are stabilized by covalent cross-links often show lower swelling degrees.[150]

Additionally, LbL films can be assembled from diblock copolymer micelles with integrated stimuli-responsive properties.[76-82] Such assemblies offer the advantage of fabricating porous thin films[77] with facility to control the pore closing/opening by an external signal.

2.3 Objective of the Thesis

The objective of the theses can be divided into two main parts.

The first part of the thesis deals with the fundamental understanding of the impact of the chemical structure of the LbL components on polyelectrolyte multilayer assemblies. The interest in multilayer systems arises from the possibility of precisely control the film composition and therefore properties of the coatings. As mentioned in the theoretical part, charge density of polyelectrolytes plays a major role. A potential limitation of systems based on weak polyelectrolytes is their effective pK_a value, which is strongly dependent on the local environment. This difficulty can be avoided by using strong polyelectrolytes with fixed charge density. Here, the charge density can be adjusted by "intramolecular dilution" of polyelectrolyte molecule with uncharged monomers.[18-22, 151, 152] However, the use of hydrophilic non-ionic monomers may result in the formation of water-soluble IPECs. Therefore, such polyelectrolytes could not be used to form stable films below a critical charge density.[19, 20] However, fundamental study of polyelectrolyte multilayer assemblies in the range of low charge density is of particular interest due to the counterion condentation in the "strong screening zone".

In collaboration with the Institute of Chemistry at the University of Potsdam (André Laschewsky and Patrick Ott), we found a system, which allows variations of charge densities of polyanions in the range between 100 - 21% by using a moderately hydrophilic non-ionic comonomer for the charge dilution. Further, stabilization of the LbL films can be observed by covalent-crosslinking of the assembled layers. This opens the possibility to tune both ionic and covalent crosslinking.

The aim of the second part is engineering of active coatings by the adsorption of stimuli-responsive micellar systems. According to this concept, the use of weak polyelectrolytes has been established, as their charge density has been regulated by the solution pH. The sensitivity of these coatings to a variety of chemical and physical conditions, such as pH or ionic strength of the solution, provides the ability to tune mechanical properties, adhesion,

permeability, or stability of the films. The production of stimuli-responsive coatings demands full control over the effective particle − substrate interactions. Therefore, it is important to have particles with well defined surface morphology combined with pronounced stimuli-responsive properties. Both requirements are met by self-assembled block copolymers. Self-assembly of amphiphilic block copolymers to micelles enables an easy creation of the structures, which are usually complex. The surface adsorption of such micelles leads to stimulus-responsive coatings with well defined thickness and morphology. Further, pH-regions that are inaccessible in solution due to colloidal stability issues can be investigated.

The goal is to create coatings with tunable charge density by adsorption of pH-sensitive micelles designed by the department of Macromolecular Chemistry II at the University of Bayreuth (Axel H. E. Müller and Eva Betthausen). In particular, systems which can be further extended to hierarchical structures, for instance, by the LbL technique are of the interest.

It is known that cell adhesion is closely related to the properties of the underlying substrate.[153] Therefore, the use of smart coatings allows controlled detachment of adsorbed cells by an external stimulus.[130] In collaboration with Daria Andreeva from the department of Physical Chemistry II at the University of Bayreuth and Katja Skorb from the Max Planck Institute of Colloids and Interfaces in Golm, we aim to adapt the new system for controlling bacteria adhesion.

References

1. H. Dautzenberg, W. Jaeger, J. Kötz, B. Philipp, C. Seidel and D. Stscherbina, *Polyelectrolytes*, Carl Hanser Verlag, München, 1994.

2. J. T. G. Overbeek, *Bulletin Des Societes Chimiques Belges*, 1948, 57, 252-261.

3. M. Mandel and J. C. Leyte, *Journal of Electroanalytical Chemistry*, 1972, 37, 297-&.

4. J. D. Mendelsohn, C. J. Barrett, V. V. Chan, A. J. Pal, A. M. Mayes and M. F. Rubner, *Langmuir*, 2000, 16, 5017-5023.

5. T. Mauser, C. Dejugnat and G. B. Sukhorukov, *Macromolecular Rapid Communications*, 2004, 25, 1781-1785.

6. H. H. Rmaile and J. B. Schlenoff, *Langmuir*, 2002, 18, 8263-8265.

7. S. S. Shiratori and M. F. Rubner, *Macromolecules*, 2000, 33, 4213-4219.

8. Z. J. Sui and J. B. Schlenoff, *Langmuir*, 2004, 20, 6026-6031.

9.   E. B. Zhulina, T. M. Birshtein and O. V. Borisov, *Macromolecules*, 1995, 28, 1491-1499.

10.   A. J. Parnell, S. J. Martin, C. C. Dang, M. Geoghegan, R. A. L. Jones, C. J. Crook, J. R. Howse and A. J. Ryan, *Polymer*, 2009, 50, 1005-1014.

11.   E. P. K. Currie, A. B. Sieval, G. J. Fleer and M. A. Cohen Stuart, *Langmuir*, 2000, 16, 8324-8333.

12.   F. A. Plamper, H. Becker, M. Lanzendörfer, M. Patel, A. Wittemann, M. Ballauff and A. H. E. Müller, *Macromolecular Chemistry and Physics*, 2005, 206, 1813-1825.

13.   D. Cochin, M. Passmann, G. Wilbert, R. Zentel, E. Wischerhoff and A. Laschewsky, *Macromolecules*, 1997, 30, 4775-4779.

14.   M. Passmann, G. Wilbert, D. Cochin and R. Zentel, *Macromolecular Chemistry and Physics*, 1998, 199, 179-189.

15.   X. Arys, A. Jonas, B. Laguitton, R. Legras, A. Laschewsky and E. Wischerhoff, *Progress in Organic Coatings*, 1998, 34, 108-118.

16.   X. Arys, P. Fischer, A. M. Jonas, M. M. Koetse, A. Laschewsky, R. Legras and E. Wischerhoff, *Journal of the American Chemical Society*, 2003, 125, 1859-1865.

17.   A. Laschewsky, F. Mallwitz, J. F. Baussard, D. Cochin, P. Fischer, J. L. H. Jiwan and E. Wischerhoff, *Macromolecular Symposia*, 2004, 211, 135-155.

18.   N. G. Hoogeveen, M. A. Cohen Stuart and G. J. Fleer, *Journal of Colloid and Interface Science*, 1996, 182, 133-145.

19.   R. Steitz, W. Jaeger and R. von Klitzing, *Langmuir*, 2001, 17, 4471-4474.

20.   K. Glinel, A. Moussa, A. M. Jonas and A. Laschewsky, *Langmuir*, 2002, 18, 1408-1412.

21.   E. Kharlampieva and S. A. Sukhishvili, *Macromolecules*, 2003, 36, 9950-9956.

22.   D. Qu, J. S. Pedersen, S. Garnier, A. Laschewsky, H. Möhwald and R. von Klitzing, *Macromolecules*, 2006, 39, 7364-7371.

23.   R. R. Netz and D. Andelman, *Physics Reports-Review Section of Physics Letters*, 2003, 380, 1-95.

24.   A. V. Dobrynin and M. Rubinstein, *Progress in Polymer Science*, 2005, 30, 1049-1118.

25.   G. S. Manning, *Journal of Chemical Physics*, 1969, 51, 924.

26.   V. A. Kabanov, *Russ. Chem. Rev.*, 2005, 74, 3-20.

27.   V. A. Kabanov and A. B. Zezin, *Pure and Applied Chemistry*, 1984, 56, 343-354.

28. D. V. Pergushov, Oleg V. Borisov, A. B. Zezin and A. H. E. Müller, *Advances in Polymer Science*, 2011, 241, 131-161.

29. L. Leibler, *Macromolecules*, 1980, 13, 1602-1617.

30. I. W. Hamley, *The Physics of Block Copolymers*, Oxford University Press, Oxford, 1998.

31. S. Förster, V. Abetz and A. H. E. Müller, *Advances in Polymer Science: Polyelectrolytes with Defined Molecular Architecture II*, 2004, 166, 173-210.

32. J. F. Gohy, *Block Copolymers II*, 2005, 190, 65-136.

33. O. V. Borisov, E. B. Zhulina, F. A. M. Leermakers and A. H. E. Müller, *Self Organized Nanostructures of Amphiphilic Block Copolymers I*, 2011, 241, 57-129.

34. J. N. Israelachvili, *Intermolecular and surface forces*, Acad. Press, London, 1992.

35. J. Rodriguez-Hernandez, F. Checot, Y. Gnanou and S. Lecommandoux, *Progress in Polymer Science*, 2005, 30, 691-724.

36. C. A. Fustin, V. Abetz and J. F. Gohy, *European Physical Journal E*, 2005, 16, 291-302.

37. J. F. Gohy, N. Willet, S. Varshney, J. X. Zhang and R. Jerome, *Angewandte Chemie-International Edition*, 2001, 40, 3214.

38. R. Erhardt, M. F. Zhang, A. Böker, H. Zettl, C. Abetz, P. Frederik, G. Krausch, V. Abetz and A. H. E. Müller, *Journal of the American Chemical Society*, 2003, 125, 3260-3267.

39. S. Förster, N. Hermsdorf, C. Böttcher and P. Lindner, *Macromolecules*, 2002, 35, 4096-4105.

40. M. Ballauff, *Progress in Polymer Science*, 2007, 32, 1135-1151.

41. J. Selb and Y. Gallot, *Makromolekulare Chemie-Macromolecular Chemistry and Physics*, 1980, 181, 2605-2624.

42. T. Nicolai, O. Colombani and C. Chassenieux, *Soft Matter*, 2010, 6, 3111-3118.

43. R. K. O'Reilly, C. J. Hawker and K. L. Wooley, *Chemical Society Reviews*, 2006, 35, 1068-1083.

44. D. V. Pergushov, Oleg V. Borisov, A. B. Zezin and A. H. E. Müller, *Advances in Polymer Science*, 2011, DOI: 10.1007/1012_2010_1102.

45. C. L. McCormick, J. D. Flores, X. W. Xu and N. J. Treat, *Macromolecules*, 2009, 42, 4941-4945.

46. F. Schacher, A. Walther and A. H. E. Müller, *Langmuir*, 2009, 25, 10962-10969.

47.   F. Schacher, E. Betthausen, A. Walther, H. Schmalz, D. V. Pergushov and A. H. E. Müller, *ACS Nano*, 2009, 3, 2095-2102.

48.   E. Betthausen, M. Drechsler, M. Förtsch, F. H. Schacher and A. H. E. Müller, *Soft Matter*, 2011, 7, 8880-8891.

49.   G. J. Fleer, M. A. Cohen Stuart, J. M. H. M. Scheutjens, T. Cosgrove and B. Vincent, *Polymers at Interfaces*, Chapman & Hall, London, 1993.

50.   P. Linse, *Macromolecules*, 1996, 29, 326-336.

51.   H. G. M. Van de Steeg, M. A. Cohen Stuart, A. De Keizer and B. H. Bijsterbosch, *Langmuir*, 1992, 8, 2538-2546.

52.   J. F. Joanny, *European Physical Journal B*, 1999, 9, 117-122.

53.   C. B. Bucur, Z. Sui and J. B. Schlenoff, *Journal of the American Chemical Society*, 2006, 128, 13690-13691.

54.   J. B. Schlenoff, A. H. Rmaile and C. B. Bucur, *Journal of the American Chemical Society*, 2008, 130, 13589-13597.

55.   R. K. Iler, *Journal of Colloid and Interface Science*, 1966, 21, 569-594.

56.   G. Decher and J. Schmitt, *Progress in Colloid & Polymer Science*, 1992, 89, 160-164.

57.   G. Decher, J. D. Hong and J. Schmitt, *Thin Solid Films*, 1992, 210, 831-835.

58.   G. Decher, *Science*, 1997, 277, 1232-1237.

59.   P. Bertrand, A. Jonas, A. Laschewsky and R. Legras, *Macromolecular Rapid Communications*, 2000, 21, 319-348.

60.   G. Decher and J. B. Schlenoff, *Multilayer Thin Films: Sequential Assembly of Nanocomposite Materials*, Wiley-VCH Verlag GmbH & Co. KGaA, Weinheim, Germany, 2003.

61.   G. Decher, J. D. Hong and J. Schmitt, *Thin Solid Films*, 1992, 210, 831-835.

62.   J. B. Schlenoff, S. T. Dubas and T. Farhat, *Langmuir*, 2000, 16, 9968-9969.

63.   A. Izquierdo, S. S. Ono, J. C. Voegel, P. Schaaff and G. Decher, *Langmuir*, 2005, 21, 7558-7567.

64.   P. A. Chiarelli, M. S. Johal, J. L. Casson, J. B. Roberts, J. M. Robinson and H. L. Wang, *Advanced Materials*, 2001, 13, 1167-+.

65.   S. S. Lee, J. D. Hong, C. H. Kim, K. Kim, J. P. Koo and K. B. Lee, *Macromolecules*, 2001, 34, 5358-5360.

66.   N. G. Hoogeveen, M. A. Cohen Stuart, G. J. Fleer and M. R. Böhmer, *Langmuir*, 1996, 12, 3675-3681.

67.   F. Caruso, E. Donath and H. Möhwald, *Journal of Physical Chemistry B*, 1998, 102, 2011-2016.

68.   G. Ladam, P. Schaad, J. C. Voegel, P. Schaaf, G. Decher and F. Cuisinier, *Langmuir*, 2000, 16, 1249-1255.

69.   Y. Lvov, G. Decher and H. Möhwald, *Langmuir*, 1993, 9, 481-486.

70.   S. T. Dubas and J. B. Schlenoff, *Macromolecules*, 1999, 32, 8153-8160.

71.   M. R. Linford, M. Auch and H. Möhwald, *Journal of the American Chemical Society*, 1998, 120, 178-182.

72.   J. B. Schlenoff and M. Li, *Berichte Der Bunsen-Gesellschaft-Physical Chemistry Chemical Physics*, 1996, 100, 943-947.

73.   Y. Lvov, K. Ariga, M. Onda, I. Ichinose and T. Kunitake, *Langmuir*, 1997, 13, 6195-6203.

74.   P. Podsiadlo, S. Paternel, J. M. Rouillard, Z. F. Zhang, J. Lee, J. W. Lee, L. Gulari and N. A. Kotov, *Langmuir*, 2005, 21, 11915-11921.

75.   C. H. Lu, I. Dönch, M. Nolte and A. Fery, *Chemistry of Materials*, 2006, 18, 6204-6210.

76.   K. Emoto, M. Iijima, Y. Nagasaki and K. Kataoka, *Journal of the American Chemical Society*, 2000, 122, 2653-2654.

77.   J. H. Cho, J. K. Hong, K. Char and F. Caruso, *Journal of the American Chemical Society*, 2006, 128, 9935-9942.

78.   N. Ma, Y. P. Wang, Z. Q. Wang and X. Zhang, *Langmuir*, 2006, 22, 3906-3909.

79.   S. Biggs, K. Sakai, T. Addison, A. Schmid, S. P. Armes, M. Vamvakaki, V. Bütün and G. Webber, *Advanced Materials*, 2007, 19, 247-250.

80.   B. S. Kim, S. W. Park and P. T. Hammond, *ACS Nano*, 2008, 2, 386-392.

81.   T. Addison, O. J. Cayre, S. Biggs, S. P. Armes and D. York, *Langmuir*, 2008, 24, 13328-13333.

82.   T. Addison, O. J. Cayre, S. Biggs, S. P. Armes and D. York, *Langmuir*, 2010, 26, 6281-6286.

83.   S. Disawal, H. H. Qiu, B. B. Elmore and Y. M. Lvov, *Colloids and Surfaces B-Biointerfaces*, 2003, 32, 145-156.

84.   T. G. Shutava, D. S. Kommireddy and Y. M. Lvov, *Journal of the American Chemical Society*, 2006, 128, 9926-9934.

85.   Z. Adamczyk, M. Zembala, B. Siwek and P. Warszynski, *Journal of Colloid and Interface Science*, 1990, 140, 123-137.

86.   C. A. Johnson and A. M. Lenhoff, *Journal of Colloid and Interface Science*, 1996, 179, 587-599.

87.   M. R. Talingting, Y. H. Ma, C. Simmons and S. E. Webber, *Langmuir*, 2000, 16, 862-865.

88.   G. B. Webber, E. J. Wanless, S. P. Armes, F. L. Baines and S. Biggs, *Langmuir*, 2001, 17, 5551-5561.

89.   R. Pericet-Camara, G. Papastavrou and M. Borkovec, *Langmuir*, 2004, 20, 3264-3270.

90.   R. Pericet-Camara, B. P. Cahill, G. Papastavrou and M. Borkovec, *Chemical Communications*, 2007, 266-268.

91.   K. Sakai, E. G. Smith, G. B. Webber, M. Baker, E. J. Wanless, V. Butun, S. P. Armes and S. Biggs, *Langmuir*, 2006, 22, 8435-8442.

92.   A. Kumar and G. M. Whitesides, *Science*, 1994, 263, 60-62.

93.   Y. N. Xia and G. M. Whitesides, *Annual Review of Materials Science*, 1998, 28, 153-184.

94.   Y. N. Xia and G. M. Whitesides, *Angewandte Chemie-International Edition*, 1998, 37, 551-575.

95.   X. P. Jiang and P. T. Hammond, *Langmuir*, 2000, 16, 8501-8509.

96.   X. P. Jiang, H. P. Zheng, S. Gourdin and P. T. Hammond, *Langmuir*, 2002, 18, 2607-2615.

97.   M. Pretzl, A. Schweikart, C. Hanske, A. Chiche, U. Zettl, A. Horn, A. Böker and A. Fery, *Langmuir*, 2008, 24, 12748-12753.

98.   Y. J. Zhan and W. L. Mattice, *Macromolecules*, 1994, 27, 683-688.

99.   H. D. Bijsterbosch, M. A. Cohen Stuart and G. J. Fleer, *Macromolecules*, 1998, 31, 9281-9294.

100.   J. C. Meiners, A. Quintel-Ritzi, J. Mlynek, H. Elbs and G. Krausch, *Macromolecules*, 1997, 30, 4945-4951.

101.   B. Mahltig, J. F. Gohy, R. Jerome, C. Bellmann and M. Stamm, *Colloid and Polymer Science*, 2000, 278, 502-508.

102. B. Mahltig, J. F. Gohy, S. Antoun, R. Jerome and M. Stamm, *Colloid and Polymer Science*, 2002, 280, 495-502.

103. G. B. Webber, E. J. Wanless, V. Bütün, S. P. Armes and S. Biggs, *Nano Letters*, 2002, 2, 1307-1313.

104. G. B. Webber, E. J. Wanless, S. P. Armes, Y. Q. Tang, Y. T. Li and S. Biggs, *Advanced Materials*, 2004, 16, 1794-1798.

105. I. W. Hamley, S. D. Connell and S. Collins, *Macromolecules*, 2004, 37, 5337-5351.

106. G. B. Webber, E. J. Wanless, S. P. Armes and S. Biggs, *Faraday Discussions*, 2005, 128, 193-209.

107. Y. Pomeau, *Journal of Physics A-Mathematical and General*, 1980, 13, L193-L196.

108. P. Schaaf, J. C. Voegel and B. Senger, *Journal of Physical Chemistry B*, 2000, 104, 2204-2214.

109. H. Walter, C. Harrats, P. Müller-Buschbaum, R. Jerome and M. Stamm, *Langmuir*, 1999, 15, 1260-1267.

110. C. Hanske, C. Schneider, M. Drechsler, A. Wittemann and A. Fery, *Physical Chemistry Chemical Physics*, 2012, DOI 10.1039/C2CP23408D.

111. H. Motschmann, M. Stamm and C. Toprakcioglu, *Macromolecules*, 1991, 24, 3681-3688.

112. P. Schaaf and J. Talbot, *Journal of Chemical Physics*, 1989, 91, 4401-4409.

113. J. Feder, *Journal of Theoretical Biology*, 1980, 87, 237-254.

114. E. L. Hinrichsen, J. Feder and T. Jossang, *Journal of Statistical Physics*, 1986, 44, 793-827.

115. B. W. Xin and J. C. Hao, *Chemical Society Reviews*, 2010, 39, 769-782.

116. Y. Liu, L. Mu, B. H. Liu and J. L. Kong, *Chemistry-A European Journal*, 2005, 11, 2622-2631.

117. K. Glinel, C. Dejugnat, M. Prevot, B. Schöler, M. Schönhoff and R. V. Klitzing, *Colloids and Surfaces A-Physicochemical and Engineering Aspects*, 2007, 303, 3-13.

118. J. F. Mano, *Advanced Engineering Materials*, 2008, 10, 515-527.

119. V. Kozlovskaya, E. Kharlampieva, I. Erel and S. A. Sukhishvili, *Soft Matter*, 2009, 5, 4077-4087.

120. P. M. Mendes, *Chemical Society Reviews*, 2008, 37, 2512-2529.

121. I. Tokarev and S. Minko, *Soft Matter*, 2009, 5, 511-524.

122. I. Tokarev and S. Minko, *Advanced Materials*, 2010, 22, 3446-3462.

123. I. Tokarev, M. Motornov and S. Minko, *Journal of Materials Chemistry*, 2009, 19, 6932-6948.

124. M. A. Cohen Stuart, W. T. S. Huck, J. Genzer, M. Müller, C. Ober, M. Stamm, G. B. Sukhorukov, I. Szleifer, V. V. Tsukruk, M. Urban, F. Winnik, S. Zauscher, I. Luzinov and S. Minko, *Nature Materials*, 2010, 9, 101-113.

125. S. T. Milner, *Science*, 1991, 251, 905-914.

126. E. B. Zhulina, O. V. Borisov and T. M. Birshtein, *Journal De Physique II*, 1992, 2, 63-74.

127. S. Minko, *Polymer Reviews*, 2006, 46, 397-420.

128. A. Synytska, M. Stamm, S. Diez and L. Ionov, *Langmuir*, 2007, 23, 5205-5209.

129. P. Uhlmann, H. Merlitz, J. U. Sommer and M. Stamm, *Macromolecular Rapid Communications*, 2009, 30, 732-740.

130. S. Schmidt, M. Zeiser, T. Hellweg, C. Duschl, A. Fery and H. Möhwald, *Advanced Functional Materials*, 2010, 20, 3235-3243.

131. K. Sakai, E. G. Smith, G. B. Webber, M. Baker, E. J. Wanless, V. Bütün, S. P. Armes and S. Biggs, *Langmuir*, 2006, 22, 8435-8442.

132. K. Sakai, E. G. Smith, G. B. Webber, M. Baker, E. J. Wanless, V. Bütün, S. P. Armes and S. Biggs, *Journal of Colloid and Interface Science*, 2007, 314, 381-388.

133. J. Hiller and M. F. Rubner, *Macromolecules*, 2003, 36, 4078-4083.

134. J. Rühe, M. Ballauff, M. Biesalski, P. Dziezok, F. Grohn, D. Johannsmann, N. Houbenov, N. Hugenberg, R. Konradi, S. Minko, M. Motornov, R. R. Netz, M. Schmidt, C. Seidel, M. Stamm, T. Stephan, D. Usov and H. N. Zhang, *Polyelectrolytes with Defined Molecular Architecture I*, 2004, 165, 79-150.

135. M. F. Zhang and A. H. E. Müller, *Journal of Polymer Science Part A-Polymer Chemistry*, 2005, 43, 3461-3481.

136. S. S. Sheiko, B. S. Sumerlin and K. Matyjaszewski, *Progress in Polymer Science*, 2008, 33, 759-785.

137. P. Pincus, *Macromolecules*, 1991, 24, 2912-2919.

138. O. V. Borisov, T. M. Birshtein and E. B. Zhulina, *Journal De Physique II*, 1991, 1, 521-526.

139. R. Israels, F. A. M. Leermakers and G. J. Fleer, *Macromolecules*, 1994, 27, 3087-3093.

140. E. B. Zhulina, J. K. Wolterink and O. V. Borisov, *Macromolecules*, 2000, 33, 4945-4953.

141. G. B. Webber, E. J. Wanless, V. Butun, S. P. Armes and S. Biggs, *Nano Letters*, 2002, 2, 1307-1313.

142. B. Mahltig, P. Müller-Buschbaum, M. Wolkenhauer, O. Wunnicke, S. Wiegand, J.-F. Gohy, R. Jérôme and M. Stamm, *Journal of Colloid and Interface Science*, 2001, 242, 36-43.

143. Z. C. Zhu and S. A. Sukhishvili, *ACS Nano*, 2009, 3, 3595-3605.

144. S. Pioge, A. Nesterenko, G. Brotons, S. Pascual, L. Fontaine, C. Gaillard and E. Nicol, *Macromolecules*, 2011, 44, 594-603.

145. J. F. Quinn and F. Caruso, *Langmuir*, 2004, 20, 20-22.

146. R. Steitz, V. Leiner, K. Tauer, V. Khrenov and R. Von Klitzing, *Applied Physics A-Materials Science & Processing*, 2002, 74, S519-S521.

147. J. A. Jaber and J. B. Schlenoff, *Macromolecules*, 2005, 38, 1300-1306.

148. S. T. Dubas and J. B. Schlenoff, *Macromolecules*, 2001, 34, 3736-3740.

149. L. Richert, F. Boulmedais, P. Lavalle, J. Mutterer, E. Ferreux, G. Decher, P. Schaaf, J. C. Voegel and C. Picart, *Biomacromolecules*, 2004, 5, 284-294.

150. E. Kharlampieva, I. Erel-Unal and S. A. Sukhishvili, *Langmuir*, 2007, 23, 175-181.

151. N. Delorme, M. Dubois, S. Garnier, A. Laschewsky, R. Weinkamer, T. Zemb and A. Fery, *Journal of Physical Chemistry B*, 2006, 110, 1752-1758.

152. R. Köhler, I. Dönch, P. Ott, A. Laschewsky, A. Fery and R. Krastev, *Langmuir*, 2009, 25, 11576-11585.

153. B. D. Ratner and S. J. Bryant, *Annual Review of Biomedical Engineering*, 2004, 6, 41-75.

3   Overview of the Thesis

The theses consist of four individual publications presented in Chapters 4 - 7. The results presented are focused on surface modification by polyelectrolytes with variable charge densities.

The first part (Chapter 4) of the theses deals with the construction of passive coating by the layer-by-layer assembly of strong polyelectrolytes with tunable charge density and post-modification of resulting films by cross-linking reaction.

In the second part, active surface construction by polyelectrolyte triblock terpolymer micelles with pH-sensitive weak polyelectrolyte block is demonstrated (Chapters 5 -7). Chapter 5 describes the adsorption behavior and response of adsorbed micelles to pH-variation. Chapter 6 demonstrates the way how such coatings may be used as active surface to control cell-surface interactions. Chapter 7 expands the use of pH-sensitive micelles for the layer-by-layer assembly creating novel double-end-tethered brush-like structures, which are pH-sensitive due to pH-tunable charge density.

In the following, a summary of main results is presented.

3.1   Strong Polyelectrolyte System with Different Charge Densities

To understand the impact of the linear charge density on structural properties of the LbL films, we studied the assembly of a novel system (Fig. 3.1) developed in the Institute of Chemistry at the University of Potsdam by André Laschewsky and Patrick Ott.
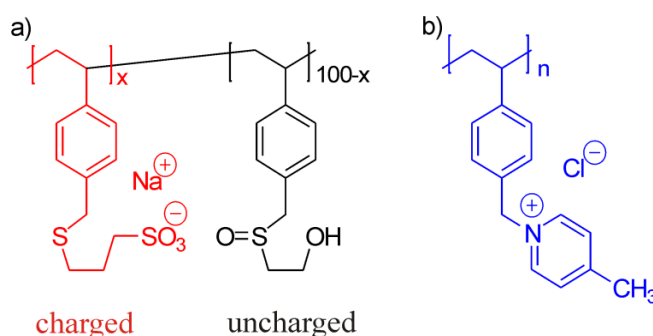

Fig. 3.1: Chemical structure of the polyelectrolytes used.

As anionic component we use strong polyanions with different fractions of charged monomers f between 100 and 21 % (Fig. 3.1a). The charge density f is adjusted by balancing the ratio of charged and uncharged monomers in the copolymerization process and is listed in the Table 1. The distance between two charged monomers d_m and the linear charge density can be calculated using the C-C distance (154 pm) and C-C angle (109.5°) of the backbone.

Table 3.1: The charge densities with corresponding calculated linear charge densities for different polyanions.

notation	f, [%]	d_m, [Å]	linear charge density, [e/Å]
PA-100	100	2.5	0.40
PA-81	81	3.1	0.32
PA-65	65	3.8	0.26
PA-36	36	6.9	0.14
PA-21	21	11.9	0.08

The main result of the multilayer buildup study indicates that for all studied ionic strengths of the solution, the charge density of polyanion only slightly affect the buildup behavior if the charge density is high ($f > 36$ %) as shown in Fig. 3.2. This can be attributed to the Manning counterion condensation,[1] whereby some of the charges on the polymer backbone are effectively neutralized by the counterions if the length between two charged groups is smaller than the Bjerrum length (Fig 2.1). In fact, in the „strong screening zone" ($f > 36\%$), Manning condensation reduces the linear charge density resulting in a constant effective distance between charges.

However, low charged polyanions (36 % and 21 %) lead to much thicker films (Fig. 3.2). The distance between two charged monomersof PA-36 is ~6.9 Å, while the Bjerrum length in water is around 7 Å. Thus, at 36% the linear charge density approaches one charge per Bjerrum length. Therefore, the counterion condensation is suppressed and the effective charge density is equal to the linear charge density.
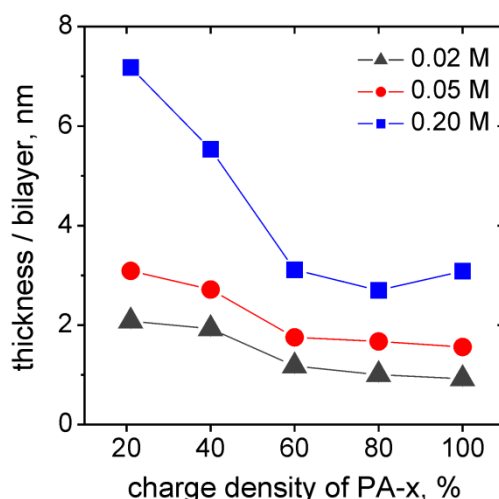
Fig. 3.2: Thickness per bilayer of PA/PC *vs.* charge density of the polyanion PA for films assembled from solutions containing 0.02 (▲), 0.05 (●), and 0.20 M NaCl (■).

Fig. 3.3a exemplarily shows the average bilayers thickness of studied multilayers as a function of the linear charge density. In the strong screening zone (charge density > 36%), the resulting film structure (thickness, roughness) is independent on the fraction of charged monomers (Fig. 3.3c). In contrast, if the linear charge density is lower than one chargeper Bjerrum length, the thickness and roughness of films increase significantly with decreasing linear charge density (Fig. 3.3b).
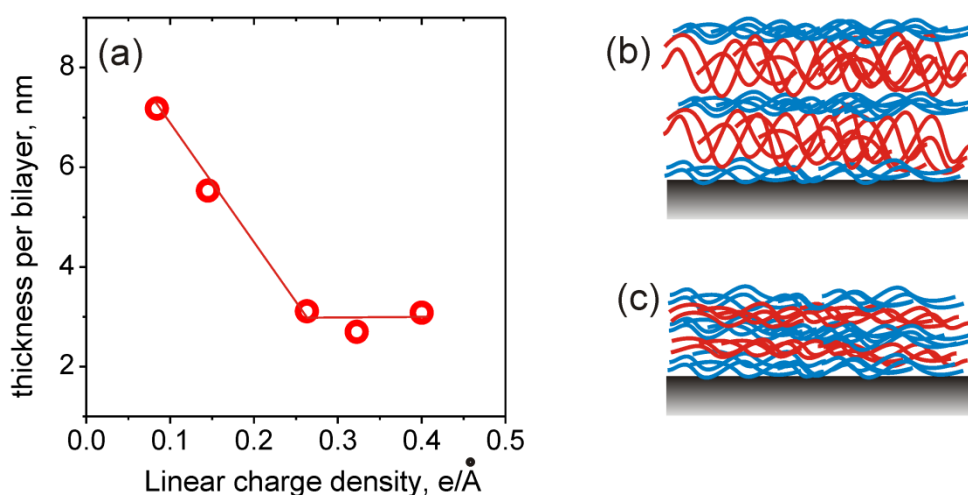

Fig. 3.3: Average bilayers-thickness *vs.* linear charge density of polyanion for LbL films assembled from 0.20 M NaCl solutions (a) and proposed schematic representation of multilayer structure at low linear charge density (36 and 21%) (b), and at high linear charge density (strong screening zone, 100, 81, and 65%) (c).

3.2   Stable Multilayers via Post-Chemical Cross-Linking

Due to the reactive methyl group of the cationic pyridinium moieties (Fig. 3.1b), we have studied cross-linking of the films by a piperidine catalysed condensation, which offers the possibility of inter- and intramolecular crosslinking of cationic units without affecting the number of ionic cross-links. The scheme of the applied aldol reaction is shown in Fig. 3.4a. The new crosslinked groups are strong chromophores and show a characteristic absorption peak at 365 nm. Thus, the formation of a colored product enables identifying the correct cross-linking product by UV-vis spectroscopy (Fig. 3.4b). Furthermore, it is possible to see when the reaction product reaches its maximum.
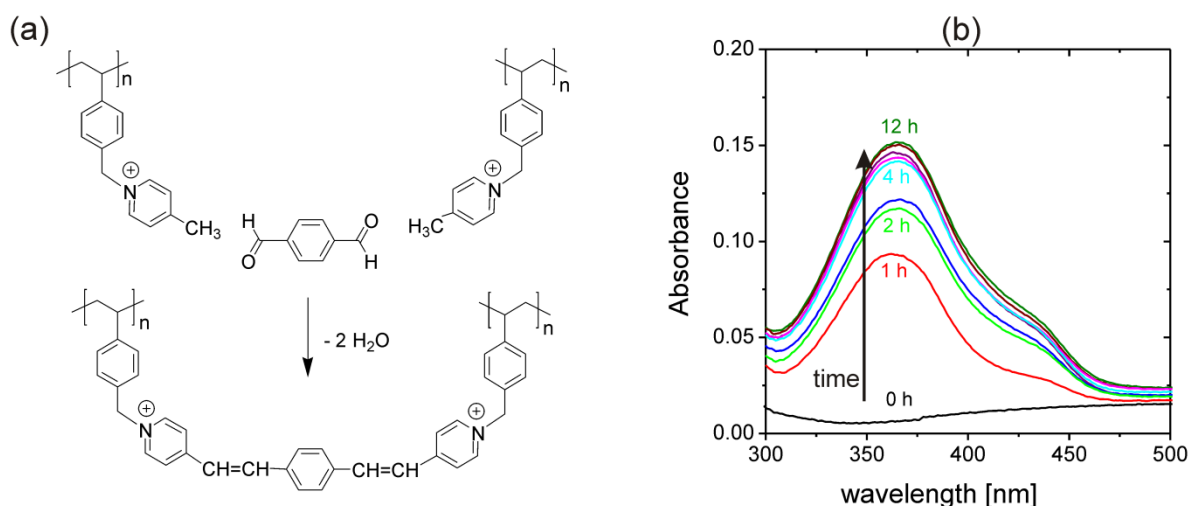

Fig. 3.4: Scheme of the aldol reaction applied for cross-linking (a) and UV-vis absorbance spectra showing the progressive reaction (b).

Due to the additional covalent cross-linking, films show increased stability against solutions where non-cross-linked films dissolved. Combined with the UV-light sensitive nature of the formed chromophore, cross-linked films can be used to generate patterns if performing UV-light treatment through a mask followed by a subsequent dissolution of unstable parts. Fig. **3.5** illustrates the schematic procedure and an example of observed patterns.
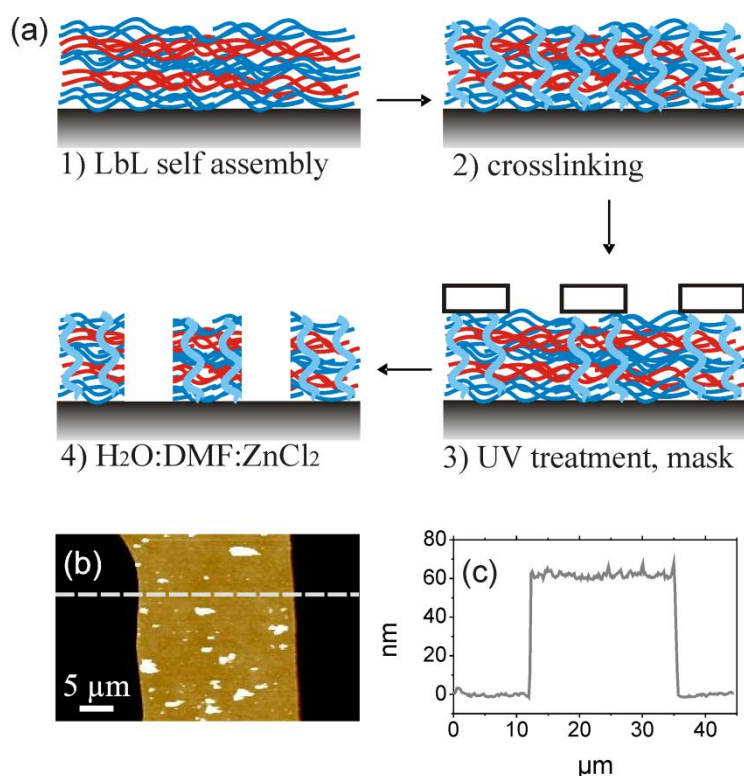
Fig. 3.5: Schematic representation of the patterning process (a), AFM height image (b) and cross-sectional height profile (c) of a patterned (PA/PC)$_{30}$ film.

3.3   Adsorption of Polyelectrolyte Micelles

For the construction of pH-responsive coatings, we used an amphiphilic triblock terpolymer consisting of a hydrophobic polybutadiene (B) block, a pH-sensitive poly(methacrylic acid) (MAA) middle block and a permanently charged block of quarternized poly(dimethyl-amino-ethyl-methacrylate) (Dq) designed in the group of A. H. E Müller by E. Betthausen.[2] In water, the polymer chains self-assemble to micelles with a well defined structure and, since MAA is a weak polyelectrolyte (p$K_{a,app}$ ~ 5.5[3]), with integrated pH-responsive properties. The pH-dependent molecular structure is given in Figure 3.6a. In water, BMAADq self-assembles into core-shell-corona micelles with a hydrophobic B core, a pH-sensitive shell and a cationic Dq corona (Fig. 3.6b). In water at low pH (pH 4), the MAA block is neutral; the triblock terpolymer self-assembles into micelles with hydrophobic B core / neutral MAA shell / highly positively charged and dense corona. At high pH (pH 10), this block is negatively charged through the deprotonation of the carboxylic acid groups leading to the interpolyelectrolyte complex (IPEC) formation with the cationic corona of Dq. Due to the higher polymerization

degree of the cationic block, the corona of micelles is always positively charged. Hence, the composition of the micellar shell as well as the charge density of the corona can be controlled by the solution pH.
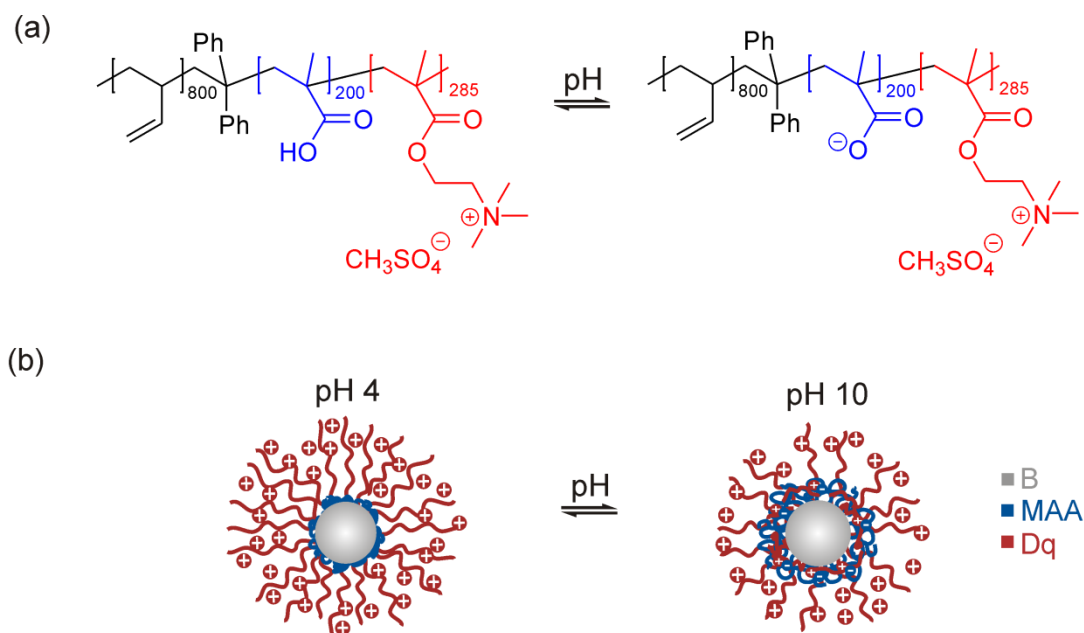

Fig. 3.6: Chemical structure of pH-sensitive BMAADq triblock terpolymer (a) and the structure of self-assembled micelles in water of different pH.

We found that the adsorption of positively charged micelles onto negatively charged silica (Chapter 5) as well as aluminum sponge-like surfaces (Chapter 6) resulted in a monolayer of micelles (Fig. 3.7). The adsorption of BMAADq micelles on silica is adequately described by the Random Sequential Adsorption (RSA) model with a maximal density of adsorbed micelles of 35 micelles per $1 \times 1 \ \mu m^2$ corresponding to the maximum coverage of 54%. Thus, one can tune the coverage between $0 - 54\%$ by the deposition time.
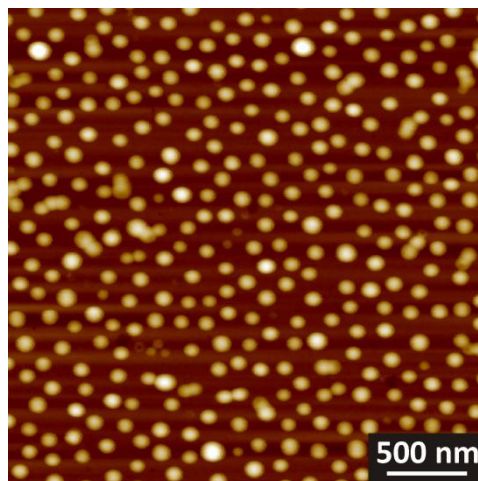
Fig. 3.7: AFM height image (0 nm – 100 nm) of BMAADq micelles adsorbed on silica.

3.4   Reversible Stimulus Response on the Short Time-Scale

The behavior of adsorbed BMAADq micelles was studied by complementary *in situ* atomic force microscopy (AFM) and quartz crystal microbalance (QCM-D) measurements in water. The main results are summarized in Fig. 3.8.
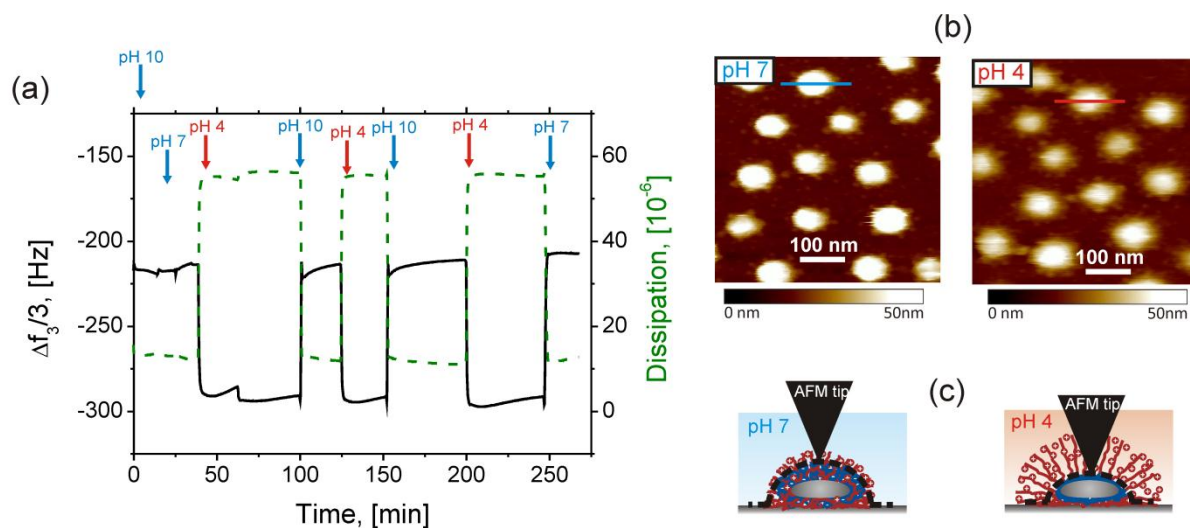

Fig. 3.8: QCM-D frequency shifts (continuous lines) and dissipation changes (dashed green lines) (a), AFM height images (b), and proposed schematic representation of adsorbed BMAADq micelles (c) in water with different pH.

The QCM data show the decrease in the frequency shift and increase in dissipation at pH 4, *i.e.* increase in thickness. Increasing the pH to 10 leads to an increase in frequency shift

combined with a decrease in dissipation. The results are consistent with the protonation of the MAA block ($\alpha \sim 0$) leading to *im*-IPEC dissolution at pH 4. Indeed, longer coronal chains involve swelling of the micelles due to the sorption of additional water and counterions (Fig. 3.8c). In contrast, at pH 10, micelles deswell due to the IPEC regeneration. The proposed morphology switching is confirmed by AFM measurements. AFM images indicate a decrease in height at pH 4. Here, the long corona is penetrable for the AFM tip and therefore not detectable in the topography images.

Thus, by controlling the solution pH on the solid-liquid interface, it is possible to reversibly switch the micellar morphology, composition and charge density of the corona (Chapter 5).

3.5   Control over the Cell-Surface Interactions

The cell-surface interaction properties were tested by using *Lactoccocus Lactis* bacteria as a model system (Chapter 6). We investigated the adhesion of these bacteria on sponge-like aluminum which was modified by a layer of micelles.

The sponge-like metal surfaces can be produced by intensive etching and oxidation of metal under ultrasound irradiation.[4-8] The generated mesoporous layer ("surface metal sponge") is typically ~200 nm and is well-adhered to the bulk metal. By additional sonication, the porous surfaces can be uploaded with low molecular weight compounds, such as silver.[5, 7]

The procedures of experiment are sketched in Fig. 3.9a. During their life process, lactic acid bacteria produce lactic acid in the self-regulated process, leading to a stepwise decrease of the pH of the media. The pH-trigged transition of the micellar morphology towards a swollen state affects the adhesion of bacteria. As a consequence, the number of attached bacteria decreases during the experiment (Fig. 3.9b, c). Hence, the release of bacteria occurs without receiving energy from an external source as the bacteria themselves are the trigger. Further, the deactivation of bacteria by silver incorporated into the porous aluminum matrix was achieved.
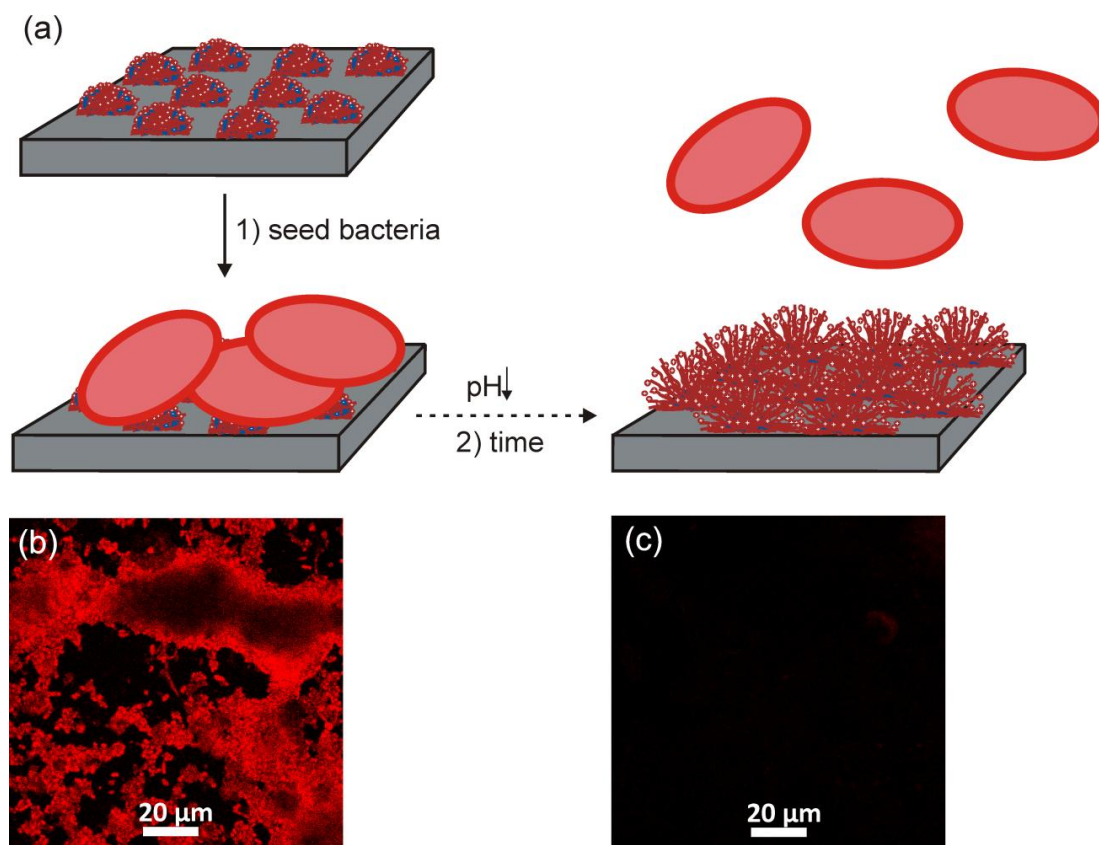
Fig. 3.9: Schematic illustration of the self-regulated bacteria release experiment with corresponding confocal microscopy images.

3.6 Formation of Hydrophobic Pockets by Long-Term Treatment

In contrast to the short-term pH-variations, the long-term treatment under acidic conditions causes irreversible changes in the morphology of adsorbed BMAADq micelles which are not accessible in solution (Chapter 5).
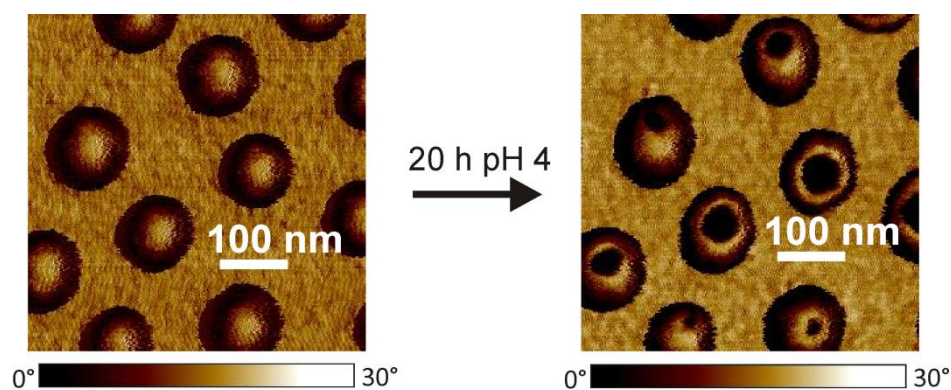

Fig. 3.10: AFM phase images of adsorbed BMAADq micelles before (left) and after long-term treatment in pH 4 (right).

50

Fig. 3.10 shows the AFM phase images of adsorbed micelles, which indicate an "opening" of the micelles due to the *im*-IPEC dissolution under these conditions and slow micelle reorganization.

These better accessible hydrophobic domains open new interesting opportunities. For instance, they can be further modified by thiol-ene click reaction (Fig. 3.11).[9, 10]
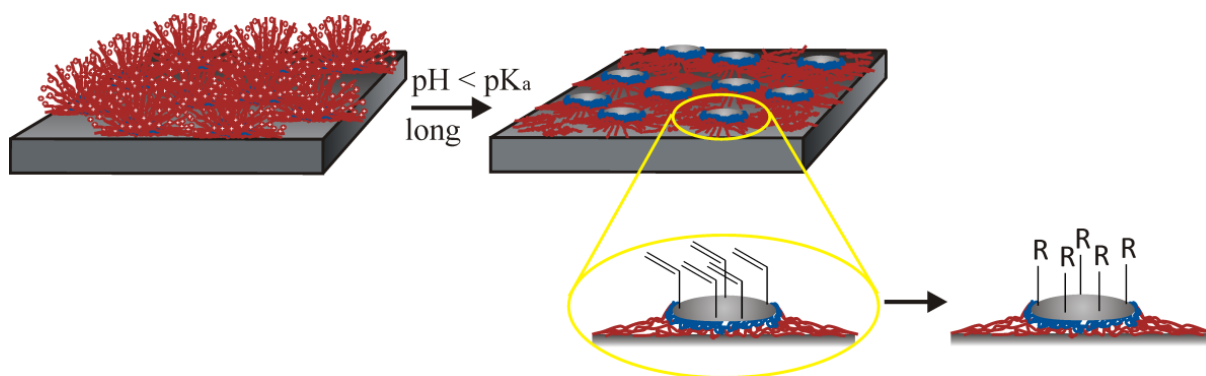

Fig. 3.11: Sketch of the observed micellar monolayer with hydrophobic pockets and a possible way of further modification.

Irreversible changes are prevented by the covalent cross-linking of the core rendering this system of potential interest for long-term experiments such as drug delivery or the use as switchable surfaces.

3.7   Layer-by-Layer Assembly of Micelles

Using the layer-by-layer approach, the BMAADq micelles were included within multilayer films (Chapter 7). Our goal was to create novel highly responsive double-end-tethered weak polyelectrolyte brush structures by complexing the strong polycationic corona of micelles with a strong polyanion. For this reason, we co-assembled micelles with poly(sodium 4-styrenesulfonate) (PSS) by the layer-by-layer technique. As deposition condition we chose pH 4 buffer solution, because MAA block is uncharged at this pH and no *im*-IPECs with Dq corona are formed. Therefore, all of the coronal chains are involved in formation of stable complexes with PSS.

Upon incorporation into multilayers, the micellar structure remains intact and the film architecture, in particular, porosity can be easily tuned between ~50% and ~0% by the number of deposition steps.

The swelling degree, the morphology as well as the mechanical properties of the (BMAADq/PSS) films are reversibly tunable by the solution. The results are summarized in Fig. 3.12. The pH-triggered swelling transition as investigated by *in situ* ellipsometry (Fig. **3.12**a) occurs at pH ~ 9.5. The shift to higher transition pH values (compared to the apparent pK_a of PMAA reported in the literature ($pK_{a,app}$ ~5.5 [Ref. 3])) agrees with experiments on polyelectrolyte brushes.[11, 12] The increase in thickness corresponds to the deprotonation of the carboxylic groups of the MAA shell. Due to the strong swelling, pore opening / closing can be regulated by the pH (Fig. 3.12b). Closely correlated to the swelling and water uptake, the mechanical properties (between pH 8 and pH 11) are changed by two orders of magnitude (Fig. 3.12a).

Moreover, controlling the porosity by the number of deposition steps allows tuning the equilibrium swelling degree between 200 − 1200%.
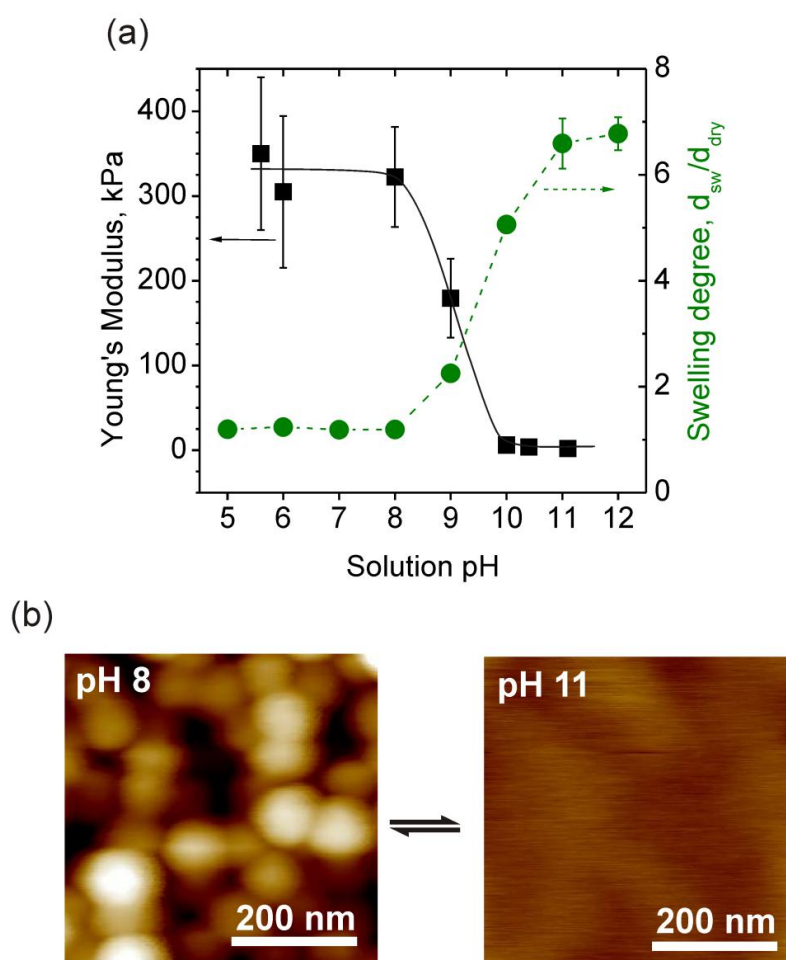

Fig. 3.12: pH-triggered swelling (●) and Young's modulus (■) transitions of a three-bilayers (BMAADq/PSS) film (a) and corresponding AFM height images (0 nm − 100 nm) in water at pH 8 and pH 11.

3.8   Individual Contributions to Joint Publications

The results presented in the thesis were obtained in collaboration with others. In the following, the contributions of each coauthor are specified. The asterisks denote the corresponding authors.

Chapter 4

Chapter 4 is reproduced with permission. Copyright (2010) American Chemical Society.

This work is published in *Chemistry of Materials* 2010, 22, 3323-3331 under the title:

"Cross-Linkable Polyelectrolyte Multilayer Films of Tailored Charge Density"

by Patrick Ott, Julia Gensel, Sina Roesler, Katja Trenkenschuh, Daria Andreeva, André Laschewsky, and Andreas Fery*.*

I performed most of the described experiments and wrote the publication.
Patrick Ott conducted the synthesis and characterization of polymers used.
Sina Rösler performed some of the ellipsometric measurements within the scope of her Bachelor Thesis under my guidance.
Katja Trenkenschuh and Daria Andreeva were involved in scientific discussions and correcting the manuscript.
André Laschewsky and Andreas Fery supervised the project, wrote the manuscript and were involved in scientific discussion.

Chapter 5

Chapter 5 is reproduced by permission of The Royal Society of Chemistry.

This work is published in *Soft Matter* 2011, 7, 11144-11153 under the title:

"Surface Immobilized Block Copolymer Micelles with Switchable Accessibility of Hydrophobic Pockets"

by Julia Gensel, Eva Betthausen, Christoph Hasenöhrl, Katja Trenkenschuh, Markus Hund, Fouzia Boulmedais, Pierre Schaaf, Axel. H. E. Müller, and Andreas Fery.*

I performed most of the experiments and wrote the publication.

Eva Betthausen conducted the synthesis and characterization of polymer used and was involved in scientific discussion and correcting the manuscript.

Christoph Hasenöhrl reproduced some AFM results within the scope of his Bachelor Thesis under my guidance.

Markus Hund contributed with valuable remarks concerning AFM measurements and was involved in scientific discussion and correcting the manuscript.

Fouzia Boulmedais performed QCM-D measurements and was involved in scientific discussion and correcting the manuscript.

Katja Trenkenschuh, Pierre Schaaf, Axel. H. E. Müller and Andreas Fery were involved in scientific discussion and correcting the manuscript.

Chapter 6

Chapter 6 is reproduced with permission. Copyright (2012) by Wiley-VCH Verlag GmbH & Co KGaA.

This work is published in *Advanced Materials* 2012, 24, 985-989 under the title:

"Cavitation engineered 3-D sponge networks and their application in active surface construction"

by Julia Gensel, Tina Borke, Nicolas Pazos Perez, Andreas Fery, Axel H. E. Müller, Eva Betthausen, Daria V. Andreeva*, Helmuth Möhwald and Ekaterina V. Skorb*.

I performed AFM measurements and wrote a part of the manuscript.

Tina Borke and Nicolas Pazos Perez prepared Al and Al/Ag sponge-like substrates and were involved in scientific discussion and correcting the manuscript.

Daria V. Andreeva performed SEM, TEM and EDX measurements of Al and Al/Ag sponge-like substrates and wrote a part of the manuscript.

Eva Betthausen conducted the synthesis of polymer used and was involved in correcting the manuscript.

Andreas Fery, Axel H. E. Müller, and Helmuth Möhwald were involved in scientific discussion and correcting the manuscript.

Katja Skorb performed bacteria release experiments and wrote a part of the manuscript.

Chapter 7

Chapter 7 is reproduced by permission of The Royal Society of Chemistry.

This work is accepted in *Chemical Science* DOI: 10.1039/C2SC20836A under the title:

"Reversible swelling transitions in stimuli-responsive layer-by-layer films containing block copolymer micelles"

by Julia Gensel, Inna Dewald, Johann Erath, Eva Betthausen, Axel. H. E. Müller and Andreas Fery*.

I and Inna Dewald performed most of the experiments. I wrote the manuscript.

Inna Dewald performed AFM and ellipsometry experiments within the scope of her research module under my guidance.

Johann Erath performed Colloidal Probe AFM measurements, wrote a part of the manuscript, and was involved in scientific discussion and correcting the manuscript.

Eva Betthausen conducted the synthesis and characterization of polymer used and was involved in scientific discussion and correcting the manuscript.

Axel. H. E. Müller and Andreas Fery were involved in scientific discussion and correcting the manuscript.

References

1.   G. S. Manning, *Journal of Chemical Physics*, 1969, **51**, 924.

2.   E. Betthausen, M. Drechsler, M. Förtsch, F. H. Schacher and A. H. E. Müller, *Soft Matter*, 2011, **7**, 8880-8891.

3.   H. Dautzenberg, W. Jaeger, J. Kötz, B. Philipp, C. Seidel and D. Stscherbina, *Polyelectrolytes*, Carl Hanser Verlag, München, 1994.

4.   E. V. Skorb, H. Möhwald, T. Irrgang, A. Fery and D. V. Andreeva, *Chemical Communications*, 2010, **46**, 7897-7899.

5.   E. V. Skorb, D. Fix, D. G. Shchukin, H. Möhwald, D. V. Sviridov, R. Mousa, N. Wanderka, J. Schäferhans, N. Pazos-Perez, A. Fery and D. V. Andreeva, *Nanoscale*, 2011, **3**, 985-993.

6.   D. V. Andreeva, D. V. Sviridov, A. Masic, H. Möhwald and E. V. Skorb, *SMALL*, 2011, doi: 10.1002/smll.201102365

7.   E. Skorb, D. Shchukin, H. Möhwald and D. Andreeva, *Langmuir*, 2010, **26**, 16973-16979.

8.   D. Andreeva, *International Journal of Materials Research*, 2011, **102**, 597-598.

9.   K. Griesbaum, *Angewandte Chemie-International Edition*, 1970, **9**, 273-287.

10.   M. J. Kade, D. J. Burke and C. J. Hawker, *Journal of Polymer Science Part A-Polymer Chemistry*, 2010, **48**, 743-750.

11.   A. J. Parnell, S. J. Martin, C. C. Dang, M. Geoghegan, R. A. L. Jones, C. J. Crook, J. R. Howse and A. J. Ryan, *Polymer*, 2009, **50**, 1005-1014.

12.   E. P. K. Currie, A. B. Sieval, G. J. Fleer and M. A. Cohen Stuart, *Langmuir*, 2000, **16**, 8324-8333.

4 Cross-Linkable Polyelectrolyte Multilayers of Tailored Charge Density

Patrick Ott,[a] Julia Gensel,[b] Sina Roesler,[b] Katja Trenkenschuh,[b] Daria Andreeva,[b] André Laschewsky,[a, c] and Andreas Fery [b]**

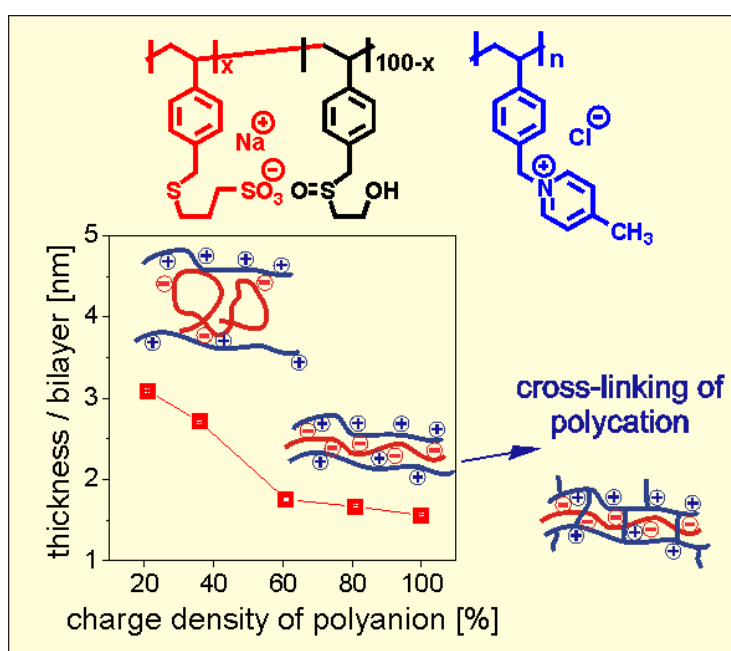[a] Institute for Chemistry, University of Potsdam, Karl-Liebknecht-Str. 24-25, 14476 Potsdam-Golm, Germany

[b] Department of Physical Chemistry II, University of Bayreuth, Universitätsstr. 30, 95440 Bayreuth, Germany

[c] Fraunhofer Institute for Applied Polymer Chemistry, Geiselbergstr. 69, 14476 Potsdam-Golm, Germany

* e-mail: Andreas.Fery@uni-bayreuth.de

* e-mail: laschews@rz.uni-potsdam.de

Abstract

The layer-by-layer (LbL) deposition technique of anionic and cationic polyelectrolytes allows formation of thin and ultrathin nanostructured films with tunable properties and, therefore, functionality. Here, we report on synthesis and characterization of new polyelectrolyte multilayer system consisting of anionic copolymer poly(sodium 3-(4-vinylbenzylsulfanyl)-propane-1-sulfonate)-*co*-poly(2-hydroxyethyl-vinylbenzyl sulfoxide), with different charge densities (21%, 36%, 65%, 81% and 100%) and cross-linkable cationic poly(4-methyl-1-(4-vinylbenzyl)-pyridinium chloride. We study the impact of salt concentration on film thickness and roughness for the different charge densities and discuss the observed trends with regard to charge effects. Furthermore we covalently cross-link the films by an aldol reaction, which preserves the number of charged groups while being easily followed via UV-vis-spectroscopy due to characteristic absorbance band of the coupling product. Cross-linking increases film stability markedly. Thus the new multilayer system allows tuning of both ionic and covalent crosslinking in a quantitative fashion.

4.1 Introduction

The layer-by-layer (LbL) alternating adsorption of anionic and cationic species, mostly polyelectrolytes, is an attractive method to prepare ultrathin multilayer films on most various types of substrates.[1-6] The LbL deposition technique is enabled to control the films' structure and properties, by varying the chemical structure of the polyelectrolytes, for instance their charge density, the number of adsorbed layers, and the conditions of adsorption, thus providing a convenient way for their functionalization.[5, 6] A further way to influence the properties of multilayer films is the use of polyelectrolyte blends [7-9] or of inorganic nanomaterials [10, 11] for their construction. Multilayer films have been therefore intensively developed and increasingly studied with respect to diverse applications, *e.g.* for controlling wetting properties or interactions with biological systems [12] as anti-corrosion coatings,[13-16] free-standing membranes,[17-22] osmotic pressure sensors [23], and micro- and nanocapsules.[24, 25]

The sensitivity of the polyelectrolyte film to a variety of chemical and physical conditions, such as charge density or ionic strength of solution, provides the ability to tune mechanical properties, permeability or stability of the films. Charge density of polymers is a major

parameter to control structure and property of LbL films. In the case of weak polyelectrolytes, the charge density can be varied with pH, determining their degree of dissociation.[26] A potential limitation of systems based on weak polyelectrolytes is the polymer local charge density, which polymer chains adjust to accommodate different molecular environments. This difficulty is avoided, when strong polyelectrolytes with fixed charge density are employed. In their case, the charge density can be controlled by "intramolecular dilution", either by fixing the distance between neighboring charged groups in the polymers via the use of complex constitutional repeat units,[27-31] or by using copolymers of charged and uncharged monomers, [32-38] thus reducing the charge statistically by their relative contents.

The former strategy has the advantage to provide regular, extremely well defined charge densities. However, the synthetic pathways to such polyelectrolytes are limited. Moreover, the mostly hydrophobic character of the uncharged spacer groups separating the charged moieties in such polymers give rise to strong hydrophobic interactions and complications.[27, 28, 30, 31] Therefore, the control of the charge density by copolymerizing charged and uncharged monomers is not only a much more convenient but also more versatile strategy, as the appropriate choice of hydrophilic non-ionic comonomers may circumvent the pitfalls of increasing hydrophobicity with charge reduction. However, care must be taken to use comonomer systems with reactivity ratios close to 1, in order to provide defined, true random copolymers under so-called azeotropic conditions, as otherwise broad mixtures of copolymers with strongly differing charge content are obtained. Particular useful in this respect have been copolymers of diallydimethylammonium chloride and vinylamides,[33, 34] or copolymers of 2-acrylamido-2-methylpropanesulfonate and acrylamides.[36, 37] Still, it was found that the use of strongly hydrophilic comonomers may pose a problem for the LbL process, as with increasing share of the non-ionic units (*i.e.* at low charge densities) in the copolymers, film growth is inhibited. This finding has been often justified by evoking a critical charge density for successful LbL deposition.[33, 34] However, there is a high chance that the stoichiometric polyelectrolyte complexes formed by such strongly hydrophilic hybrid ionic-nonionic copolymers may be water-soluble and, thus, do not adsorb onto the substrate.

Here, we study a new polyelectrolyte multilayer system, which consists of the reactive polycation poly(4-methyl-1-(4-vinylbenzyl)-pyridinium chloride, PC, and polyanions with different charge densities, namely the copolymers poly(sodium 3-(4-vinylbenzylsulfanyl)-propane-1-sulfonate)-*co*-poly(2-hydroxyethyl vinylbenzyl sulfoxide) PA-x. The copolymer is obtained by copolymerization of ionic sodium 3-(4-vinylbenzylsulfanyl)-propane-1-sulfonate

with the non-ionic 2-hydroxyethyl-vinylbenzyl sulfoxide. As both monomers contain the same polymerizable group, the formation of random copolymers can be expected. Moreover, the non-ionic comonomer is only moderately hydrophilic. Therefore, it is polar enough to be water soluble, but the homopolymer is only capable of swelling in water without dissolving. These features were aimed at providing control over the charge-density of the resulting copolymers by adjusting the comonomer composition, without affecting on the one hand the overall hydrophobic/hydrophilic balance severely, while avoiding on the other hand the formation of water-soluble polyelectrolyte complexes at high contents of the non-ionic comonomer. As the methyl substituent of the pyridinium moiety of PC is activated by the conjugated quaternary nitrogen atom, it is reactive towards carbonyl compounds to undergo aldol condensations.[39, 40] This opens the possibility to cross-link the multilayer films with *e.g.* dialdehydes without affecting the number of charged groups. Therefore, the newly used polyelectrolyte system allows varying simultaneously parameters such as the charge density and the degree of cross-linking in the multilayer films. Hence, we investigated the effect of charge density of polyanion and degree of cross-linking of polycation on film morphology, structure and properties. Film growth, its surface morphology and inner structure as well as film stability were studied by atomic force microscopy (AFM), ellipsometry and UV-Vis spectroscopy in dependence on the preparation condition (ionic strength) and the polymers' chemical nature (degree of cross-linking and charge density of the chain).

4.2 Materials and Methods

Materials

4-Vinylbenzyl chloride (technical $\geq$ 90%, Fluka) was passed through basic alumina before use. Sodium 3-mercapto-1-propanesulfonate (technical grade, 90% Sigma-Aldrich), 4-methylpyridine (γ-picoline, 99%, Acros), 2,6-di-tert-butyl-4-methylphenol (99%, Acros), terephthaldialdehyde (99%, Sigma-Aldrich), piperidine (99.9%, Iris Biotech), sodium chloride (99.8%, Riedel-de Haën), zinc chloride (pure, Merck), basic Al_2O_3 (for chromatographie, Acros) and NaOH solution (1 M, Merck) were used as received. DMSO (dimethylsulfoxide), THF (tetrahydrofurane), *n*-hexane, methanol, and N,N-dimethylformamide (DMF) were analytical grade. Initiators V-50 (2,2'-Azobis(2-methylpropionamidine)dihydrochloride) and VA-044 (2,2'-Azobis[2-(2-imidazolin-2-yl) propane]dihydrochloride) were a kind gift of Wako Chemicals GmbH**.** Branched polyethyleneimine (PEI, M_w ~ 25 000 g mol^{-1}) was from Sigma-Aldrich. Milli-Q water

(18.2 MΩ cm) was used in all experiments. All aqueous polymer solutions were used after filtration. Dialysis tubes "ZelluTrans" (Roth, Germany) had a nominal molar mass cut off of 3500 D. The synthesis of sodium 2-benzylsulfanylthiocarbonylsulfanyl-ethanesulfonate,[41] (UV-Vis in water: band at λ_{max}= 425 nm, extinction coefficient ε = 49.3 l·mol^{-1}·cm^{-1}), and polycation poly(4-methyl-1-(4-vinylbenzyl)-pyridinium chloride, PC,[40] were reported before.

Synthesis of sodium 3-(4-vinyl-benzylsulfanyl)-propane-1-sulfonate

Sodium 3-mercaptopropanesulfonate (12.11 g, 67 mmol) in THF (30 mL) and 82 mL of 1M NaOH were refluxed for 30 min. Then, 4-vinylbenzylchloride (10.38 g, 68 mmol) and a small amount of 2,6-di-tert-butyl-4-methylphenol in THF (56 mL) were added dropwise within 25 min. The mixture is refluxed for 4 h and stirred at ambient temperature over night, then diluted with water (200 mL) and precipitated into acetone. The resulting suspension was filtrated and the filtrate concentrated under reduced pressure. The resulting precipitate was filtered off and dried in vacuo at 40°C. Yield: 9.4 g (32 mmol, 48 %) of sodium 3-(4-vinyl-benzylsulfanyl)-propane-1-sulfonate, colorless powder that decomposes at 132 °C.

Elemental analysis ($C_{12}H_{15}O_3S_2Na$, M_r = 294.37): Calc.: C 48.96, H 5.14, S 21.78. Found: C 48.84, H 5.08, S 21.62.

^{1}H-NMR (200 MHz, in D_2O, δ in ppm) 7.36 (d, 2H,. CH aryl); 7.23 (d, 2H, -CH aryl); 6.68 (dd, 1H, Aryl-CH=); 5.77 (dd, 1H, Aryl-C=CH (Z)); 5.22 (dd, 1H, Aryl-C=CH (E)); 3.65 (s, 2H, aryl-CH$_2$-S), 2.85 (t, 2H, -CH$_2$-SO$_3$); 2.46 (t, 2H, S-CH$_2$-C) 1.90 (m, 2H, -CH$_2$-).

^{13}C-NMR (75 MHz, in D_2O, δ in ppm) 138.6, 136.7, 129.7, 126.7, 114.6 (-C= aryl + alkene); 50.2 (CH$_2$-SO$_3$); 35.0 (aryl-CH$_2$-S); 29.7 (-S-CH$_2$-); 24.3 (-CH$_2$-).

MS (ESI) m/z (%) =271.04 (100) (M$^+$-Na); m/z 148.9 (7.2) (M$^+$-S-CH$_2$CH$_2$CH$_2$-SO$_3$Na)

Synthesis of 2-(4-vinyl-benzylsulfanyl)-ethanol

4-vinylbenzylchloride (38.87 g, 0.257 mol) was added during 60 min to a solution of 2-mercaptoethanol (21.17 g, 0.257 mol) and a small amount of 2,6-di-tert-butyl-4-methylphenol in 250 mL of 1 M aqueous NaOH and 150 mL of THF, while refluxing. The mixture was refluxed over night, diluted with 500 mL of water, and extracted four times with 500 mL of CH$_2$Cl$_2$. The organic phases were combined, dried over MgSO$_4$ and evaporated to give the product as colorless, waxy solid (m.p. 39 °C). Yield: 48.85 g (0.251 mol, 98 %).

^{1}H-NMR (200 MHz, in methanol-d4, δ in ppm) 7.40,7.36 (d+d, 2H+2H, CH aryl); 6.71 (dd, 1H, Aryl-CH=); 5.78 (dd, 1H, Aryl-C=CH (Z)); 5.22 (dd, 1H, Aryl-C=CH (E)); 3.74 (s, 2H, aryl-CH_2-S); 3.32 (t, 2H, -CH_2-O); 2.55 (t, 2H, S-CH_2-).

^{13}C-NMR (75 MHz, in $CDCl_3$, δ in ppm) 137.9 , 136.7, 136.6, 129.4, 126.7, 114.3 (-C= aryl + alkene), 61.2 (-CH_2-OH)), 35.7 (aryl-CH_2-S-); 33.4 (S-CH_2-).

MS (ESI): m/z (%) = 195 [M^+]; 117 [M^+- SCH_2CH_2OH].

Synthesis of 2-(4-vinyl-phenylmethanesulfinyl)-ethanol

Sodium periodate (30.87 g, 0.144 mol) in water (300 mL) was added at 0°C dropwise 2-(4-vinyl-benzylsulfanyl)-ethanol (24.42 g, 0.126 mol) in methanol (400 mL). The mixture is stirred for 2 days at ambient temperature, filtered, and extracted 4 times with 400 mL of $CHCl_3$. The combined organic phases were dried over $MgSO_4$ and evaporated. The residue was crystallized from *n*-hexane after adding of a small amount of 2,6-di-tert-butyl-4-methylphenol to give colorless crystals (m.p. 83 °C). Yield 15.82 g (80 mmol, 64 %).

Elemental analysis: ($C_{11}H_{14}O_2S$, M_r = 210.29): Calc.: C 62.83, H 6.71, S 15.25. Found: C62.72, H 6.67, S 15.25.

^{1}H-NMR (200 MHz, in methanol-d4, δ in ppm) 7.48 (d, 2H, CH aryl); 7.36 (d, 2H, CH aryl); 6.77 (dd, 1H, Aryl-CH=); 5.83 (dd, 1H, Aryl-C=CH (Z)); 5.28 (dd, 1H, Aryl-C=CH (E)); 4.06, 3.96 (d + d, 2H + 2H, aryl-CH_2-S(=O)-); 3.99-3.96 (m, 2H, -CH_2-OH); 3.02, 2.84 (m + m, 2H + 2H, S(=O)-CH_2-).

^{13}C-NMR (75 MHz, in MeOH-d4, δ in ppm) 139.0, 137.3, 131.8, 131.1, 127.5, 114.7 (-C= aryl + alkene); 58.4 (-CH_2-O); 55.7 (aryl-CH_2-S(=O)-); 54.9 (S(=O)-CH_2-).

MS (ESI):m/z (%) = 210 [M^+]; 117 [M^+- S(=O)-CH_2CH_2OH].

Synthesis of the polyanions

In a typical polymerization procedure, sodium 3-(4-vinyl-benzylsulfanyl)-propane-1-sulfonate (3.599g, 12.2 mol), 2-(4-vinyl-phenylmethanesulfinyl)ethanol (0.2848g, 1.2 mmol) and RAFT agent sodium 2-benzylsulfanyl-thiocarbonylsulfanylethanesulfonate (0.0446g, 0.1368 mmol) were dissolved in 50 aqueous methanol (52 vol%). Then 2 mL of a solution containing initiator V-50 (0.00454 g, 0.0167mmol in water (10 mL) were added. The mixture was purged with nitrogen for 15 min, and then heated to 60°C for 150 min. The polymer was isolated and purified by dialysis and lyophilized, to yield 1.16 g of polymer (colorless hygroscopic powder).

Multilayer Film Preparation by Spraying

The LbL films were assembled on silicon wafers (CrysTec) and on quartz slides (QSIL AG, Germany). from 1 mg/mL polymer solutions by the spray coating method.[42, 43] The substrates were cleaned using RCA method (sonication in a 1:1 mixture of water and 2-propanol for 15 min),[44] followed by heating at 70 °C in a 5:1:1 mixture of water, 25% ammonia solution, and 30% hydrogen peroxide solution for 10 min. The freshly cleaned substrate was than precoated with one layer of PEI which was allowed to adsorb onto the negatively charged surface during 20 min before rinsing with water.

The PEI coated substrate was vertically placed in a homemade spray unit. The polyelectrolyte solutions containing precise concentrations of NaCl (0.02 M, 0.05 M, or 0.20 M) were filled into spray bottles (10 mL, NeoLab Migge GmbH, Germany) which were manually pressurized twice for each deposition step. After each step, the polymer was allowed to adsorb during 10 s before spraying of water during 10 s (200 mL spray bottles "air boy", Carl Roth GmbH, Germany) to rinse the surface. The films were dried in a stream of nitrogen before characterization.

Cross-linking

Cross-linking was performed on films deposited on quartz slides. The film coated substrate was immersed at room temperature into the solution of terephthalaldehyde (20 mg) in methanol (5 mL) adding piperidine (2 drops) as catalyst,[45] followed by rinsing with methanol and water and drying with a stream of nitrogen. The progress of the reaction was monitored by UV-vis spectroscopy, following the evolving absorbance band of the newly formed chromophore.

In order to investigate the stability of films, multilayer-covered quartz slides were immersed into a ternary mixture of H_2O:DMF:$ZnCl_2$ (5:3:2, w/w/w).

Characterization Methods

Ellipsometry measurements were performed with a Sentech SE 850 spectroscopic ellipsometer at a constant incidence angle of 70°.

Atomic force microscopy (AFM) images were taken with a commercial AFM (DI Dimension 3100 Metrology) operating in Tapping Mode[TM] using Si_3N_4 cantilevers (Olympus) with a spring constant of 43.0 – 63.8 N/m. The surface mean roughness (R_a) was determined from the plain fitted and flattened images of 5 μm × 5 μm size using the DI NanoScope 7.20 software.

UV-vis spectra were recorded between 200 and 600 nm with 1 nm resolution using a Perkin Elmer Lambda 19 UV-vis spectrometer, using a RCA-treated quartz slide for reference. When investigating the cross-linking process, absorbance spectra were recorded only above 300 nm, to protect the UV-light sensitive newly formed chromophore.

4.3 Results

The new homopolymer poly(sodium 3-(4-vinylbenzylsulfanyl)-propane-1-sulfonate), and its copolymers with 2-hydroxyethyl-vinylbenzyl sulfoxide were synthesized for their use as strong polyanion PA-x with different charge densities x, expressed in mole% of ionic monomer incorporated (Figure 4.1a). Accordingly, the charge density is adjusted by balancing the ratio of charged and uncharged monomers in the copolymerization (Table 4.1), independent of the pH of the solutions. Due to the similarity of the polymerizable moieties, the comonomers have similar reactivities, and thus are evenly distributed within the polymer chains. As intended, the balanced polarity of the non-ionic comonomer has the effect, that the copolymers with markedly reduced charge density are still fully water-soluble, but that the complexation with the polycation PC results in thick precipitates, demonstrating the water-insolubility of their polyion complexes ("PIC", "symplex"). This contrasts *e. g.* with the behavior of symplexes made from poly(diallyldimethyl ammonium chloride) and copolymers of anionic 3-acrylamido-2-methylpropanesulfonate (AMPS) and the strongly hydrophilic trismethylolmethylacrylamide.
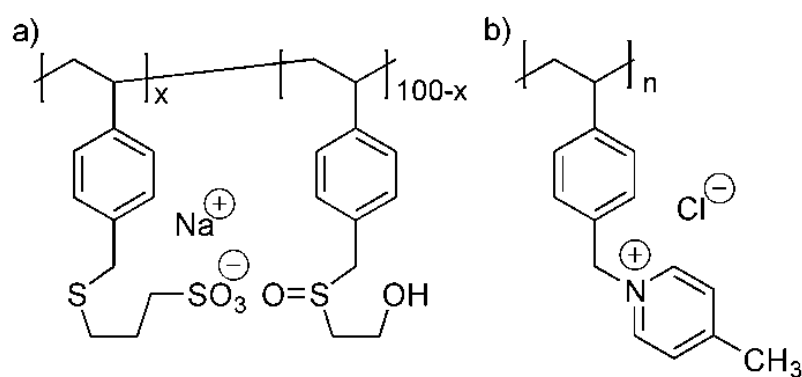

Fig. 4.1: Polyelectrolytes used for the multilayer buildup. (a) Anionic copolymers PA-x (x = 100%, 81%, 65%, 36%, and 21%); (b) reactive polycation PC.

Table 4.1. Anionic polymers of sodium 3-(4-vinylbenzylsulfanyl)-propane-1-sulfonate and 2-hydroxyethylvinylbenzyl sulfoxide synthesized.

polymer	yield [%]	M_n [a)] [g/mol]	sulfonate content in the reaction mixture [mol%]	sulfonate content in the polymer (=charge density) [b)] [mol%]
PA-100	49	13000	100	100
PA-81	51	7500	80	81
PA-65	26	6200	60	65
PA-36	20	5000	40	36
PA-21	30	7800	25	21

[a)] number average molar mass, as determined by vis-spectroscopy (based on the absorbance of the trithiocarbonate moiety of the RAFT agent used at $\lambda = 425$ nm and assuming exactly 1 RAFT end group per polymer [41, 72]).

[b)] mole fraction x of anionic sodium 3-(4-vinylbenzylsulfanyl)-propane-1-sulfonate in the copolymer, as determined from the C/S ratio by microanalysis.

The used polyanions are listed in Table 4.1. As cationic counterpart we chose the reactive homopolymer PC (Figure 4.1b). Due to the conjugation with the quaternary nitrogen atom of the pyridinium moiety, the methyl substituent in 4-position is activated toward proton abstraction, and thus participates *e.g.* easily in aldol-type reactions catalyzed by mild bases.[45] However, this reactive group is inert toward radical attack and hence, the monomer is suitable well for free radical polymerization. Moreover, chemical transformations at this reactive site do not affect the cationic charge, so that *e.g.* chemical cross-linking with bifunctional carbonyl compounds becomes possible over a wide range (theoretically, from 0 to 100% of γ-picolinium moieties may reacted), while the number of ionic cross-links is preserved. In contrast, the hitherto most used cross-linking reactions in LbL multilayers, namely the amide formation of carboxylic groups with amines,[18, 46-49] or the unspecific decomposition of

diazonium salts,[50-52] characteristically sacrifice ionic groups. Furthermore, the cross-linking products of the γ-picolinium moieties are strong chromophores and even fluorophores, if the carbonyl reagents are appropriately chosen.[39, 40, 45, 53] This allows to follow positively and most conveniently the increase of coupling products. This differs from the typical photo-cross-linking reactions used in the past,[54-59] which conserve the number of ionic groups, but which allow only following the conversion of the reactive groups to non-identified putative coupling products.

Here, the layer-by-layer (LbL) sequential adsorption of oppositely charged polyelectrolytes was performed by spray deposition. Spray coating is known to simplify and speed up the polyelectrolyte multilayer deposition as compared to conventional dip coating.[42, 43] Schlenoff et al.[42] used spray deposition technique to construct poly(diallyldimethyl ammonium chloride)/ poly(sodium styrenesulfonate) multilayers and found similar buildup and composition of resulting films. Later Izquierdo et al.[43] showed that spray deposition allows achieving regular multilayer growth even for extremely short contact times for which dipping fails to produce homogeneous films.

4.3.1 Multilayer formation at different solution ionic strength.

Polyelectrolyte multilayer films from aqueous homopolymer (100% charge density) solutions of varying salt concentrations were prepared via LbL spray assembly in order to analyze the influence of solution ionic strength on the film buildup. Figure 4.2 displays a plot of ellipsometric film thickness versus the deposited polyelectrolyte layer number. The driving force for the buildup process of multilayer assemblies is the alternate overcompensation of the surface charge after each deposition. As often reported for the absorption behavior of strong polyelectrolytes from pure aqueous solutions,[5, 29, 60, 61] only very low thickness increment was observed, when the films were adsorbed from solutions without any added salt (see Supporting Information, Figure S4). In contrast, linear buildup behavior was found for systems containing salt. The concentration of NaCl has a significant effect on the multilayer formation as the conformation of polyelectrolytes is highly dependent on the ionic strength of solutions. The increasing salt concentration leads to a more coiled conformation due to the screening of repulsive interactions within the chain, leading to thicker layers.[2, 62, 63]
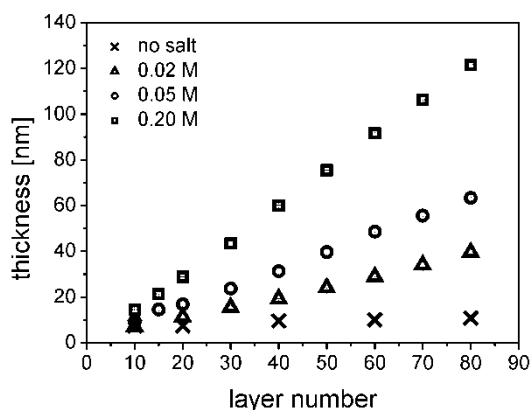
Fig. 4.2: Plot of the ellipsometric thickness vs. the number of layers of PEI(PA-100/PC)$_n$ films deposited by alternated spraying of polyelectrolyte solutions without added salt ($\times$), and in the presence of 0.02 M ($\triangle$), 0.05 M (o), 0.2 M ($\square$) NaCl. The error bars are smaller than the size of the symbols.

To obtain detailed structural information about the LbL film deposited from different ionic strength solutions, AFM measurements were performed. Figure 4.3a displays the mean roughness (R_a) of multilayered films assembled from solutions containing 0.20 M, 0.05 M, 0.02 M NaCl, and without added salt as a function of layer number. If deposition is performed from solution without added salt, only marginal film growth was observed, so the roughness is very low (similar to substrate roughness) and independent from layer number as the thickness hardly evolves. The films deposited from 0.02 and 0.05 M NaCl solutions show a similar roughness increasing with the layer number. For adsorption from solutions with 0.20 M salt concentration, the roughness increased significantly in comparison to lower ionic strength solutions. AFM images of the 80-layer-films show clear differences in the surface morphology between the four films deposited from varying salt concentration of polymer solutions (Fig. 4.3b-e). In the absence of added salt, the film is very smooth with the mean roughness of 0.8 nm. With an increasing ionic strength of solution, the polyelectrolytes have more coiled conformation, leading to thicker, but also rougher layers, as commonly observed for polyelectrolyte multilayers.[6] The surface topography of films formed from solutions containing 0.02 and 0.05 M sodium chloride shows slightly topographical differences (Fig. 4.3c, d) with the roughness for 80 layers of 1.6 nm and 1.9 nm, respectively. When 0.20 M sodium chloride solution is used, the surface of 80-layer film becomes much rougher than other samples ($R_a \sim 3.5$ nm).
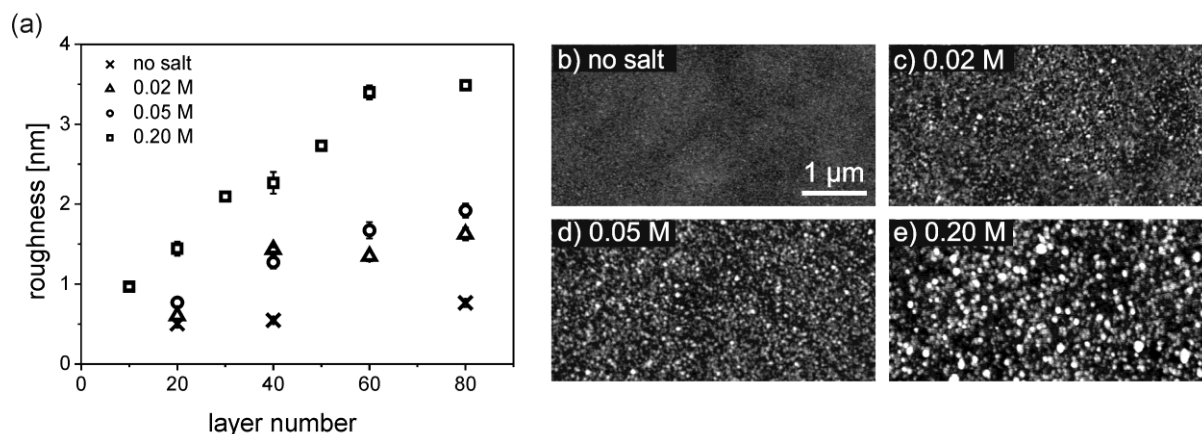
Fig. 4.3. Roughness of the LbL films deposited from polyion solutions of different ionic strength measured by AFM: (a) dependence on layer number; (b) - (e) typical AFM height images (scale 0 nm – 20 nm) of PEI(PA-100/PC)$_{40}$ films, deposited from solutions (b) without added salt, (c) with 0.02 M, (d) with 0.05 M, and (e) with 0.20 M NaCl added.

4.3.2 Effect of charge density

Polyelectrolyte multilayers were prepared by adsorption of polyanions with different charge densities (PA-100, PA-81, PA-65, PA-36, and PA-21) from 0.20 M, 0.05 M, and 0.02 M NaCl solutions in order to analyze the influence of the ionic strength and the polyelectrolyte charge density, respectively, on the film properties. Thicknesses of the films were measured by ellipsometry and are displayed in Figure 4.4. All three salt concentrations show a similar trend with respect to charge density: Only slight differences in the growth are observed between films from PA-100, PA-81 and PA-65. Virtually no differences are found at high ionic strength. But when lowering ionic strength, film thickness increases slightly as a function of decreasing charge density. In contrast, films deposited from PA-36 and PA-21 result in much thicker layers at all salt concentrations.
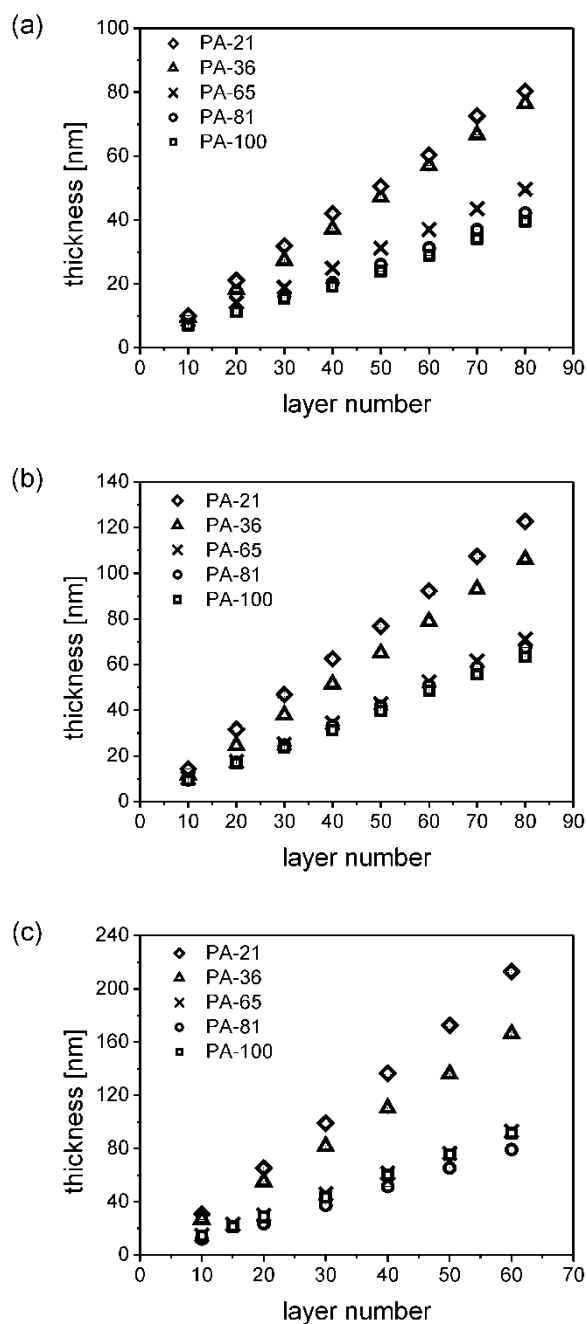
Fig. 4.4: Plot of the ellipsometric thickness as a function of the layer number (with PEI as first layer) of films with different charge densities (PA-21 (◊), PA-36 (Δ), PA-65 (×), PA-81 (○), PA-100 (□)) adsorbed from solutions containing (a) 0.02 M sodium chloride, (b) 0.05 M sodium chloride, and (c) 0.20 M sodium chloride. The error bars are smaller than the size of the symbols.

Figure 4.5a shows the thickness per adsorbed bilayer for the three salt concentrations studied. This behavior can be understood taking into account that secondary interactions for

our system are expected to be comparable for the charged and uncharged monomers. Therefore, mainly charge-related effects should dominate the film buildup. In all cases, multilayer formation is observed, indicating that the polyelectrolyte charge density is above the critical value for charge reversal.[33] The assumption that charge effects are dominating is corroborated by the fact that the thickness scales for all charge densities with the square-root of the ionic strength, as illustrated in Figure 4.5b. This scaling exponent was already found in several studies [64-66] for multilayers built up from linear polyelectrolytes.
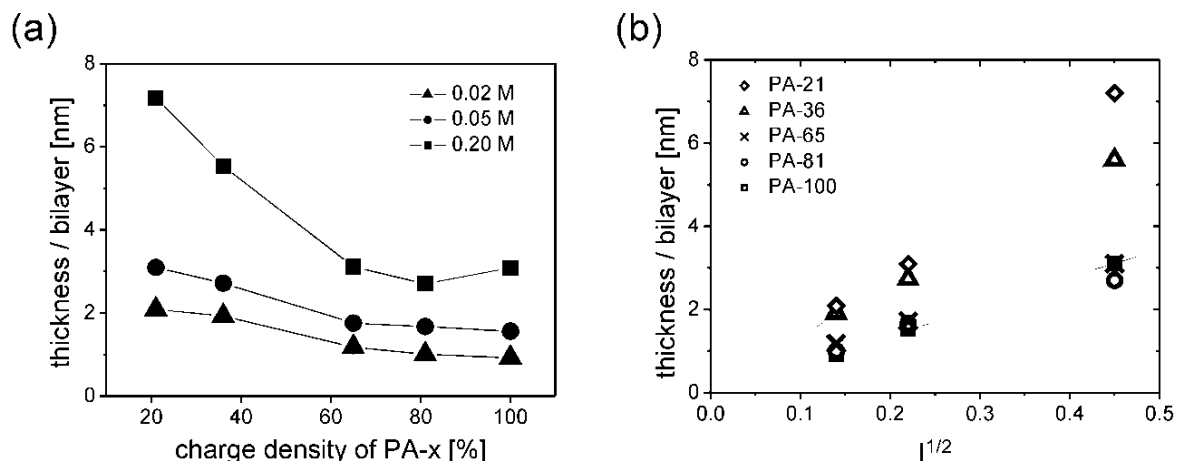

Fig. 4.5: (a) Thickness per bilayer versus charge density of PEI(PA-x/PC)$_n$ films deposited by alternated spraying of polyelectrolyte solutions in the presence of 0.02 M (Δ), 0.05 M (o), 0.20 M ($\square$) NaCl. (b) Thickness per bilayer of films prepared from PA-100 ($\square$), PA-81 (o), PA-65 ($\times$), PA-36 (Δ), and PA-21 ($\lozenge$) as a function of the square root of ionic strength (I). The lines are the fits to the data.

The differences in layer thickness can therefore be attributed to the fact that self-repulsion of the polyelectrolytes decreases with decreasing charge density, giving raise to higher film thicknesses as charge density decreases. The Rubner group[67] describes a different mechanism whereby it takes more material for the surface charge overcompensation if the linear charge density of the polyelectrolyte is reduced. Both mechanisms could account for the trends observed in our measurements. The added electrolyte screens the self-repulsion, as reflected in the fact, that at higher ionic strength, the differences between 65 to 100 percent charge density are vanishing, while they become more pronounced at lower ionic strength. While the trend of increasing thickness as a function of decreasing charge density can thus be rationalized, the pronounced increase of film thickness at a linear charge density below 36% especially at high ionic strength requires a more complex discussion. A possible reason for

the qualitative change of the adsorption behavior is that the linear charge density of the polyelectrolytes approaches the Manning-condensation threshold at this linear charge density, as proposed by Glinel *et al.*[34] The linear charge density (projected onto the backbone) is 6.9 Å, while the Bjerrum length in water is around 7 Å. Thus one expects that for charge densities above 36% Manning condensation effectively reduces the linear charge density in solution to a similar value for the polyelectrolytes with 65, 81 and 100%, resulting in a similar effective linear charge density for these species. In contrast, for lower charge densities, this "masking" effect of counterion condensation diminishes. In several studies on multilayers formed from polystyrene-sulfonate and charge-diluted poly[(diallyl-dimethyl-ammonium chloride)-*rand*-(N-methyl-N-vinyl acetamide)] (P(DADMAC-*rand*-NMVA)), an opposite trend was observed.[33, 66] Here, film thickness showed a pronounced decrease below a critical threshold of 40% − 50% DADMAC-content. The main difference between the system investigated here and P(DADMAC-*stat*-NMVA) is the highly hydrophilic nature of both the ionic as well as the non-ionic comonomers in P(DADMAC-*rand*-NMVA). This favors soluble polyelectrolyte complexes and acts against adsorption at low charge densities, thus preventing multilayer formation in this regime. Accordingly, the new system presented here might offer an access to low charge density regime.

The film roughness of these systems as a function of layer number was determined by AFM imaging, as shown in Figure 4.6. Here trends are less pronounced with regard to charge density. At high ionic strength, films show a nearly linear increase of the roughness with the number of added layers. Whereas the thicknesses of PA-65 and PA-100 films do not vary with the charge density, the film roughness is significantly influenced by it, decreasing with the increasing charge density. The mean roughness (R_a) of 60-layer for the fully charged system is 3.4 nm, while that of the 65% charged is 5.7 nm. This is in accordance with more coiled conformation of lower charged polymers in solution.[68] The roughness of 36% charged system remains almost constant about 3.0 − 3.1 nm over the studied range. With decreasing salt concentration, roughness decreases for all samples, which is as well in agreement with the picture that roughness is dominated by solution conformation of the polyelectrolytes.
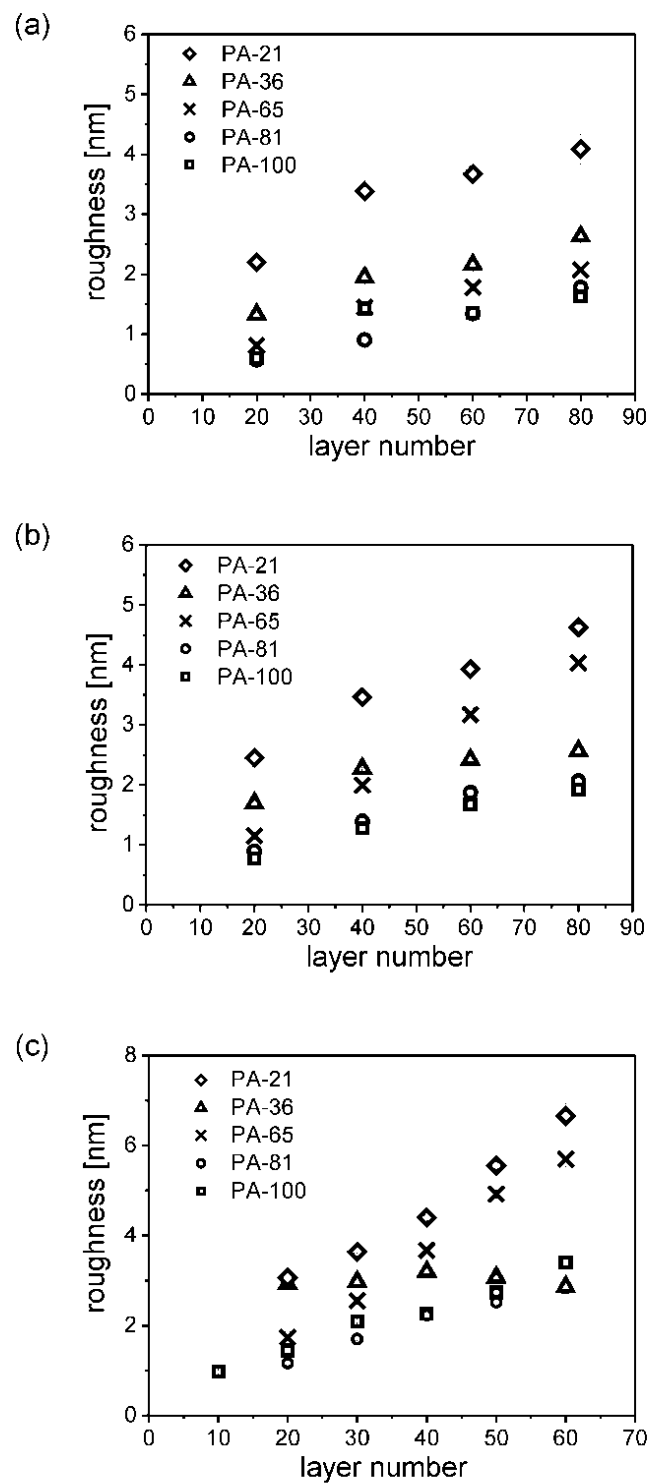
Fig. 4.6: Surface roughness (R_a) determined by AFM measurements *versus* the layer number of films with different charge densities (PA-21 (◊), PA-36 (Δ), PA-65 (×), PA-81 (○), PA-100 (□)) adsorbed from solutions containing (a) 0.02 M NaCl, (b) 0.05 M NaCl , and (c) 0.20 M NaCl.

4.3.3 Film cross-linking

The monomer units of the PC contain a CH-acidic methyl group, which offers the possibility of inter- and intramolecular cross-linking *via* a base catalyzed condensation reaction without affecting the number of ionic cross-links (Figure 4.7).
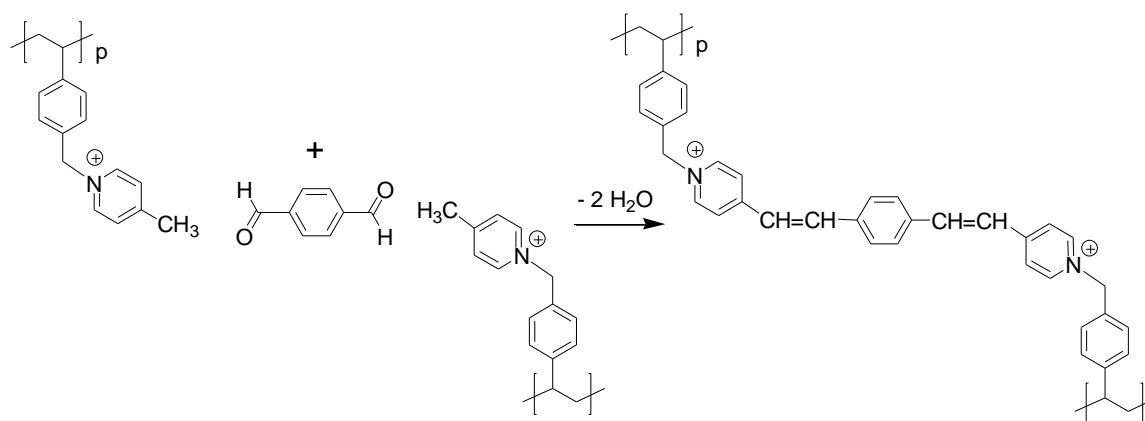

Fig. 4.7: Scheme of the aldol reaction applied for cross-linking multilayer films $(PA-x/PC)_n$.

The product of the cross-linking reaction shows a characteristic absorption at 365 nm, which offers the possibility to follow the process by UV-vis spectroscopy. Figure 4.8 shows the absorbance spectra of quartz-supported $PEI(PA-65/PC)_{25}$ multilayer film sprayed from solutions containing 0.20 M NaCl. While before cross-linking, the film is transparent between 300 nm and 600 nm, a new absorbance band of the coupling product is clearly visible after 1h of reaction and grows with time, indicating the increasing number of cross-links in the film.

The inset in Figure 4.8 shows that the absorption increment decreases with time, approaching asymptotically a final maximum value after about 9 h. To verify the success of the cross-linking reaction, the sample was immersed in to the cross-linking mixture for additional 3 h. No changes in the absorbance maximum were observed.
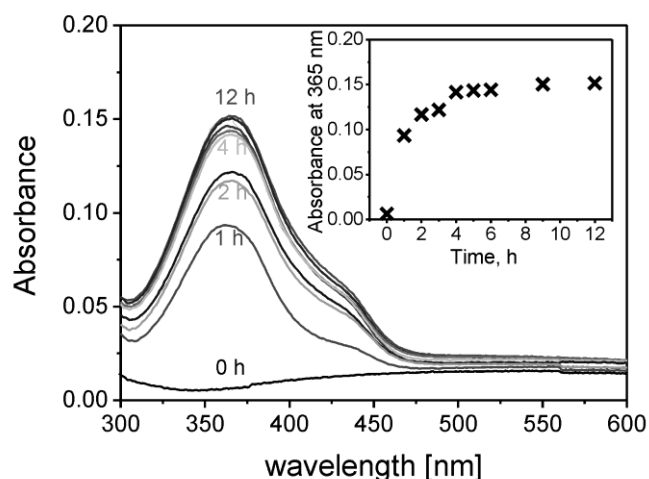
Fig. 4.8: Evolution of the UV-vis absorption spectra of films PEI(PA-65/PC)$_{25}$ film deposited from solutions containing 0.20 M NaCl with increasing time of cross-linking. The inset shows the absorbance at 365 nm *versus* the time of cross-linking.

4.3.4 Film stability

The stability of the cross-linked films relative to not cross-linked films, which are stabilized only by ionic bonds, was tested by immersion in a solution of H$_2$O:DMF:ZnCl$_2$. This ternary system is known to dissolve similar polyelectrolyte complexes efficiently.[69] Figure 4.9 displays the UV-vis absorption spectra of PEI(PA-65/PC)$_{25}$ assembled on quartz. The adsorption spectra of the non-crosslinked multilayer films (Fig. 4.9a) show characteristic peaks at 220 nm attributed to the benzylidene group of PA, and at 256 nm attributed to the pyridinium group of PC. After cross-linking, a new absorbance band at 365 nm appears, indicating the formation of the dicationic 1,4-bis(pyridinioethenyl) benzene chromophore as coupling product of two cationic pyridinium units (Fig. 4.9b).[53, 70] Note, that for cross-linked film only the absorbance spectra were recorded from 300 nm upwards, to exclude rigorously any possibly occuring photo induced side reaction, as the newly formed chromophore might be sensitive against intense UV light, inducing for instance a 2+2 photo cycloaddition.[71]

As can be clearly seen, the cross-linked samples are stable and no polymer desorption is detected, as demonstrated by the unchanged absorbance at 365 nm, when the film was treated in the ternary solvent 30 min (Fig 4.9c). In strong contrast, the absorbances at 220 nm and 256 nm of uncross-linked film nearly disappears after solvent treatment of only 10 seconds

74

(Fig. 4.9d), indicating the fast dissolution of the purely electrostatically stabilized LbL films, without any additional covalent bonds between the complementary polyelectrolytes.
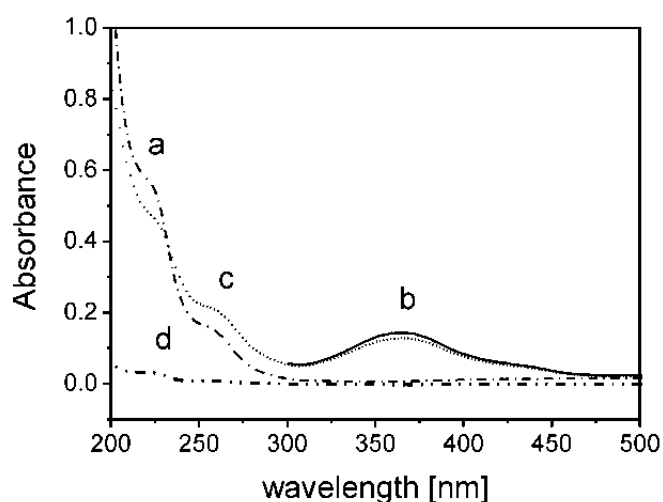

Fig. 4.9: UV-vis spectra of films PEI(PA-65/PC)$_{25}$ sprayed from solutions containing 0.2 M NaCl: (a) before cross-linking (·······) , (b) after cross-linking (——), (c) after cross-linking and treatment by a ternary solution of H$_2$O-DMF-ZnCl$_2$ for 30 min (·······), and (d) not cross-linked film after treatment by the ternary solution for 10 s (·········).

4.4 Summary and Conclusions

The assembly of novel polyanions with variable charge density and cross-linkable cationic polyelectrolyte prepared by spray-coating was studied, with focus on film buildup and crosslinking of the films.

Investigating the influence of ionic strength and charge density on the film buildup, a linear film growth as a function of the number of deposition cycles was found in all cases. Film thickness increased with increasing ionic strength, exhibiting a scaling behavior of the thickness proportional to the square-root of ionic strength. For all ionic strengths studied, film thicknesses increase with decreasing charge density. This trend can be rationalized by decreasing self-repulsion of the polyelectrolytes. Interestingly, a qualitative change between the charge densities of 65, 81 and 100% as compared to linear charge densities below 36% is observed: Especially at higher ionic strength, film thickness only varies little for the multilayers containing higher charge densities, while below 36% an increase up to a factor of two is observed. A possible explanation for this behavior is that at this charge level, the linear

charge density approaches one charge per Bjerrum length, the so-called Manning condensation threshold. Therefore, at higher charge densities, counterion condensation would reduce the effective charge of the polyelectrolytes to effectively the same value (strong screening).

Subsequently, we have studied cross-linking of the films by a base catalysed condensation. We took advantage of the fact that the crosslinks in this system can be easily detected by UV/Vis spectroscopy. The kinetics of the reaction could thus be quantified and we found a constant absorption after 4 hours of reaction time. The reaction mechanism allows for both inter- and intramolecular crosslink formation. In order to check whether the stability of the films was improved due to intermolecular crosslinks, we carried out stability tests on crosslinked and non-crosslinked samples which show a stabilizing effect of the crosslinking procedure.

In conclusion, the system offers several advantages as compared to charge-diluted polyelectrolytes previously introduced in the literature: It combines a statistical copolymer nature which allows tuning of linear charge density with a hydrophobic backbone. This ensures multilayer assembly even for low charge densities, because the additional hydrophobic interactions and the corresponding lower solubility favor adsorption of the polyelectrolytes. This regime was previously often not accessible, although it is interesting from a fundamental point-of-view: Especially the case, that charge densities approach or drop below the Manning condensation threshold gives raise to novel and more pronounced charge density effects than the regime of higher charge densities, because effects are no longer "masked" by counterion-condensation. The data for the lowest charge densities reported here points towards such effects and the synthetic approach could provide a good route towards even lower charge densities.

As well, the system reported here can be cross-linked. The cross-linking pathway offers two main advantages: First, the charge density of the charge diluted part is not affected in the process. Thus the system remains controlled in its anionic charge density even in the crosslinked state, which provides perspectives for studying the correlations between crosslinking and charge density on mechanical properties in the future. Second, cross-linking causes spectroscopic changes. A characteristic absorption wavelength is linked to the formation of crosslinks. Therefore, crosslinking of the films can be directly followed by UV-Vis spectroscopy. Thus the system gives perspectives for quantifying crosslinking kinetics and crosslink densities. Additionally, rupture of crosslinks due to chemical degradation or mechanical strains could be directly detected *in situ*.

Acknowledgements

References

1.   Iler, R. K., Multilayers of Colloidal Particles. *Journal of Colloid and Interface Science* **1966,** 21, (6), 569-594.

2.   Decher, G.; Schmitt, J., Fine-tuning of the film thickness of ultrathin multilayer films composed of consecutively alternating layers of anionic and cationic polyelectrolytes. *Progress in Colloid & Polymer Science* **1992,** 89, 160-164.

3.   Decher, G.; Hong, J. D.; Schmitt, J., Buildup of Ultrathin Multilayer Films by a Self-Assembly Process. 3. Consecutively Alternating Adsorption of Anionic and Cationic Polyelectrolytes on Charged Surfaces. *Thin Solid Films* **1992,** 210, (1-2), 831-835.

4.   Decher, G., Fuzzy nanoassemblies: Toward layered polymeric multicomposites. *Science* **1997,** 277, (5330), 1232-1237.

5.   Bertrand, P.; Jonas, A.; Laschewsky, A.; Legras, R., Ultrathin polymer coatings by complexation of polyelectrolytes at interfaces: suitable materials, structure and properties. *Macromolecular Rapid Communications* **2000,** 21, (7), 319-348.

6.   Decher, G.; Schlenoff, J. B., *Multilayer Thin Films: Sequential Assembly of Nanocomposite Materials. .* Wiley-VCH Verlag GmbH & Co. KGaA, Weinheim, Germany: **2003**; p 524 pp.

7.   Cho, J. H.; Quinn, J. F.; Caruso, F., Fabrication of polyelectrolyte multilayer films comprising nanoblended layers. *Journal of the American Chemical Society* **2004,** 126, (8), 2270-2271.

8.   Quinn, A.; Tjipto, E.; Yu, A. M.; Gengenbach, T. R.; Caruso, F., Polyelectrolyte blend multilayer films: Surface morphology, wettability, and protein adsorption characteristics. *Langmuir* **2007,** 23, (9), 4944-4949.

9. Quinn, A.; Such, G. K.; Quinn, J. F.; Caruso, F., Polyelectrolyte blend multilayers: A versatile route to engineering interfaces and films. *Advanced Functional Materials* **2008,** 18, (1), 17-26.

10. Podsiadlo, P.; Paternel, S.; Rouillard, J. M.; Zhang, Z. F.; Lee, J.; Lee, J. W.; Gulari, L.; Kotov, N. A., Layer-by-layer assembly of nacre-like nanostructured composites with antimicrobial properties. *Langmuir* **2005,** 21, (25), 11915-11921.

11. Lu, C. H.; Dönch, I.; Nolte, M.; Fery, A., Au nanoparticle-based multilayer ultrathin films with covalently linked nanostructures: Spraying layer-by-layer assembly and mechanical property characterization. *Chemistry of Materials* **2006,** 18, (26), 6204-6210.

12. Jaber, J. A.; Schlenoff, J. B., Recent developments in the properties and applications of polyelectrolyte multilayers. *Current Opinion in Colloid & Interface Science* **2006,** 11, (6), 324-329.

13. Mamedov, A. A.; Kotov, N. A., Free-standing layer-by-layer assembled films of magnetite nanoparticles. *Langmuir* **2000,** 16, (13), 5530-5533.

14. Farhat, T. R.; Schlenoff, J. B., Corrosion control using polyelectrolyte multilayers. *Electrochemical and Solid State Letters* **2002,** 5, (4), B13-B15.

15. Andreeva, D. V.; Fix, D.; Mohwald, H.; Shchukin, D. G., Self-healing anticorrosion coatings based on pH-sensitive polyelectrolyte/inhibitor sandwichlike nanostructures. *Advanced Materials* **2008,** 20, (14), 2789-2794.

16. Andreeva, D. V.; Fix, D.; Mohwald, H.; Shchukin, D. G., Buffering polyelectrolyte multilayers for active corrosion protection. *Journal of Materials Chemistry* **2008,** 18, (15), 1738-1740.

17. Jiang, C. Y.; Markutsya, S.; Tsukruk, V. V., Compliant, robust, and truly nanoscale free-standing multilayer films fabricated using spin-assisted layer-by-layer assembly. *Advanced Materials* **2004,** 16, (2), 157-161.

18. Mallwitz, F.; Laschewsky, A., Direct access to stable, freestanding polymer membranes by layer-by-layer assembly of polyelectrolytes. *Advanced Materials* **2005,** 17, (10), 1296-1299.

19. Lavalle, P.; Boulmedais, F.; Ball, V.; Mutterer, J.; Schaaf, P.; Voegel, J. C., Free standing membranes made of biocompatible polyelectrolytes using the layer by layer method. *Journal of Membrane Science* **2005,** 253, (1-2), 49-56.

20. Nolte, M.; Schoeler, B.; Peyratout, C. S.; Kurth, D. G.; Fery, A., Filled microcavity arrays produced by polyelectrolyte multilayer membrane transfer. *Advanced Materials* **2005,** 17, (13), 1665-1669.

21. Nolte, M.; Fery, A., Freestanding polyelectrolyte multilayers as functional and construction elements. *IEE Proceedings-Nanobiotechnology* **2006,** 153, (4), 112-120.

22. Ferri, J. K.; Dong, W. F.; Miller, R.; Möhwald, H., Elastic moduli of asymmetric ultrathin free-standing polyelectrolyte nanocomposites. *Macromolecules* **2006,** 39, (4), 1532-1537.

23. Nolte, M.; Dönch, I.; Fery, A., Freestanding polyelectrolyte films as sensors for osmotic pressure. *Chemphyschem* **2006,** 7, (9), 1985-1989.

24. Sukhorukov, G.; Fery, A.; Möhwald, H., Intelligent micro- and nanocapsules. *Progress in Polymer Science* **2005,** 30, (8-9), 885-897.

25. Johnston, A. P. R.; Cortez, C.; Angelatos, A. S.; Caruso, F., Layer-by-layer engineered capsules and their applications. *Current Opinion in Colloid & Interface Science* **2006,** 11, (4), 203-209.

26. Choi, J.; Rubner, M. F., Influence of the degree of ionization on weak polyelectrolyte multilayer assembly. *Macromolecules* **2005,** 38, (1), 116-124.

27. Cochin, D.; Passmann, M.; Wilbert, G.; Zentel, R.; Wischerhoff, E.; Laschewsky, A., Layered nanostructures with LC-polymers, polyelectrolytes, and inorganics. *Macromolecules* **1997,** 30, (16), 4775-4779.

28. Passmann, M.; Wilbert, G.; Cochin, D.; Zentel, R., Nematic ionomers as materials for the build-up of multilayers. *Macromolecular Chemistry and Physics* **1998,** 199, (2), 179-189.

29. Arys, X.; Jonas, A.; Laguitton, B.; Legras, R.; Laschewsky, A.; Wischerhoff, E., Structural studies on thin organic coatings built by repeated adsorption of polyelectrolytes. *Progress in Organic Coatings* **1998,** 34, (1-4), 108-118.

30. Arys, X.; Fischer, P.; Jonas, A. M.; Koetse, M. M.; Laschewsky, A.; Legras, R.; Wischerhoff, E., Ordered polyelectrolyte multilayers. Rules governing layering in organic binary multilayers. *Journal of the American Chemical Society* **2003,** 125, (7), 1859-1865.

31. Laschewsky, A.; Mallwitz, F.; Baussard, J. F.; Cochin, D.; Fischer, P.; Jiwan, J. L. H.; Wischerhoff, E., Aggregation phenomena in polyelectrolyte multilayers made from polyelectrolytes bearing bulky functional, hydrophobic fragments. *Macromolecular Symposia* **2004,** 211, 135-155.

32. Hoogeveen, N. G.; Stuart, M. A. C.; Fleer, G. J., Polyelectrolyte adsorption on oxides .1. Kinetics and adsorbed amounts. *Journal of Colloid and Interface Science* **1996,** 182, (1), 133-145.

33. Steitz, R.; Jaeger, W.; von Klitzing, R., Influence of charge density and ionic strength on the multilayer formation of strong polyelectrolytes. *Langmuir* **2001,** 17, (15), 4471-4474.

34. Glinel, K.; Moussa, A.; Jonas, A. M.; Laschewsky, A., Influence of polyelectrolyte charge density on the formation of multilayers of strong polyelectrolytes at low ionic strength. *Langmuir* **2002,** 18, (4), 1408-1412.

35. Kharlampieva, E.; Sukhishvili, S. A., Polyelectrolyte multilayers of weak polyacid and cationic copolymer: Competition of hydrogen-bonding and electrostatic interactions. *Macromolecules* **2003,** 36, (26), 9950-9956.

36. Qu, D.; Pedersen, J. S.; Garnier, S.; Laschewsky, A.; Möhwald, H.; von Klitzing, R., Effect of polymer charge and geometrical confinement on ion distribution and the structuring in semidilute polyelectrolyte solutions: Comparison between AFM and SAXS. *Macromolecules* **2006,** 39, (21), 7364-7371.

37. Delorme, N.; Dubois, M.; Garnier, S.; Laschewsky, A.; Weinkamer, R.; Zemb, T.; Fery, A., Surface immobilization and mechanical properties of catanionic hollow faceted polyhedrons. *Journal of Physical Chemistry B* **2006,** 110, (4), 1752-1758.

38. Köhler, R.; Dönch, I.; Ott, P.; Laschewsky, A.; Fery, A.; Krastev, R., Neutron Reflectometry Study of Swelling of Polyelectrolyte Multilayers in Water Vapors:

Influence of Charge Density of the Polycation. *Langmuir* **2009,** 25, (19), 11576-11585.

39. Laschewsky, A.; Mayer, B.; Wischerhoff, E.; Arys, X.; Jonas, A.; Kauranen, M.; Persoons, A., A new technique for assembling thin, defined multilayers. *Angewandte Chemie-International Edition* **1997,** 36, (24), 2788-2791.

40. Koetse, M.; Laschewsky, A.; Mayer, B.; Rolland, O.; Wischerhoff, E., Ultrathin coatings by multiple polyelectrolyte adsorption/surface activation (CoMPAS). *Macromolecules* **1998,** 31, (26), 9316-9327.

41. Baussard, J. F.; Habib-Jiwan, J. L.; Laschewsky, A.; Mertoglu, M.; Storsberg, J., New chain transfer agents for reversible addition-fragmentation chain transfer (RAFT) polymerisation in aqueous solution. *Polymer* **2004,** 45, (11), 3615-3626.

42. Schlenoff, J. B.; Dubas, S. T.; Farhat, T., Sprayed polyelectrolyte multilayers. *Langmuir* **2000,** 16, (26), 9968-9969.

43. Izquierdo, A.; Ono, S. S.; Voegel, J. C.; Schaaff, P.; Decher, G., Dipping versus spraying: Exploring the deposition conditions for speeding up layer-by-layer assembly. *Langmuir* **2005,** 21, (16), 7558-7567.

44. Kern, W.; Puotinen, D. A., Cleaning Solutions Based on Hydrogen Peroxide for Use in Silicon Semiconductor Technology. *RCA Review* **1970,** 31, (2), 187-206.

45. Phillips, A. P., Condensation of Aromatic Aldehydes with Gamma-Picoline Methiodide. *Journal of Organic Chemistry* **1949,** 14, (2), 302-305.

46. Harris, J. J.; DeRose, P. M.; Bruening, M. L., Synthesis of passivating, nylon-like coatings through cross-linking of ultrathin polyelectrolyte films. *Journal of the American Chemical Society* **1999,** 121, (9), 1978-1979.

47. Wu, G. J.; Su, Z. H., Polyhedral oligomeric silsesquioxane nanocomposite thin films via layer-by-layer electrostatic self-assembly. *Chemistry of Materials* **2006,** 18, (16), 3726-3732.

48. Hendricks, T. R.; Lee, I., Wrinkle-free nanomechanical film: Control and prevention of polymer film buckling. *Nano Letters* **2007,** 7, (2), 372-379.

49. Crouzier, T.; Picart, C., Ion Pairing and Hydration in Polyelectrolyte Multilayer Films Containing Polysaccharides. *Biomacromolecules* **2009,** 10, (2), 433-442.

50. Sun, J. Q.; Wu, T.; Sun, Y. P.; Wang, Z. Q.; Zhang, X.; Shen, J. C.; Cao, W. X., Fabrication of a covalently attached multilayer via photolysis of layer-by-layer self-assembled films containing diazo-resins. *Chemical Communications* **1998**, (17), 1853-1854.

51. Yang, Z. H.; Cao, W. X., Self-assemblies based on poly (4-diazonium styrene). *Macromolecular Chemistry and Physics* **2004,** 205, (2), 241-246.

52. Zhang, L. L.; Peng, Z. H.; Yao, L. H.; Lv, F. Z.; Li, X., Photoalignment of liquid crystals using a covalently attached self-assembled ultrathin film fabricated from diazoresin and cinnamate polyelectrolyte. *Journal of Materials Chemistry* **2007,** 17, (29), 3015-3022.

53. Stathatos, E.; Lianos, P.; Rakotoaly, R. H.; Laschewsky, A.; Zana, R., Photophysical behavior of a new gemini surfactant in neat solvents and in micellar environments. *Journal of Colloid and Interface Science* **2000,** 227, (2), 476-481.

54. Laschewsky, A.; Wischerhoff, E.; Bertrand, P.; Delcorte, A., Polyelectrolyte multilayers containing photoreactive groups. *Macromolecular Chemistry and Physics* **1997,** 198, (10), 3239-3253.

55. Vuillaume, P. Y.; Jonas, A. M.; Laschewsky, A., Ordered polyelectrolyte "multilayers". 5. Photo-cross-linking of hybrid films containing an unsaturated and hydrophobized poly(diallylammonium) salt and exfoliated clay. *Macromolecules* **2002,** 35, (13), 5004-5012.

56. Park, M. K.; Deng, S. X.; Advincula, R. C., Sustained release control via photo-cross-linking of polyelectrolyte layer-by-layer hollow capsules. *Langmuir* **2005,** 21, (12), 5272-5277.

57. Olugebefola, S. C.; Ryu, S. W.; Nolte, A. J.; Rubner, M. F.; Mayes, A. M., Photo-cross-linkable polyelectrolyte multilayers for 2-D and 3-D patterning. *Langmuir* **2006,** 22, (13), 5958-5962.

58.   Vazquez, C. P.; Boudou, T.; Dulong, V.; Nicolas, C.; Picart, C.; Glinel, K., Variation of Polyelectrolyte Film Stiffness by Photo-Cross-Linking: A New Way To Control Cell Adhesion. *Langmuir* **2009,** 25, (6), 3556-3563.

59.   Connal, L. A.; Kinnane, C. R.; Zelikin, A. N.; Caruso, F., Stabilization and Functionalization of Polymer Multilayers and Capsules via Thiol-Ene Click Chemistry. *Chemistry of Materials* **2009,** 21, (4), 576-578.

60.   Schlenoff, J. B.; Li, M., Kinetics and multilayering in the adsorption of polyelectrolytes to a charged surface. *Berichte Der Bunsen-Gesellschaft-Physical Chemistry Chemical Physics* **1996,** 100, (6), 943-947.

61.   Lvov, Y.; Ariga, K.; Onda, M.; Ichinose, I.; Kunitake, T., Alternate assembly of ordered multilayers of SiO_2 and other nanoparticles and polyions. *Langmuir* **1997,** 13, (23), 6195-6203.

62.   Lvov, Y.; Decher, G.; Möhwald, H., Assembly, Structural Characterization, and Thermal-Behavior of Layer-by-Layer Deposited Ultrathin Films of Poly(Vinyl Sulfate) and Poly(Allylamine). *Langmuir* **1993,** 9, (2), 481-486.

63.   Dubas, S. T.; Schlenoff, J. B., Factors controlling the growth of polyelectrolyte multilayers. *Macromolecules* **1999,** 32, (24), 8153-8160.

64.   Steitz, R.; Leiner, V.; Siebrecht, R.; von Klitzing, R., Influence of the ionic strength on the structure of polyelectrolyte films at the solid/liquid interface. *Colloids and Surfaces A-Physicochemical and Engineering Aspects* **2000,** 163, (1), 63-70.

65.   Ruths, J.; Essler, F.; Decher, G.; Riegler, H., Polyelectrolytes I: Polyanion/polycation multilayers at the air/monolayer/water interface as elements for quantitative polymer adsorption studies and preparation of hetero-superlattices on solid surfaces. *Langmuir* **2000,** 16, (23), 8871-8878.

66.   Voigt, U.; Jaeger, W.; Findenegg, G. H.; Klitzing, R. V., Charge effects on the formation of multilayers containing strong polyelectrolytes. *Journal of Physical Chemistry B* **2003,** 107, (22), 5273-5280.

67.   Shiratori, S. S.; Rubner, M. F., pH-dependent thickness behavior of sequentially adsorbed layers of weak polyelectrolytes. *Macromolecules* **2000,** 33, (11), 4213-4219.

68.   Kolarik, L.; Furlong, D. N.; Joy, H.; Struijk, C.; Rowe, R., Building assemblies from high molecular weight polyelectrolytes. *Langmuir* **1999,** 15, (23), 8265-8275.

69.   Sun, J. Q.; Long, C. B.; Liu, F.; Dong, S. J.; Wang, Z. Q.; Zhang, X.; Shen, J. C., Covalently attached multilayer assemblies containing photoreactive diazo-resins and conducting polyaniline. *Colloids and Surfaces A-Physicochemical and Engineering Aspects* **2000,** 169, (1-3), 209-217.

70.   Zheng, H. P.; Zhang, R. F.; Wu, Y.; Shen, J. C., Blue-green light emission from self-assembled bipyridinium thin films. *Chemistry Letters* **1998**, (9), 909-910.

71.   Gromov, S. P.; Ushakov, E. N.; Fedorova, O. A.; Baskin, I. I.; Buevich, A. V.; Andryukhina, E. N.; Alfimov, M. V.; Johnels, D.; Edlund, U. G.; Whitesell, J. K.; Fox, M. A., Novel photoswitchable receptors: Synthesis and cation-induced self-assembly into dimeric complexes leading to stereospecific [2+2]-photocycloaddition of styryl dyes containing a 15-crown-5 ether unit. *Journal of Organic Chemistry* **2003,** 68, (16), 6115-6125.

72.   Skrabania, K.; Kristen, J.; Laschewsky, A.; Akdemir, O.; Hoth, A.; Lutz, J. F., Design, synthesis, and aqueous aggregation behavior of nonionic single and multiple thermoresponsive polymers. *Langmuir* **2007,** 23, (1), 84-93.

4.5 Supporting Information

Table S1. Elemental analysis of the copolymers prepared

entry	polymer	C [%]	H [%]	S [%]
1	PA-100	47.67	5.24	20.94
2	PA-81	50.98	5.29	21.19
3	PA-65	51.91	5.61	18.80
4	PA-36	52.83	5.58	19.97
5	PA-21	58.19	6.44	17.02

Figure S1.   Copolymerization diagramm of monomers 3-(4-vinylbenzylsulfanyl)-propane-1-sulfonate) (1) and poly(2-hydroxyethyl-vinylbenzyl sulfoxide (2).
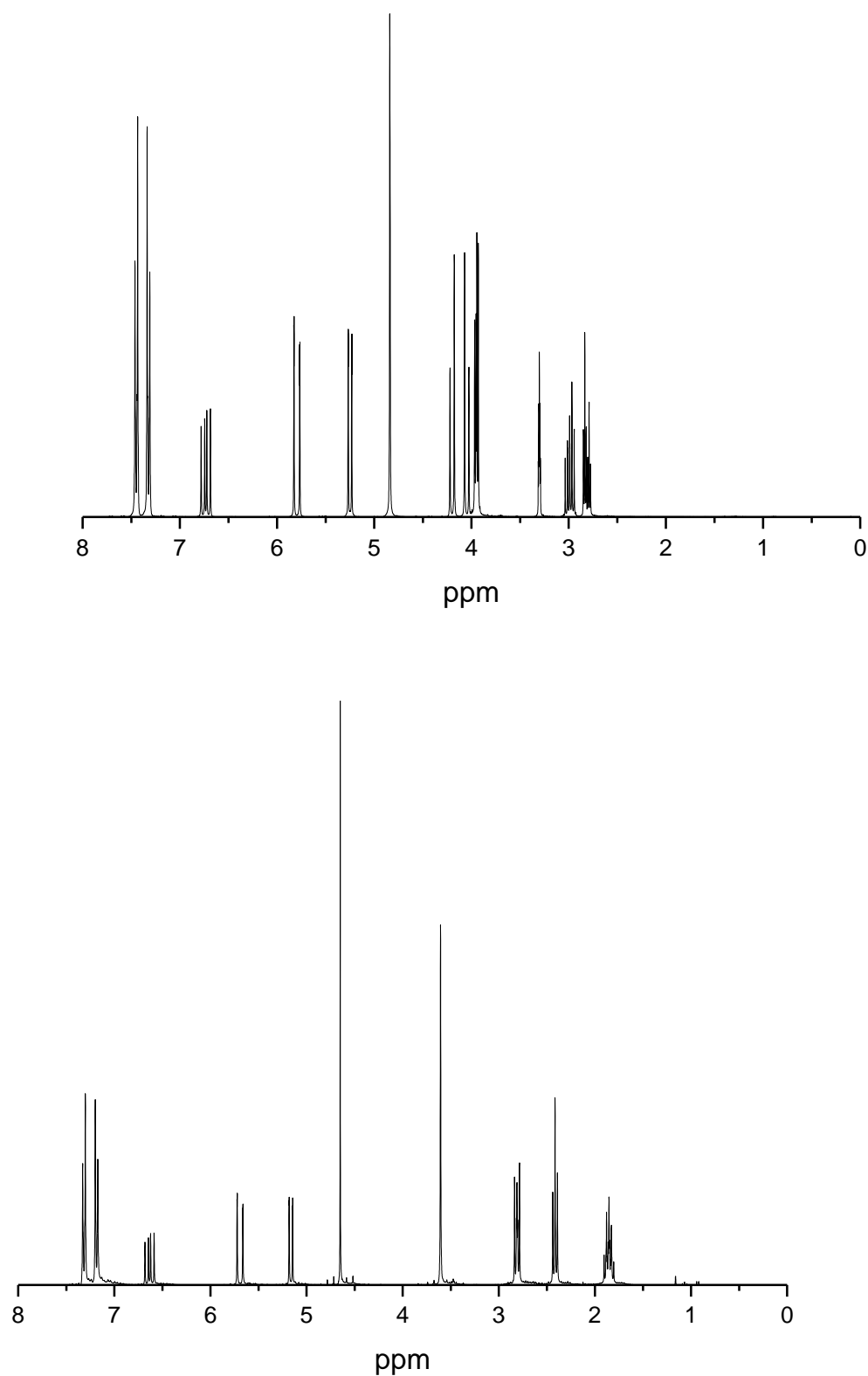
Figure S2. 1H-NMR spectra of monomers 3-(4-vinylbenzylsulfanyl)-propane-1-sulfonate) (1) in D2O (bottom) and of 2-hydroxyethyl-vinylbenzyl sulfoxide (2) in CD3OD (top).
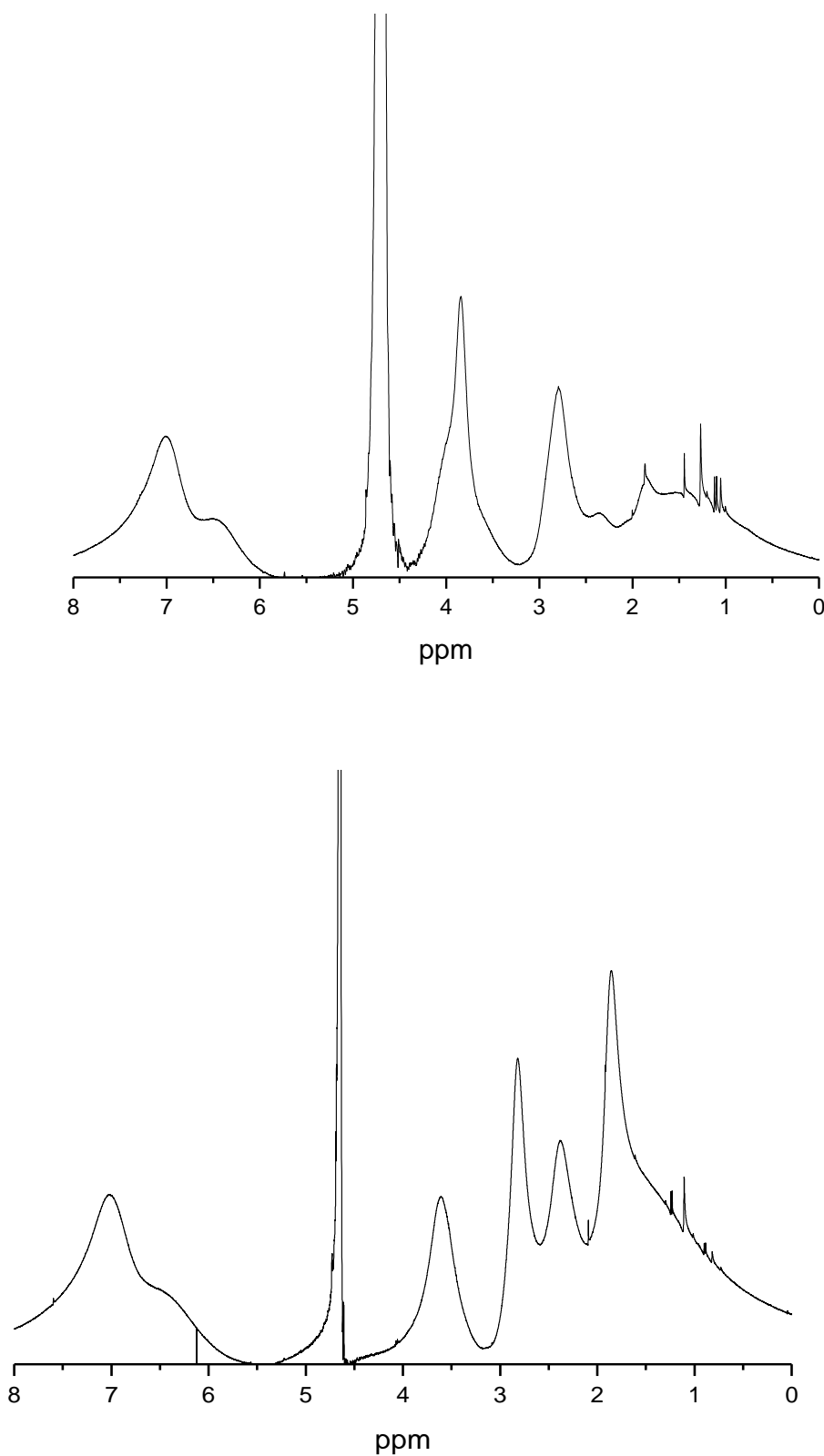
Figure S3.   1H-NMR spectra of homopolymer poly(3-(4-vinylbenzylsulfanyl)-propane-1-sulfonate) (PA-100) (bottom) and of copolymer poly[(3-(4-vinylbenzylsulfanyl)-propane-1-sulfonate)-co-2-hydroxyethyl-vinylbenzyl sulfoxide] (PA-36) in CD3OD (top) in D_2O.
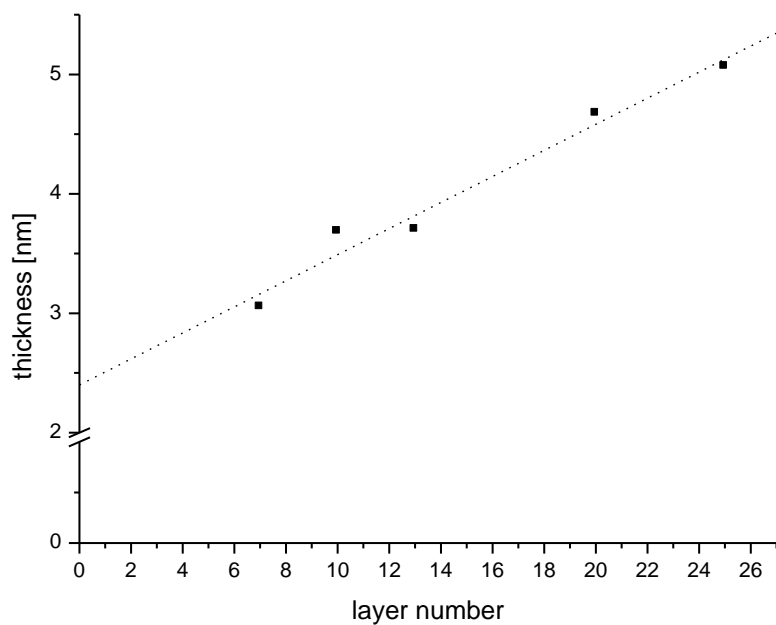
Figure S4. Build-up of layer-by-layer films from PA-100 and PC from aqueous solutions without any additional salt, as prepared by dip-coating. Thicknesses measured by ellipsometry.

5 Surface Immobilized Block Copolymer Micelles with Switchable Accessibility of Hydrophobic Pockets

Julia Gensel,[a] Eva Betthausen,[b] Christoph Hasenöhrl,[a] Katja Trenkenschuh,[a] Markus Hund,[a] Fouzia Boulmedais,[c] Pierre Schaaf,[c] Axel. H. E. Müller,[b] Andreas Fery[a,]*
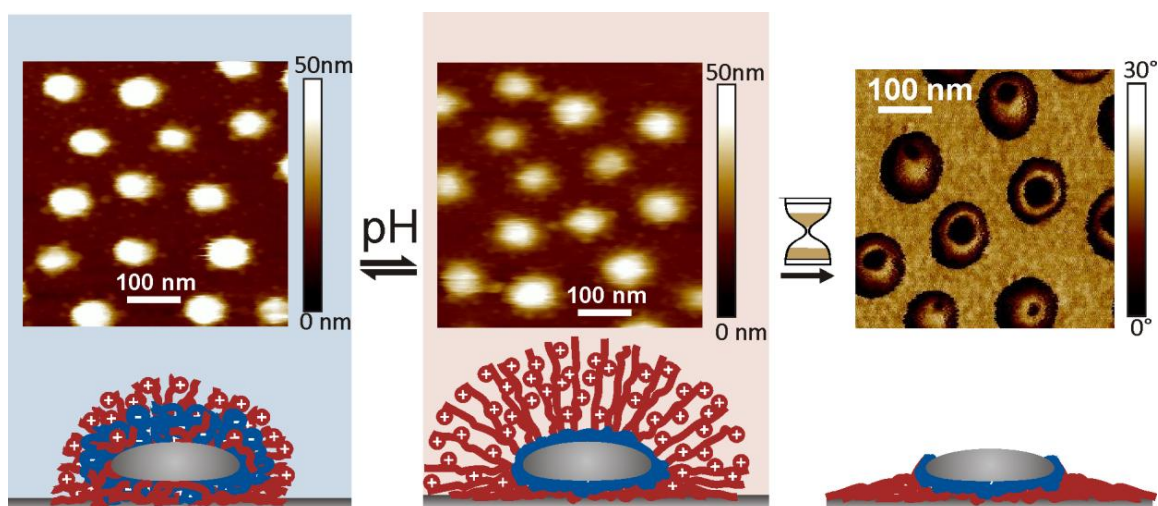
[a] Physical Chemistry II, University of Bayreuth, Universitätsstr. 30, 95440 Bayreuth, Germany

[b] Macromolecular Chemistry II, University of Bayreuth, Universitätsstr. 30, 95440 Bayreuth, Germany

[c] Institut Charles Sadron, Université de Strasbourg, Centre National de la recherche scientifique, UPR 22, 23 rue du Loess, 67034 Strasbourg Cedex, France.

* e-mail: Andreas.Fery@uni-bayreuth.de

Abstract

We report on a novel approach for the design of stimuli-responsive surfaces based on the immobilization of charged ABC triblock terpolymer micelles. The terpolymer consists of a hydrophobic polybutadiene (B) block, a weak anionic poly(methacrylic acid) (MAA) middle block, and a strong cationic end block of quaternized poly(2-(dimethylamino)ethyl methacrylate) (Dq) (BMAADq). In alkaline solutions, this polymer self-assembles into core-shell-corona micelles with a hydrophobic B core, a pH-sensitive MAA/Dq intramicellar interpolyelectrolyte complex (*im*-IPEC) shell, and a cationic corona of excess Dq. These micelles were directly adsorbed onto charged silica as a monolayer creating lateral structured surfaces. The adsorption kinetics was found to follow the theoretical model of random sequential adsorption (RSA). Exposure of the adsorbed micelles to external stimuli (at pH < $pK_{a,apparent}$ of PMAA) induces *im*-IPEC dissolution due to protonation of the MAA block resulting in a changed composition of the shell and both the length and charge density of the corona. Two types of conformational response to pH trigger and therefore, two types of dynamics coupled to short and long relaxation times are involved in the system. The response to pH cycling was shown to be reversible on the short-term scale while the long-term exposure to acidic media causes irreversible changes in the morphology of the micelles as a consequence of the micelles' core mobility and slow rearrangement. In particular, we find that exposure to low pH causes a shape transition to a "doughnut"-like morphology, exposing the core parts of the micelles. In contrast, adsorbed micelles with covalently crosslinked B cores show higher stability to irreversible morphology changes while maintaining the reversible response to pH cycling.

5.1 Introduction

The creation of functional surface coatings based on soft matter systems with lateral structure continues to be an attractive research objective in current materials science. Laterally homogeneous surfaces can be obtained by grafting of polymer or polyelectrolyte brushes onto a solid support.[1-3] Alternatively, layer-by-layer deposition of oppositely charged polyelectrolytes allows the formation of laterally homogeneous multilayer films.[4-7] The patterning of these systems can be achieved by additional processes, such as photolithography or micro-contact printing (μCP)[8-10] and selective deposition of polymeric material to pre-patterned surfaces.[11-13]

An alternative approach for laterally structured surfaces is the use of block copolymers by means of spontaneous self-assembly[14-16] or by adsorption of micellar systems.[17-25] The latter case has the advantage to provide regular monolayers of isolated round-shaped particles. Moreover, patterning is possible on the nano-scale, which is difficult to obtain by the methods mentioned above.

One special class of systems used for the preparation of surface coatings is that of stimuli-responsive materials.[26] The interest in such systems originates from the possibility to develop surface coatings for a number of applications[26] including triggerable drug delivery[27-29], nanoreactors for *in-situ* preparation of metal nanoparticles[18, 25, 30], and "smart" surfaces.[23, 31-34] They show reversible or irreversible response to external stimuli like temperature, pH, ionic strength, or light. In particular after the introduction of stimuli-responsive self-assembly of amphiphilic polystyrene-*block*-poly(acrylic acid) diblock copolymers by Eisenberg and co-workers,[35] stimuli-responsive block copolymer micelles have attracted the attention of many research groups[36, 37]

Generally, block copolymer micelles are dynamic structures and show responsiveness to environmental changes.[38,39] Micellar structures can be "quenched" by covalent crosslinking of the core or shell.[39-41] Another approach to stabilize block copolymer micelles is the reversible ionic complexation of oppositely charged blocks.[42, 43] Unlike the covalently crosslinked systems, interpolyelectrolyte complexes (IPECs) can be disassembled by increasing the ionic strength of the solution or, in the case of weak polyelectrolytes, by changes in pH.[44, 45] ABC triblock terpolymer micelles,[46, 47] having both cationic and anionic blocks, are of specific interest as they can form intramicellar IPECs (*im*-IPECs) without extrinsic crosslinking agents. Recently, Müller and co-workers have reported on dynamic micelles of different triblock terpolymers, which exhibit a core-shell-corona structure with an *im*-IPEC shell.[48, 49, 50] The McCormick group introduced the term "self-locked" micelles to clearly distinguish this intramicellar crosslinking process from ionic crosslinking by an extrinsic homopolymer.[51] Very recently, double-layered micellar IPECs were prepared from "self-locked" triblock terpolymer precursor micelles with an *im*-IPEC and a second IPEC with an extrinsic homopolymer resulting in a core-shell-shell-corona structure.[49, 52]

Several research groups have studied the adsorption of diblock copolymer micelles onto planar surfaces.[19-21, 23, 24] The immobilization of stimuli-responsive block copolymer micelles onto solid substrates provides an opportunity to design "smart" surfaces with nano-patterned structure combined with the response to external stimuli, which in solution would lead to

aggregation. At the same time, pH-regions that are inaccessible in solution due to colloidal stability issues can be investigated.

Herein, we report on the surface immobilization of stimuli-responsive ABC triblock terpolymer micelles. The terpolymer is composed of a hydrophobic polybutadiene (B) block, a pH-responsive poly(methacrylic acid) (MAA) middle block, and a permanently charged cationic end block of quaternized poly(2-(dimethylamino)ethyl methacrylate) (Dq) (BMAADq). Since the middle block, MAA, is a weak polyacid, the micelles should be pH-sensitive. In alkaline solutions (pH > $pK_{a,\text{apparent}}$ of PMAA ~ 5.5), this polymer self-assembles into core-shell-corona micelles with a hydrophobic B core, a MAA/Dq intramicellar interpolyelectrolyte complex (*im*-IPEC) shell, and a cationic corona of uncomplexed Dq. The structure of the micelles in solution was studied by cryogenic transmission electron microscopy (cryo-TEM) and dynamic light scattering (DLS) and is described in detail elsewhere.[50] In the present work, the morphology of a monolayer of adsorbed micelles, their adsorption kinetics on silica as well as the pH response of adsorbed micelles on both short and long-term scales were studied by atomic force microscopy (AFM), scanning electron microscopy (SEM), and quartz crystal microbalance with dissipation monitoring (QCM-D). The slow irreversible response of adsorbed micelles to acidic pH was compared with that of micelles with a covalently crosslinked B core.

5.2 Materials and Methods

5.2.1 Materials

The triblock terpolymer $B_{800}MAA_{200}Dq_{285}$ (subscripts denoting the degrees of polymerization of the corresponding blocks, M_n ~ 110 000 g/mol, PDI = 1.10) was synthesized via sequential living anionic polymerization in THF followed by polymer-analogous modifications. Details about polymerization and characterization can be found elsewhere.[50] The crosslinking of the micellar B core (x-BMAADq) was performed in aqueous solutions with a UV photoinitiator, Lucirin-TPO (2,4,6-trimethylbenzoylphosphine oxide, BASF), and irradiation with an UV lamp (Hoehnle UVAHAND 250 GS, cut-off at 300 nm).[53, 54]

The adsorption experiments were performed with BMAADq micelles at concentrations of 0.11, 0.23, and 0.45 g/L and with x-BMAADq micelles at a concentration of 0.45 g/L in commercial pH 10 buffer solutions (AVS Titrinorm from VWR, ionic strength ~ 0.05 M).

5.2.2 Adsorption of BMAADq micelles on solid surfaces

For the adsorption experiments, silicon wafers (CrysTec) with a silica layer of 1.3 nm were used. The silicon substrates were cleaned using the RCA method (sonication in a 1:1 mixture of water and 2-propanol for 15 min),[55] followed by heating at 70 °C in a 5:1:1 mixture of water, 25 % ammonia solution, and 30 % hydrogen peroxide solution for 10 min. For the QCM-D experiments, QCM sensor crystals (Q-Sense) coated with a ~50 nm thick SiO_2 layer were used.

The triblock terpolymer micelles were adsorbed on freshly cleaned substrates from a 0.45 g/L BMAADq in pH 10 buffer solution via the dip coating method. After one hour the substrate was rinsed with milli-Q water (18.2 MΩ cm) and dried with a stream of nitrogen.

For the kinetic study, Si-wafers were dipped into 0.11, 0.23, and 0.45 g/L BMAADq in pH 10 buffer solution for controlled periods of time (1-120 min). The substrates were then removed from the solution, rinsed with milli-Q water and dried with nitrogen.

5.2.3 pH treatment of pre-adsorbed micelles

Short-term treatment was performed *in situ* in contact with aqueous solutions of different pH. For the pH adjustment, HCl and NaOH were used. For the long-term treatment, substrates with pre-adsorbed micelles were immersed into aqueous solutions of pH 4. After treatment, the substrates were intensively rinsed with milli-Q water and dried with nitrogen.

5.2.4 Characterization methods

Atomic force microscopy (AFM) images of dried samples were taken with a commercial AFM (Dimension[TM] 3100 equipped with a NanoScope® V controller, Veeco Instruments Inc., USA) operating in TappingMode[TM] using Si_3N_4 cantilevers (OMCL-AC160TS, Olympus) with a typical spring constant of 42 N/m, a typical resonance frequency of 300 kHz and a tip radius less than 7 nm. For the imaging, light tapping (ratio of setpoint amplitude to free amplitude ~ 0.9) was applied. The mean number of adsorbed micelles was determined from at least three images of 5 μm × 5 μm size for each sample using the NanoScope Analysis software version 1.20. To study the morphology changes of adsorbed micelles after

long-term treatment in pH 4, *ex situ* AFM measurements on the same spot of the sample were performed before and after the treatment.

Liquid cell AFM measurements were performed on a Dimension[TM] 3100 Nanoscope® V operating in TappingMode[TM] using cantilevers (SNL-10, Bruker) with a spring constant of 0.24 N/m.

Scanning electron microscopy (SEM) measurements were obtained on a Gemini Leo 1550 instrument operating at 3 keV. Samples were sputtered with a 1.3 nm thin platinum layer.

Cryo-TEM studies were performed on a Zeiss EM922 OMEGA EFTEM instrument according to a standard procedure described before.[49]

The quartz crystal microbalance (QCM-D) measurements were performed on a Q-Sense E1 apparatus from Q-Sense AB (Gothenburg, Sweden) by monitoring the resonance frequencies f and the dissipation factor D of an oscillating quartz crystal upon adsorption of a viscoelastic layer.[56, 57] The silicon-coated quartz crystal was excited at its fundamental frequency (5 MHz), and the measurements were performed at the first, third, fifth and seventh overtones, corresponding to 5, 15, 25 and 35 MHz. The QCM measurement is sensitive to the amount of water associated to the adsorbed molecules and senses the viscoelastic changes in the interfacial material.[56] The thickness and the viscosity of the adsorbed layer can be estimated using the viscoelastic Voigt model.[58] For the evaluation, the fluid density (1009 kg/m^3), fluid viscosity (0.91 mPa·s) and layer density (1000 kg/m^3) were kept constant. The thickness was estimated using the 3rd, 5th and 7th overtones. The estimated chi square values for the fitted data are listed in Table S1 (Supporting Information). Prior to adding the BMAADq solution, the sensor was allowed to equilibrate in pH 4 water and pH 10 buffer solution for 25 and 15 minutes, respectively to obtain the respective baseline used for the thickness and viscosity evaluation of the adsorbed layer. After the terpolymer micelles injection and signal equilibration, the sensor was rinsed with pH 10 buffer to remove residual polymer, and then, the rinsing water was repeatedly cycled from pH 10 or 7 to pH 4.

Ellipsometry measurements were performed with a Sentech SE 850 spectroscopic ellipsometer at a constant incidence angle of 70°.

5.3 Results and Discussion

5.3.1   Solution structure

The amphiphilic polymer used in this study is a linear ABC triblock terpolymer consisting of polybutadiene (B), poly(methacrylic acid) (MAA), and quaternized poly(2-(dimethylamino)ethyl methacrylate) (Dq), $B_{800}MAA_{200}Dq_{285,}$ (subscripts denoting the degrees of polymerization of the corresponding blocks, M_n ~ 110 000 g/mol, PDI = 1.10). For simplicity, the polymer will be denoted as BMAADq throughout the manuscript. BMAADq was synthesized via sequential living anionic polymerization followed by polymer-analogous modifications as reported before.[50] Its chemical structure is shown in Figure 5.1a. In aqueous solutions, BMAADq self-assembles into core-shell-corona micelles with a hydrophobic B core. The solution structure of BMAADq is dependent on pH: at high pH, the attraction between the deprotonated MAA and the positively charged Dq blocks induces the formation of an intramicellar interpolyelectrolyte complex (*im*-IPEC) shell. According to the polymerization degrees ($DP_n(MAA) < DP_n(Dq)$), parts of the cationic Dq block remain uncomplexed forming a positively charged corona. The core-shell-corona structure of the BMAADq micelles was confirmed by cryogenic transmission electron microscopy (cryo-TEM).[50] Figure 5.1b shows a cryo-TEM micrograph of the BMAADq micelles at pH 10 with spherical shape and uniform size. The dark hydrophobic B core of 72 nm diameter is surrounded by a 31 nm thick, grey *im*-IPEC shell. The water soluble Dq corona is not visible in the cryo-TEM micrograph due to its low electron density. From dynamic light scattering (DLS) measurements, we obtained a hydrodynamic diameter of the micelles of ~208 nm.[50] The schematic representation of the obtained core-shell-corona micelles is shown in Figure 5.1b. Dyalysis of BMAADq micelles to low pH (pH 4) results in a formation of a new 11 nm thin dark shell, which could be attributed to collapsed MAA indicating the dissolution of the electrostatic complex between the MAA and Dq (Fig. 5.1c). Furthermore, the core diameter decreases from 72 to 64 nm while the hydrodynamic diameter increases slightly to ~214 nm.[50]
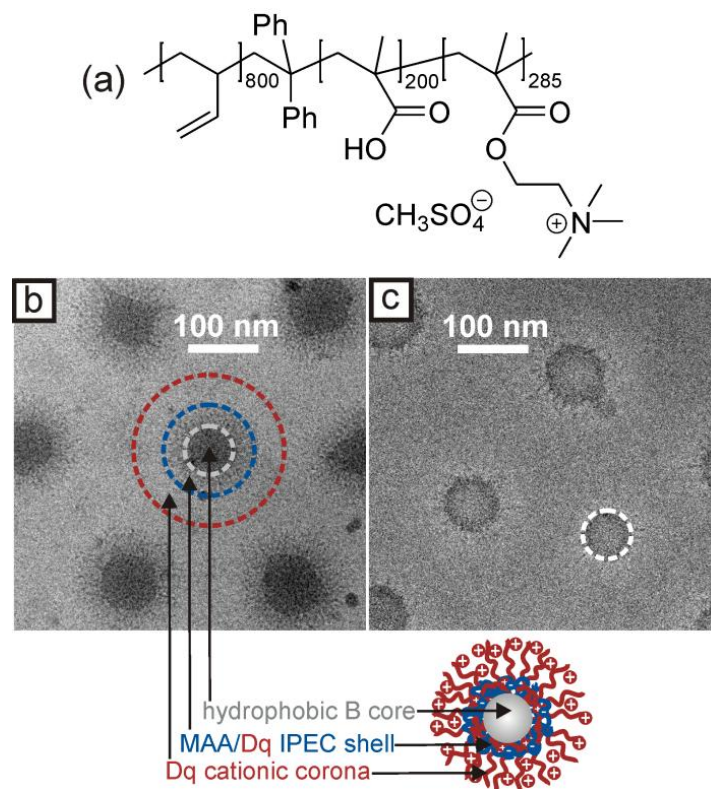
Fig. 5.1: (a) Chemical structure of the BMAADq terpolymer; (b) 500 nm × 500 nm cryo-TEM micrograph and schematic representation of BMAADq core-shell-corona micelles in alkaline solution (pH 10 buffer). Dashed circles indicate the dimensions of the core (grey) and *im*-IPEC shell (blue) obtained from cryo-TEM and the dimensions of the corona determined by DLS (red). (c) 500 nm × 500 nm cryo-TEM micrograph of BMAADq micelles in acidic solution (pH 4 buffer, dashed circle indicates the dimensions of the core (grey)).

5.3.2   Surface assembly

For all adsorption experiments, core-shell-corona micelles with *im*-IPEC shell (in pH 10 buffer, Fig. 5.1b) were used. Due to the positive charge of the Dq corona, one would expect a direct adsorption of the BMAADq micelles onto negatively charged surfaces. Therefore, negatively charged silica was used to immobilize the triblock terpolymer micelles, which were assembled by dip-coating. The characterization of the adsorbed micelles was carried out by scanning electron microscopy (SEM) and atomic force microscopy (AFM) in dry state.
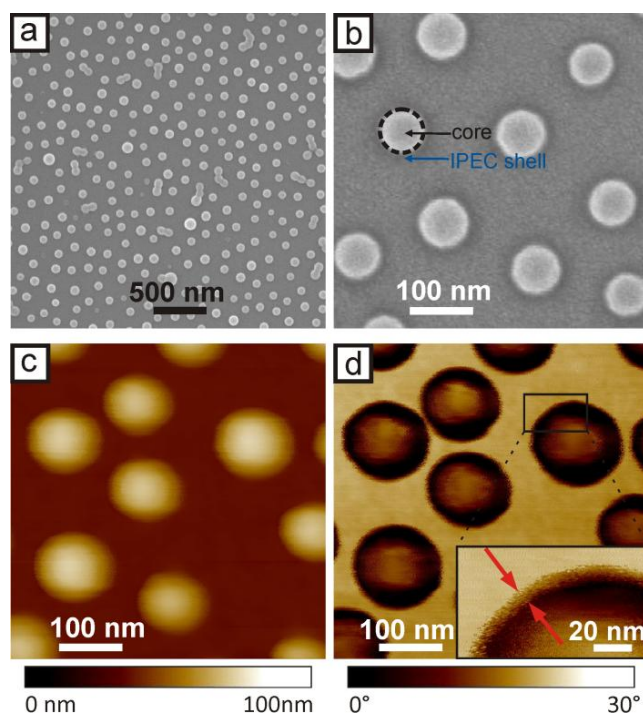
Fig. 5.2: 3 µm × 3 µm SEM image of a monolayer of dry BMAADq micelles adsorbed on a Si wafer (a), 500 nm × 500 nm SEM image of adsorbed micelles with a hydrophobic core (bright, marked by dashed circle) surrounded by an *im*-IPEC shell (dark) (b), 500 nm × 500 nm AFM height (c), and phase image (d) of BMAADq micelles adsorbed on a Si wafer and observed in dry state. Arrows in the enlarged AFM phase image (d, inset) indicate the dimensions of the adsorbed corona.

Figure 5.2a shows a SEM image of dry micelles adsorbed on a Si wafer. The BMAADq micelles form regular arrays of particles with uniform size and spherical-cap shape. The driving force for the surface immobilization is the release of counterions and hydration water upon adsorption.[59, 60] The adsorption of coronal chains onto the silica surface inhibits the rearrangement of attached micelles. Electrostatic repulsion between already adsorbed micelles and micelles in solution in conjunction with steric interactions prevent further particle adsorption. As a result, a monolayer of micelles is formed, as often reported for the adsorption behavior of charged soft[19, 20, 61-63] or rigid colloidal particles.[64, 65]

An enlarged SEM image in Figure 5.2b shows adsorbed micelles in a dry state with a hydrophobic core (bright) surrounded by an *im*-IPEC shell and a collapsed corona (dark) indicating that the core-shell-corona structure of the triblock terpolymer micelles remains intact upon adsorption to a solid support. The diameter of the micellar core is (78 ± 4) nm based on the average of at least 30 micelles. The average diameter of the adsorbed micelles in

the dry state as measured by AFM, corresponding to the diameter of the core and shell, is (124 ± 9) nm and the height is (42 ± 5) nm based on the average of at least 50 micelles. The convolution effect of the tip shape can introduce overestimated lateral dimensions. This effect is of particular relevance for structures having a high aspect ratio and small lateral sizes comparable to the tip radius. However, in our case, the sample features are much larger than the tip radius (Fig. 5.2c). Therefore, the convolution effect can be neglected.

Compared to the dimensions in solution the core diameter increases slightly upon adsorption and drying while the height decreases. The flattening of the micelles upon adsorption could be explained by a relaxation of attached chains, while the non-adsorbed coronal chains on the top collapse upon drying. Similar flattening of block copolymer micelles due to the relaxation of coronal chains upon adsorption was also reported before.[19, 21] The AFM phase image (Fig. 5.2d, inset) gives additional information about the thickness of the surrounding adsorbed Dq corona, which is 7-8 nm. Including the thickness of the adsorbed corona, which is not detectable in the topography images, the total diameter of the adsorbed micelles is (139 ± 7) nm. Compared to the dimensions in solution, the micellar diameter is decreased and is comparable with the diameter of the micelles in solution excluding the corona (~134 nm).

Due to the additional quantitative analysis of the morphology (phase images), AFM was chosen for further investigations. Moreover, the ability of scanning surfaces in liquids by AFM gives the possibility of monitoring particle response to external stimuli (pH).

5.3.3   Adsorption kinetics

To gain insight into the kinetic aspects of the adsorption process, we used *ex situ* AFM to study the density of adsorbed micelles as a function of time. As the micelles were adsorbed from a buffer solution with an ionic strength of ~ 0.05 M (Debye length ~ 1.4 nm), they can be handled as hard spheres due to the screening of the repulsive long-range interactions. Giving this and that the micelles adsorb on random locations, we used a method of counting particles adsorbed with cumulative time.[20, 61, 65]

Fig. 5.3 shows a series of typical AFM height images of micelles adsorbed from 0.45 g/L BMAADq solution in pH 10 buffer (ionic strength ~ 0.05 M). The amount of adsorbed micelles increases rapidly during the first five minutes. At longer adsorption times (15, 30 and 60 minutes), the silica surface appears to become saturated.
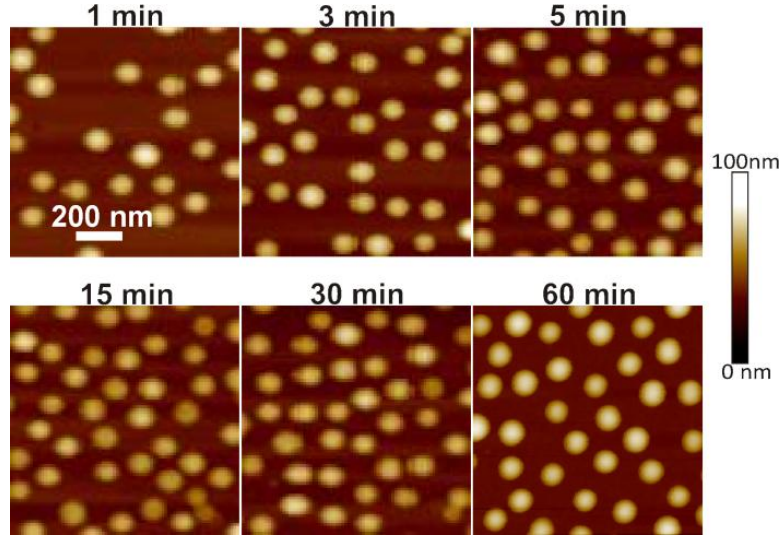
Fig. 5.3: A series of 1 μm × 1 μm AFM height images of BMAADq micelles adsorbed on Si wafers from 0.45 g/L solutions in pH 10 buffer without added salt.

The saturation effect of the adsorption process can be shown clearly by plotting the number of adsorbed micelles as a function of the adsorption time. The mean number of micelles was calculated from at least three 5 μm × 5 μm AFM images of BMAADq adsorbed from 0.11, 0.23, and 0.45 g/L solutions in pH 10 buffer without added salt and is displayed in Figure 5.4a. At all three concentrations, the amount of attached micelles increased rapidly in the initial state of adsorption and reached asymptotically the same saturation value.
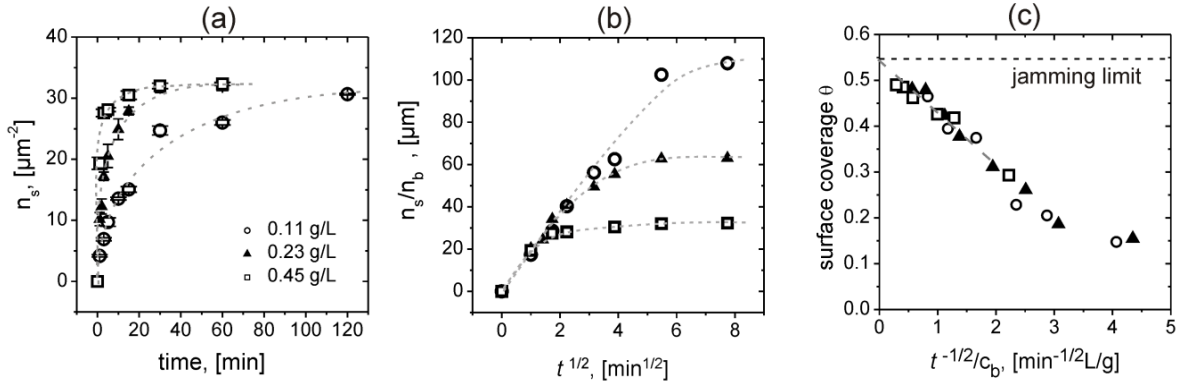

Fig. 5.4: Mean number of adsorbed micelles, n_s, for different concentrations of BMAADq (0.11 (○), 0.23 (▲), and 0.45 g/L (□) solutions in pH 10 buffer (ionic strength ~ 0.05 M)) calculated from *ex situ* AFM measurements as a function of the adsorption time t (a); mean number of adsorbed micelles normalized to the number of micelles in the bulk solution, n_b, vs. $t^{1/2}$ (b); surface coverage θ vs. $t^{-1/2}$ normalized to the solution bulk concentration c_b (c). Dashed lines are guides to the eye.

At the initial adsorption state, micelles that are transported to the surface are not influenced by already adsorbed micelles. Therefore, the adsorption process should be diffusion limited and the number of adsorbed micelles $n_s(t)$ (per unit area) should be proportional to the square root of the adsorption time t according to[66]

$$n_s(t) = 2n_b \sqrt{\frac{D_s t}{\pi}}$$

(5.1)

where n_b is the number of micelles (per unit volume) in the bulk solution, and D_s the diffusion coefficient of micelles to the silica surface.

A plot of the kinetic data normalized to the number of micelles in solution as a function of the square root of time shows the expected linear relationship at the initial state of adsorption (Figure 5.4b). For the three studied concentrations, the slope of the plots in the initial adsorption state is similar, and the mean value of D_s, calculated using Eq. (5.1) is equal 4.04 $\times 10^{-8}$ cm^2/s. The diffusion coefficient D_b of micelles in bulk solution was estimated at 2.10 $\times 10^{-8}$ cm^2/s by DLS. Although different determination methods were used, the experimentally observed initial adsorption rate of BMAADq micelles onto silica is in a reasonable agreement with the diffusion in the bulk solution, which verifies the validity of the diffusion limited regime in the initial adsorption state.

The asymptotical characteristics of micelle adsorption result from surface exclusion effects[67] and have a direct analogy to the theoretical model of random sequential adsorption (RSA) of monodisperse hard spheres.[68, 69] The RSA model describes a non-equilibrium process, in which particles are irreversibly attached one by one at random locations on a uniform surface. If the system exhibits RSA kinetics, the surface coverage should asymptotically approach a jamming limit $\theta(\infty)$ according to the relationship[68]

$$\theta(\infty) - \theta(t) \propto t^{-1/2}$$

(5.2)

The surface coverage $\theta(t)$ can be calculated according to the equation $\theta(t) = n_S \pi R_{AFM}^2$, where n_s is the mean number of adsorbed micelles (per unit area) and R_{AFM} the radius of adsorbed micelles estimated from AFM phase images. Figure 5.4c shows the surface coverage vs. $t^{-1/2}$ normalized to the concentration. For all studied concentrations, the surface coverage scales with $t^{-1/2}$ at longer adsorption times. Extrapolation to the ordinate gives a mean limiting coverage of 0.54 (corresponding to the maximum density of adsorbed micelles $n_{s,max}$ =

35 μm^{-2}), which is in a very good agreement with the theoretical jamming limit of 0.547 for the adsorption of monodisperse hard spheres.[70, 71]

5.3.4 Stimulus response

BMAADq micelles belong to the class of shell-crosslinked micelles.[41] Unlike covalent crosslinks, ion-pairing like in polyelectrolyte complexes or multilayers can be disassembled by increasing the ionic strength or, in the case of weak polyelectrolytes, by changes in pH.[44, 45] Since MAA is a weak polyelectrolyte (p$K_{a,app}$ ~ 5.5[72]), one would expect changes in the properties and structure of the micelles in response to stimuli like pH and/or ionic strength. Accordingly, the charge density of this block can be adjusted by the pH of the solution.

Reversible stimulus response: short-term effect of pH change

The charge density of the MAA block can be represented by the degree of ionization as a function of pH. In the pH range between 4 and 7, the ionization degree, denoted α, increases from 0 to unity.[73, 74] Therefore, we used an *in situ* quartz crystal microbalance with dissipation monitoring (QCM-D) to follow the pH-induced switching of adsorbed micelles in these two extreme cases. The QCM measurement is sensitive to the amount of water associated to the adsorbed micelles and senses the viscoelastic changes in the interfacial material. A decrease in QCM frequency represents as a first approximation an increase in thickness.

Representative data of frequency and dissipation changes for pH cycling are shown in Figure 5.5a. After adsorption and rinsing with pH 10 buffer, the adsorbed micelles were rinsed with aqueous solutions of pH above (pH 10 or pH 7) and below (pH 4) the pK_a of the pH-sensitive MAA middle block. The adsorbed micelles show a rapid response to pH cycling. The decrease in the frequency shift at pH 4, i.e. increase in thickness, is consistent with the protonation of the MAA block (α ~ 0) leading to *im*-IPEC dissolution. Indeed, the uncharged MAA block collapses onto the B core forming a new shell, and the length of the positively charged Dq corona then increases. Longer coronal chains involve swelling of the micelles due to the sorption of additional water and counterions. In conjunction with the decrease in frequency shift, a 6-fold increase in dissipation occurs due to micelles swelling. By increasing the pH to 10, the regeneration of the *im*-IPEC due to the deprotonation of MAA (α ~ 1) leads to an increase in frequency shift and a decrease in dissipation. The thickness and the viscosity of the adsorbed layer can be estimated using the viscoelastic Voigt model (Figure 5.5b). At

pH > pK_a of MAA, the adsorbed micelles exhibit a reduced thickness (55 nm compared to 82 nm) and a higher viscosity as compared to pH 4 respectively due to collapsed Dq corona and to a lower amount of hydration water in the presence of the *im*-IPEC. This short-term response to pH changes is completely reversible after several cycling steps. The disassembly of the *im*-IPEC was also confirmed by cryo-TEM measurements of BMAADq micelles in acidic solutions (Fig. 5.1c).[50]
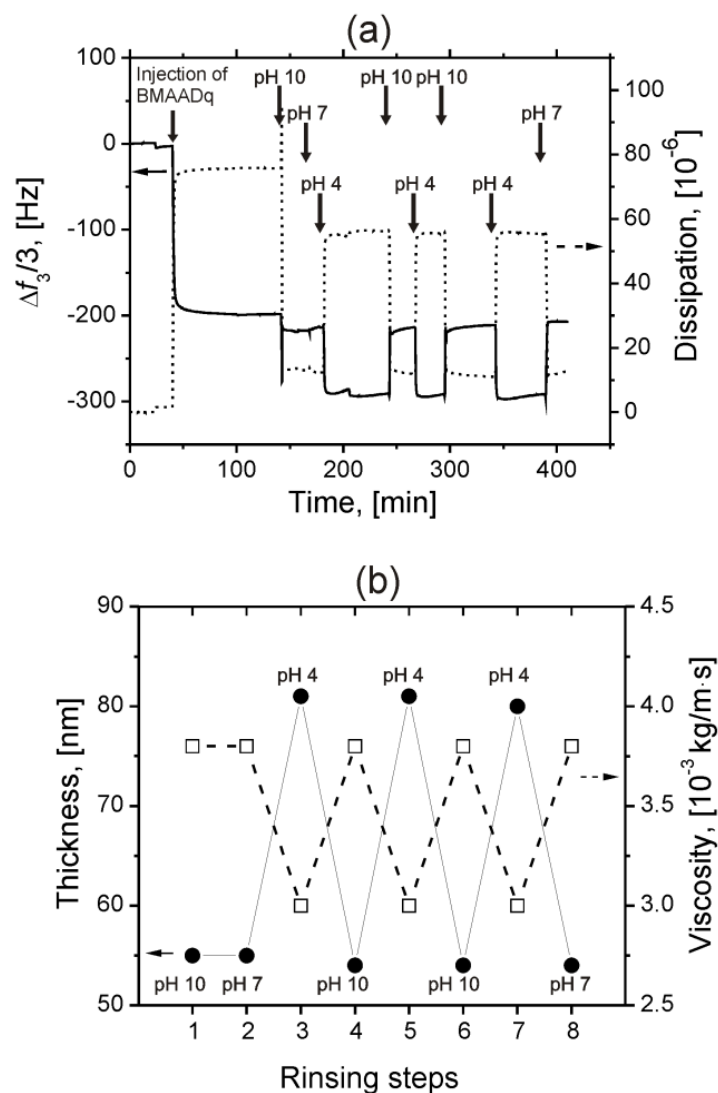

Fig. 5.5: QCM-D frequency shifts (continuous lines) and dissipation changes (dashed lines), obtained from 15 MHz harmonics (overtone *n* = 3), *versus* time during the adsorption of BMAADq micelles (0.45 g/L in pH 10 buffer) followed by several rinsing steps with water at different pH (a); calculated thickness and viscosity, using the viscoelastic Voigt model, of the monolayer of swollen micelles in response to pH cycling (b).

The corresponding AFM images of pre-adsorbed terpolymer micelles in the presence of pH 7 and pH 4 water are shown in Fig. 5.6a and 5.6b, respectively. The AFM images strongly correlate with the data observed by QCM-D measurements. Under neutral pH conditions, the height of micelles (43 ± 5) nm is comparable with the height of dry micelles (42 ± 5) nm but smaller compared to QCM data. In contrast, the height of micelles determined by AFM at pH 4 decreased to (27 ± 4) nm (*cf.* cross-sectional height profiles in Fig. 5.6c) but increased to 82 nm according to QCM. The schematic representation of the topography switching is shown in Figure 6d. The dissolution of the *im*-IPEC under acidic conditions causes the formation of an uncharged collapsed MAA shell and a long Dq corona, which is penetrable for the AFM tip and therefore not detectable in the topography images in contrary to QCM that allows determining the hydrodynamic thickness of the micelles, including the Dq corona. Similar observations have been reported in the literature: Hamley *et al.,* for example, performed *in situ* AFM imaging of amphiphilic diblock copolymer micelles observing that AFM is only imaging the core of the micelle rather than the diffuse corona.[24] Similarly, cylindrical brushes with a hard poly(acrylic acid) core and a soft poly(*n*-butyl acrylate) shell only showed the hard core in the height image.[75]
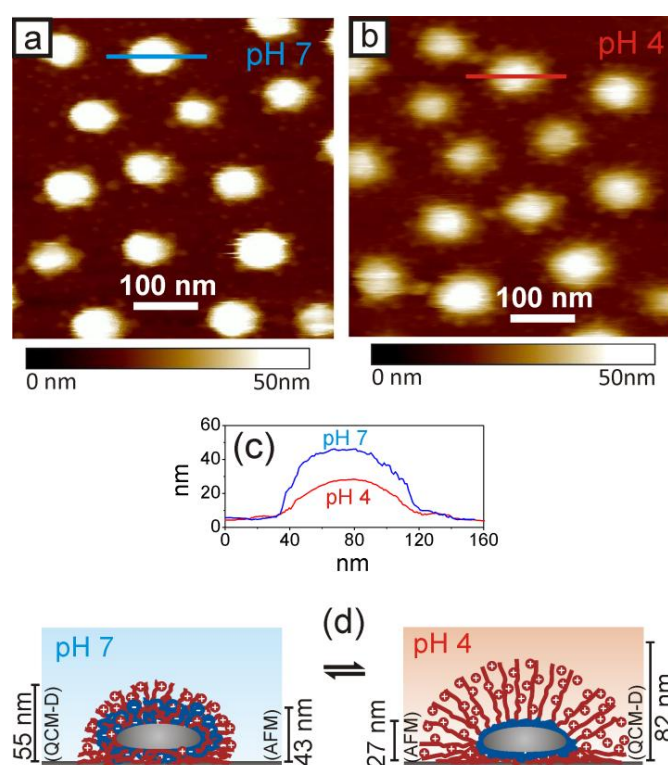

Fig. 5.6: *in situ* liquid cell AFM height images (500 nm × 500 nm) of pre-adsorbed BMAADq micelles in pH 7 water (a) and pH 4 water (b) with corresponding cross-sectional height profiles (c), and proposed reversible response of an adsorbed BMAADq micelle (d).

Irreversible stimulus response: long-term effect of pH change

On the one hand, the disassembly of the *im*-IPEC due to the loss of ionic crosslinking in acidic solutions leads to the formation of new interfaces both within the micelle and with water as well as to an increase in the coronal length and charge density. These structural rearrangements are expected to result in changes in the aggregation number of the micelles to minimize the total free energy. The analogous pH decrease from 10 to 4 in the micellar solution lead to a decreased core radius of 32 nm compared to 36 nm at high pH, which might serve as an indication for a dynamic response of the system towards pH change.[50] On the other hand, the desorption process of adsorbed polyelectrolyte chains is entropically unfavourable. This would have two effects: first, the mobility of chains within the micelle should be retarded through entanglements and physically attached chains. Secondly, the changes in the lateral dimensions of the adsorbed micelles should be hindered. This, together with the strong electrostatic repulsion of coronal chains in the absence of the *im*-IPEC, can induce intramicellar microphase separation of adsorbed micelles if the experimental time is comparable with the longest relaxation time.

The fast pH cycling process in the previous section was shown to be completely reversible as the free energy cannot be minimized on such short-time scales. To gain insight into the much slower process of thermodynamic equilibration that involves a change in the aggregation number, we performed long-term treatment of the adsorbed micelles under acidic conditions. The surface morphology was studied *ex situ* by AFM. To precisely follow structural changes of the micelles, we performed measurements on exactly the same spot of the sample before and after the pH treatment and drying. Figure 5.7 shows the AFM topography (left) and phase (right) images of the same spot of the sample observed before (Figure 5.7a) and after 20 hours contact with pH 4 water (Figure 5.7b).

The height image of the adsorbed micelles after long-term treatment in acidic solution (Fig. 5.7b, left) shows no changes in diameter, but a significant decrease in height from (42 ± 5) nm to (25 ± 6) nm. The measured height profile (Fig. 5.7c) indicates some deepening towards the middle of the treated micelle, which could be attributed to the deformation of the soft B core by the AFM tip.[76] In contrast, no shape deformation was found for the untreated micelles. Since all measurements were performed in the same light tapping regime, we conclude that the tip-induced deformation could originate from the formation of an exposed B core. Furthermore, the phase image (Fig. 5.7b, right) indicates the appearance of a soft material (glass transition temperature T_g(PB) ~ -28 °C (Ref. 77)) in the centre of each micelle, the

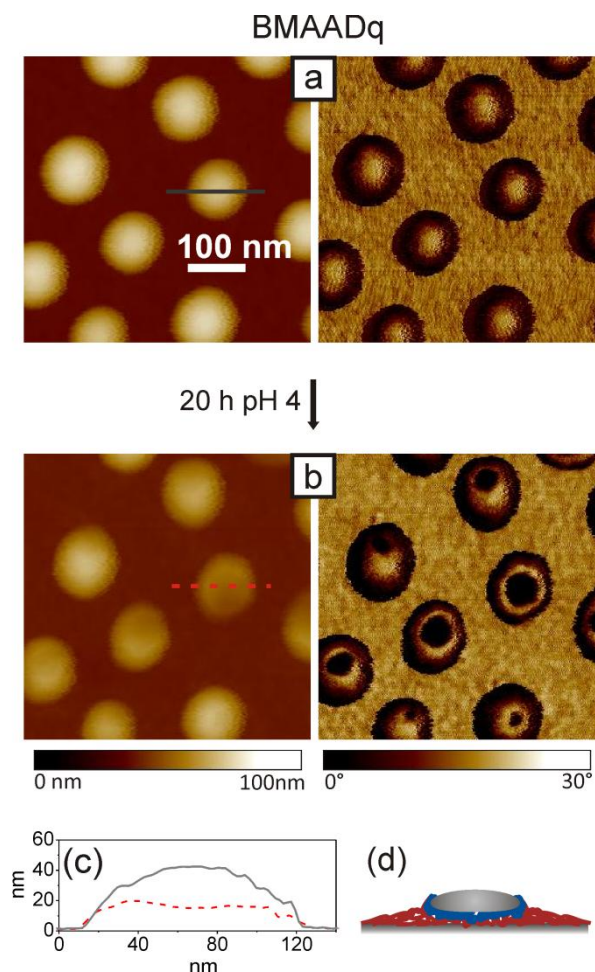lateral expansion of which corresponding to the size of the core obtained from SEM measurements (Fig. 5.2b).

Fig. 5.7: 500 nm × 500 nm AFM height (left) and phase (right) images of dried BMAADq micelles adsorbed on Si-wafers from pH 10 buffer solution (a) and after 20 hours treatment with pH 4 water (b) at the same location of the sample with corresponding cross-sectional height profiles of the same micelle (c) and a schematic representation of observed structure (d).

The resulting morphological changes may be attributed to the slow surface reorganization of polymer chains that are not electrostatically attached to the surface in order to minimize repulsion of coronal chains. In acidic media, the hydrophobically attached polymer chains within a micelle can dissociate and re-adsorb onto the uncovered silica parts, whereas electrostatically linked chains remain. Since the three blocks are covalently linked,

intramicellar microphase separation of adsorbed micelles occurs. After drying and collapse of the MAA shell, the interface of B domains with air can be formed.

To confirm this structural change, we performed ellipsometry measurements. While the morphology of the adsorbed micelles after the long-term treatment at pH 4 changed significantly, the thickness of the sample before and after treatment remains constant (~ 20 nm) indicating a rearrangement of the micelles on the surface.

Similar irreversible changes have been published by Biggs and co-workers [21, 23, 63, 78] They have demonstrated the pH-responsive behavior of an on-mica adsorbed monolayer of cationic poly(2-(dimethylamino)ethyl methacrylate)-*block*-poly(2-(diethylamino)ethyl methacrylate) (Dq-DEA) diblock copolymer micelles to pH cycling as a function of the degree of quaternization ($0 < q < 1$) of the D corona.[78] For partly and fully quaternized systems, irreversible changes in the nanomorphology of the adsorbed monolayer were observed after a long-term treatment.[21, 78] For non-quaternized systems, however, the close-packed adsorbed micellar layer was found to reversibly open and close the micellar cores in response to solution pH ("nano-anemones").[23, 63, 78] Interestingly, the same micelles, adsorbed on silica, showed irreversible pH-responsive behaviour upon long-term treatment.[63] In the latter case, the dissociation of micelles on the surface was suggested.

In contrast to these studies, we find microdomain structures with both chemical and topographical patterns of different polarity within domains of round shape on the lateral scale of ~100 nm in ultra-thin films (~20 nm). During submission of this manuscript we became aware of independent work of Tan et al. in which similar effects were observed for the systems poly(N,N-dimethylaminoethyl methacrylate)-*block*-poly(propylene oxide) diblock copolymer micelles and poly(N,N-dimethylaminoethyl methacrylate)-*block*-poly(propylene oxide)-*block*-poly(N,N-dimethyl-aminoethyl methacrylate) triblock copolymer micelles.[79]

Hence, the system provides two relaxation times coupled with the mobility of the B core: fast relaxation in the case of short-term treatment, and slow relaxation in the case of irreversible rearrangement of adsorbed micelles. To investigate the role of the core mobility and to support the observed results, we adsorbed micelles with covalently crosslinked B cores (x-BMAADq) onto silica and studied their response to long-term contact with acidic solution. x-BMAADq particles are expected to show a character similar to nanoparticles, the cores of which inhibiting any changes in the aggregation number and therefore no reorganization on the surface should be possible.
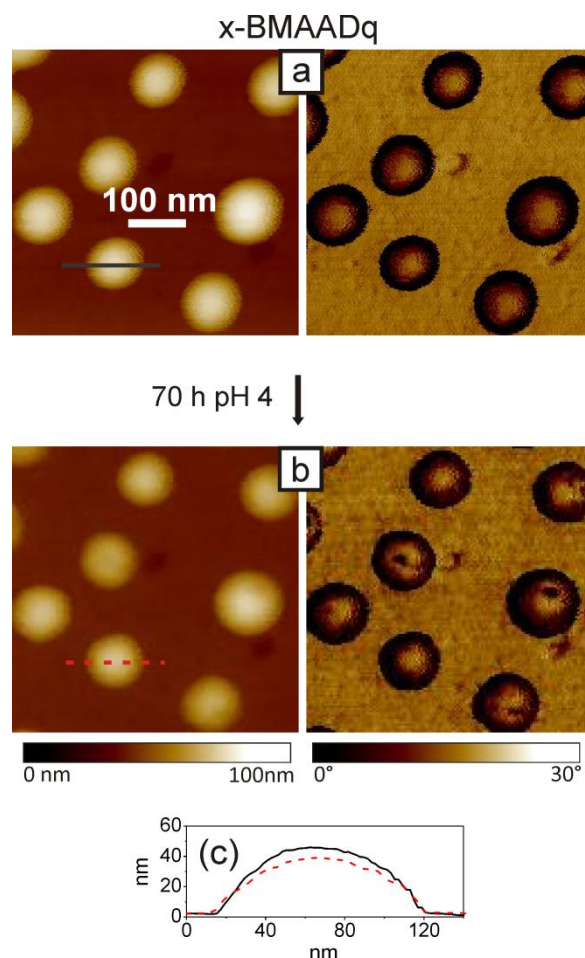
Fig. 5.8: 500 nm × 500 nm AFM height (left) and phase (right) images of dried core-crosslinked x-BMAADq particles adsorbed on Si-wafers from pH 10 buffer solution (a) and after 70 hours treatment with pH 4 water (b) at the same location of the sample, with corresponding cross-sectional height profiles of the same particle (c).

In contrast to BMAADq micelles, almost no topographical and morphological changes occur with x-BMAADq micelles even after 70 hours of pH 4 treatment (Fig. 5.8). The crosslinking of the core prevents the dynamic behaviour of the micelles and therefore the rearrangement/dissociation of terpolymer chains from adsorbed micelles. The slight decrease in the height of the micelles (Fig. 5.8c) may be attributed to the relaxation of the corona onto the silica substrate. Since the length of the positively charged corona increases in acidic media, non-adsorbed, mobile Dq chains of adsorbed micelles can adsorb onto uncovered silica. This process is entropically favoured due to the release of hydration water and counterions.[59, 60]

5.4 Conclusions

The assembly and pH-responsive behaviour of core-shell-corona micelles of a BMAADq triblock terpolymer on silica was studied. The deposition of micelles onto planar surfaces by a simple dipping method led to well-defined topographical structuring on the nanoscale.

We found that the initial adsorption kinetics of the micelles is determined by the rate of transport to the surface and therefore by the diffusion coefficient, while at later adsorption times, the surface coverage reached a limiting value of 54 % consistent with the RSA model.

By controlling the solution pH on the solid-liquid interface of pre-adsorbed micelles, it was possible to reversibly or irreversibly change the micellar morphology and composition. The system involves two types of conformational response to pH trigger and consequently two types of dynamics coupled to the time scales of treatment. On the short-time scale, the pH-responsive behaviour of adsorbed micelles is reversible and can be controlled by the ionization degree of the MAA middle block. The long-term treatment at pH $<$ p$K_{a,apparent}$ of MAA causes changes in the morphology of BMAADq micelles due to the *im*-IPEC dissolution under these conditions and slow micelle reorganization, creating irreversible morphology changes, which are not accessible in solution. This opens interesting opportunities, which will be investigated in further work: while normally the hydrophobic cores are not accessible in aqueous environment, the shape changes observed here indicate an "opening" of the micelles. This makes the micellar cores accessible for chemistry. For example, due to the good stability of such systems in organic solvents, further modifications of the better accessible polybutadiene core *via* click chemistry (*e.g.* thiol-ene reaction) are possible. As well, material (drugs) loaded in the micellar cores is expected to release in the open state.

A further interesting perspective for this system is exploiting the switchable interaction properties. Depending on the swelling state, osmotic pressure due to small counterions confined in the corona is expected to undergo dramatic changes. This results in a change of compressibility of the corona region and/or an expansion which can be used to create volume-work against an external load. Therefore, these systems are potentially interesting as nano-actuators.[79, 80] A detailed investigation of these interaction / nano-mechanical properties requires techniques like local force spectroscopy,[81, 82] which will be subject of further investigations. As well, substrates which undergo strong changes in hydration / swelling have been shown to have potential for switchable cell culture substrates.[83] This perspective will as well be explored in further work.

The two relaxation times were found to be linked to the mobility of the B core, as the covalent crosslinking of the core prevents slow irreversible changes, and therefore only one relaxation dynamics was found for the crosslinked system. In contrast to BMAADq, the crosslinked x-BMAADq micelles showed higher stability against morphology changes under long-term acidic conditions, rendering this system of potential interest for long-term experiments *e.g.* drug delivery or the use as switchable surfaces.

Acknowledgements

References

1.   S. T. Milner, *Science*, 1991, **251**, 905-914.

2.   E. B. Zhulina, O. V. Borisov and T. M. Birshtein, *Journal De Physique II*, 1992, **2**, 63-74.

3.   B. Zhao and W. J. Brittain, *Progress in Polymer Science*, 2000, **25**, 677-710.

4.   R. K. Iler, *Journal of Colloid and Interface Science*, 1966, **21**, 569-594.

5.   G. Decher, J. D. Hong and J. Schmitt, *Thin Solid Films*, 1992, **210**, 831-835.

6.   G. Decher and J. Schmitt, *Progress in Colloid & Polymer Science*, 1992, **89**, 160-164.

7.   G. Decher, *Science*, 1997, **277**, 1232-1237.

8.   A. Kumar and G. M. Whitesides, *Science*, 1994, **263**, 60-62.

9.   Y. N. Xia and G. M. Whitesides, *Annual Review of Materials Science*, 1998, **28**, 153-184.

10.   Y. N. Xia and G. M. Whitesides, *Angewandte Chemie-International Edition*, 1998, **37**, 551-575.

11.   X. P. Jiang and P. T. Hammond, *Langmuir*, 2000, **16**, 8501-8509.

12.   X. P. Jiang, H. P. Zheng, S. Gourdin and P. T. Hammond, *Langmuir*, 2002, **18**, 2607-2615.

13.   M. Pretzl, A. Schweikart, C. Hanske, A. Chiche, U. Zettl, A. Horn, A. Böker and A. Fery, *Langmuir*, 2008, **24**, 12748-12753.

14.   T. L. Morkved, M. Lu, A. M. Urbas, E. E. Ehrichs, H. M. Jaeger, P. Mansky and T. P. Russell, *Science*, 1996, **273**, 931-933.

15.   M. Park, C. Harrison, P. M. Chaikin, R. A. Register and D. H. Adamson, *Science*, 1997, **276**, 1401-1404.

16.   S. Ludwigs, A. Böker, A. Voronov, N. Rehse, R. Magerle and G. Krausch, *Nature Materials*, 2003, **2**, 744-747.

17.   J. P. Spatz, T. Herzog, S. Mossmer, P. Ziemann and M. Möller, *Advanced Materials*, 1999, **11**, 149-153.

18.   J. P. Spatz, S. Mossmer, C. Hartmann, M. Möller, T. Herzog, M. Krieger, H. G. Boyen, P. Ziemann and B. Kabius, *Langmuir*, 2000, **16**, 407-415.

19.   M. R. Talingting, Y. H. Ma, C. Simmons and S. E. Webber, *Langmuir*, 2000, **16**, 862-865.

20.   G. B. Webber, E. J. Wanless, S. P. Armes, F. L. Baines and S. Biggs, *Langmuir*, 2001, **17**, 5551-5561.

21.   G. B. Webber, E. J. Wanless, V. Butun, S. P. Armes and S. Biggs, *Nano Letters*, 2002, **2**, 1307-1313.

22.   G. Kästle, H. G. Boyen, F. Weigl, G. Lengl, T. Herzog, P. Ziemann, S. Riethmüller, O. Mayer, C. Hartmann, J. P. Spatz, M. Möller, M. Ozawa, F. Banhart, M. G. Garnier and P. Oelhafen, *Advanced Functional Materials*, 2003, **13**, 853-861.

23.   G. B. Webber, E. J. Wanless, S. P. Armes, Y. Q. Tang, Y. T. Li and S. Biggs, *Advanced Materials*, 2004, **16**, 1794-1798.

24. I. W. Hamley, S. D. Connell and S. Collins, *Macromolecules*, 2004, **37**, 5337-5351.

25. J. P. Spatz, T. Lohmueller and E. Bock, *Advanced Materials*, 2008, **20**, 2297-+.

26. M. A. Cohen Stuart, W. T. S. Huck, J. Genzer, M. Müller, C. Ober, M. Stamm, G. B. Sukhorukov, I. Szleifer, V. V. Tsukruk, M. Urban, F. Winnik, S. Zauscher, I. Luzinov and S. Minko, *Nature Materials*, 2010, **9**, 101-113.

27. T. Addison, O. J. Cayre, S. Biggs, S. P. Armes and D. York, *Langmuir*, 2008, **24**, 13328-13333.

28. Z. C. Zhu and S. A. Sukhishvili, *ACS Nano*, 2009, **3**, 3595-3605.

29. L. Xu, Z. C. Zhu and S. A. Sukhishvili, *Langmuir*, 2011, **27**, 409-415.

30. T. P. Russell, H. D. Koh and S. Park, *ACS Nano*, 2010, **4**, 1124-1130.

31. T. P. Russell, *Science*, 2002, **297**, 964-967.

32. K. Glinel, C. Dejugnat, M. Prevot, B. Schöler, M. Schönhoff and R. V. Klitzing, *Colloids and Surfaces A-Physicochemical and Engineering Aspects*, 2007, **303**, 3-13.

33. P. M. Mendes, *Chemical Society Reviews*, 2008, **37**, 2512-2529.

34. M. Stamm, P. Uhlmann, H. Merlitz and J. U. Sommer, *Macromolecular Rapid Communications*, 2009, **30**, 732-740.

35. L. F. Zhang and A. Eisenberg, *Science*, 1995, **268**, 1728-1731.

36. M. Motornov, Y. Roiter, I. Tokarev and S. Minko, *Progress in Polymer Science*, 2010, **35**, 174-211.

37. O. J. Cayre, N. Chagneux and S. Biggs, *Soft Matter*, 2011, **7**, 2211-2234.

38. J. Rodriguez-Hernandez, F. Checot, Y. Gnanou and S. Lecommandoux, *Progress in Polymer Science*, 2005, **30**, 691-724.

39. R. K. O'Reilly, C. J. Hawker and K. L. Wooley, *Chemical Society Reviews*, 2006, **35**, 1068-1083.

40. K. B. Thurmond, T. Kowalewski and K. L. Wooley, *Journal of the American Chemical Society*, 1996, **118**, 7239-7240.

41.   S. P. Armes and E. S. Read, *Chemical Communications*, 2007, 3021-3035.

42.   J. V. M. Weaver, Y. Q. Tang, S. Y. Liu, P. D. Iddon, R. Grigg, N. C. Billingham, S. P. Armes, R. Hunter and S. P. Rannard, *Angewandte Chemie-International Edition*, 2004, **43**, 1389-1392.

43.   M. A. C. Stuart, B. Hofs, I. K. Voets and A. de Keizer, *Current Opinion in Colloid & Interface Science*, 2005, **10**, 30-36.

44.   V. A. Kabanov, *Russ. Chem. Rev.*, 2005, **74**, 3-20.

45.   D. V. Pergushov, Oleg V. Borisov, A. B. Zezin and A. H. E. Müller, *Advances in Polymer Science*, 2011, DOI: 10.1007/1012_2010_1102.

46.   C. A. Fustin, V. Abetz and J. F. Gohy, *European Physical Journal E*, 2005, **16**, 291-302.

47.   J. F. Gohy, N. Willet, S. Varshney, J. X. Zhang and R. Jerome, *Angewandte Chemie-International Edition*, 2001, **40**, 3214-3216.

48.   F. Schacher, A. Walther and A. H. E. Müller, *Langmuir*, 2009, **25**, 10962-10969.

49.   F. Schacher, E. Betthausen, A. Walther, H. Schmalz, D. V. Pergushov and A. H. E. Müller, *ACS Nano*, 2009, **3**, 2095-2102.

50.   E. Betthausen, M. Drechsler, M. Förtsch, F. H. Schacher and A. H. E. Müller, *Soft Matter*, 2011, **7**, 8880-8891

51.   C. L. McCormick, J. D. Flores, X. W. Xu and N. J. Treat, *Macromolecules*, 2009, **42**, 4941-4945.

52.   F. H. Schacher, C. V. Synatschke, M. Förtsch, M. Drechsler and A. H. E. Müller, *Soft Matter*, 2011, **7**, 1714-1725.

53.   A. Walther, A. S. Goldmann, R. S. Yelamanchili, M. Drechsler, H. Schmalz, A. Eisenberg and A. H. E. Müller, *Macromolecules*, 2008, **41**, 3254-3260.

54.   E. Betthausen, F. Schacher, A. H. E. Müller, in preparation

55.   W. Kern and D. A. Puotinen, *RCA Review*, 1970, **31**, 187-206.

56.   K. A. Marx, *Biomacromolecules*, 2003, **4**, 1099-1120.

57. F. Hook, J. Voros, M. Rodahl, R. Kurrat, P. Boni, J. J. Ramsden, M. Textor, N. D. Spencer, P. Tengvall, J. Gold and B. Kasemo, *Colloids and Surfaces B-Biointerfaces*, 2002, **24**, 155-170.

58. M. V. Voinova, M. Rodahl, M. Jonson and B. Kasemo, *Physica Scripta*, 1999, **59**, 391-396.

59. C. B. Bucur, Z. Sui and J. B. Schlenoff, *Journal of the American Chemical Society*, 2006, **128**, 13690-13691.

60. J. B. Schlenoff, A. H. Rmaile and C. B. Bucur, *Journal of the American Chemical Society*, 2008, **130**, 13589-13597.

61. R. Pericet-Camara, G. Papastavrou and M. Borkovec, *Langmuir*, 2004, **20**, 3264-3270.

62. R. Pericet-Camara, B. P. Cahill, G. Papastavrou and M. Borkovec, *Chemical Communications*, 2007, 266-268.

63. K. Sakai, E. G. Smith, G. B. Webber, M. Baker, E. J. Wanless, V. Bütün, S. P. Armes and S. Biggs, *Langmuir*, 2006, **22**, 8435-8442.

64. Z. Adamczyk, M. Zembala, B. Siwek and P. Warszynski, *Journal of Colloid and Interface Science*, 1990, **140**, 123-137.

65. C. A. Johnson and A. M. Lenhoff, *Journal of Colloid and Interface Science*, 1996, **179**, 587-599.

66. H. Motschmann, M. Stamm and C. Toprakcioglu, *Macromolecules*, 1991, **24**, 3681-3688.

67. P. Schaaf and J. Talbot, *Journal of Chemical Physics*, 1989, **91**, 4401-4409.

68. Y. Pomeau, *Journal of Physics A-Mathematical and General*, 1980, **13**, L193-L196.

69. P. Schaaf, J. C. Voegel and B. Senger, *Journal of Physical Chemistry B*, 2000, **104**, 2204-2214.

70. J. Feder, *Journal of Theoretical Biology*, 1980, **87**, 237-254.

71. E. L. Hinrichsen, J. Feder and T. Jossang, *Journal of Statistical Physics*, 1986, **44**, 793-827.

72. H. Dautzenberg, W. Jaeger, J. Kötz, B. Philipp, C. Seidel and D. Stscherbina, *Polyelectrolytes*, Carl Hanser Verlag, München, 1994.

73. I. Borukhov, D. Andelman, R. Borrega, M. Cloitre, L. Leibler and H. Orland, *Journal of Physical Chemistry B*, 2000, **104**, 11027-11034.

74. G. Battaglia, C. Fernyhough and A. J. Ryan, *Soft Matter*, 2009, **5**, 1674-1682.

75. M. F. Zhang, T. Breiner, H. Mori and A. H. E. Müller, *Polymer*, 2003, **44**, 1449-1458.

76. J. Tamayo and R. Garcia, *Langmuir*, 1996, **12**, 4430-4435.

77. W. A. Lee and R. A. Rutherford, *Polymer Handbook*, 2d edn., John Wiley and Sons, New York, 1975.

78. G. B. Webber, E. J. Wanless, S. P. Armes and S. Biggs, *Faraday Discussions*, 2005, **128**, 193-209.

79. W. S. Tan, Z. Zhu, S. A. Sukhishvili, M. F. Rubner and R. E. Cohen, *Macromolecules*, 2011, **44**, 7767-7774

80. W. S. Tan, R. E. Cohen, M. F. Rubner and S. A. Sukhishvili, *Macromolecules*, 2010, **43**, 1950-1957.

81. V. V. Tsukruk, A. Sidorenko, V. V. Gorbunov and S. A. Chizhik, *Langmuir*, 2001, **17**, 6715-6719.

82. P. A. L. Fernandes, S. Schmidt, M. Zeiser, A. Fery and T. Hellweg, *Soft Matter*, 2010, **6**, 3455-3458.

83. S. Schmidt, M. Zeiser, T. Hellweg, C. Duschl, A. Fery and H. Möhwald, *Advanced Functional Materials*, 2010, **20**, 3235-3243.

6 Cavitation Engineered 3-D Sponge Networks and Their Application in Active Surface Construction

Gensel, J., Borke, T., Pérez, N. P., Fery, A., Andreeva, D. V.,* Betthausen, E., Müller, A. H. E., Möhwald, H. and Skorb, E. V.*

Email: Daria V. Andreeva (daria.andreeva@uni-bayreuth.de),

Ekaterina V. Skorb (skorb@mpikg.mpg.de)

The design of the 3D architecture surfaces with both space- and time-dependent functionality (cell attraction, pH-trigged self-cleaning, antiseptic/disinfection) is in the focus. The innovative story includes: sonochemical surface activation, formation of feedback surface component (pH-responsible micelles), proof of responsive activity (time resolved cell adhesion and bacteria deactivation) and space adhesion selectivity (surface patterning).

6.1 Introduction and Results

Controlling cell positioning, adhesion, spreading, growth and migration on surfaces is of interest in fundamental cell biology,[1] tissue engineering,[2] cell-based biosensor development,[3] bioelectronics[4] and protection of biocompatible devices.[5] Various methods have been used to direct the adhesion of cells to selected areas of a substrate, including micropatterning,[6] soft lithography,[7] patterning through pores in elastomeric membranes,[8] patterning by using three-dimensional microfluidic systems,[9] laminar-flow patterning,[10] local oxidation by using microelectrodes,[11] and a spectacular method of layer-by-layer deposition.[12] One particularly versatile approach to control cell attachment and patterning is the physical or chemical adsorption of functional molecules such as extracellular matrix proteins and pH- or temperature- sensitive polymers to selected areas of a substrate.[13] The effects significantly depend on the properties and nature of the underlying substrate,[14] and substrates with complex 3-D network are of high priority.[15]

The market for joint-implant surgery, as an example of a biocompatible device, is expected to reach \$17.4 billion by 2012 – an annual growth rate of more than 9 percent since 2008, when estimates pegged its value at \$12.2 billion.[16] Thus, green and inexpensive methods of surface modification are in focus as well as fundamental aspects of processes which can be used for surface engineering.

Ultrasound of high intensity could provide green and fast physical and chemical surface modification due to high energy localized by a sonotrode at a particular surface area.[17] The shape of the sonotrode can be adjusted to particular applications and allows easy modification of large sample areas.[18] Acoustic cavitation offers the unique potential of locally establishing high-temperature (up to 5000K) and high-pressure (several hundreds of bars) reactions, while the system remains macroscopically near room temperature and ambient pressure.[19] Thus, ultrasound could replace some expensive, multi-stage and time-consuming methods of surface engineering. For example, formation of fine porous metal structure with large pores (200 μm to 2 mm) needs special casting conditions or can be made by sputter deposition.[20] For formation of porous metals with pore size distribution between 2 and 50 nm (mesoporous materials) chemical[21] or electrochemical dealloying[22] of expensive noble metal containing alloys[23] has to be used. These syntheses normally employ high temperatures (*e.g.* >1000 °C) rendering the material chemically inert and hindering facile postchemical functionalisation. Commonly, the processes require very harsh reagents.

We suggest using ultrasonically formed metal sponges for nanoconstruction of protected biocompatible surfaces. Recently, we demonstrated that ultrasonic treatment of biocompatible metal surfaces (aluminum, magnesium, iron, and titanium) changes their morphology (roughness, porosity), chemistry (surface oxidation by the products of water sonolysis) and properties (adhesion, hydrophilic/hydrophobic *etc.*).[17,24] Intensive etching and oxidation of metals by ultrasound leads to formation of a 200-nm-thick sponge-like surface layer well-adhered to the bulk metal. The surface metal sponge is porous, has a high surface area and is covered by active OH-groups. Such kind of surfaces can provide effective storage and release on demand of functional compounds (antiseptics, disinfectants, corrosion inhibitors, drugs *etc.*) as well as excellent adhesion of protective coatings or cells. Furthermore, such sponges combining the beneficial properties of metals and porous structure have unique physical and mechanical properties such as low density, high surface-to-volume ratio, high thermal shock resistance, and high specific strength that are important for their application.[20–25]

Liquid motion in the vicinity of cavitation sites generates very large shear and strain gradients that are caused by the very rapid streaming of solvent molecules around the cavitation bubble and by the intense shock waves emanating upon collapse.[26] Thus, cavitation stimulates intercalation of low molecular weight compounds into the porous interior of metal sponges.[27] We applied here this effect of sonication to incorporate the antiseptic/ disinfectant, silver (Ag), into a porous Al surface. The ultrasonic assisted generation of surface Al sponges and their upload with Ag was performed in a step-wise mode at the same reactor unit (Figure 6.1).[24,27] The maximum silver concentration was estimated by EDS 0.03 wt%.
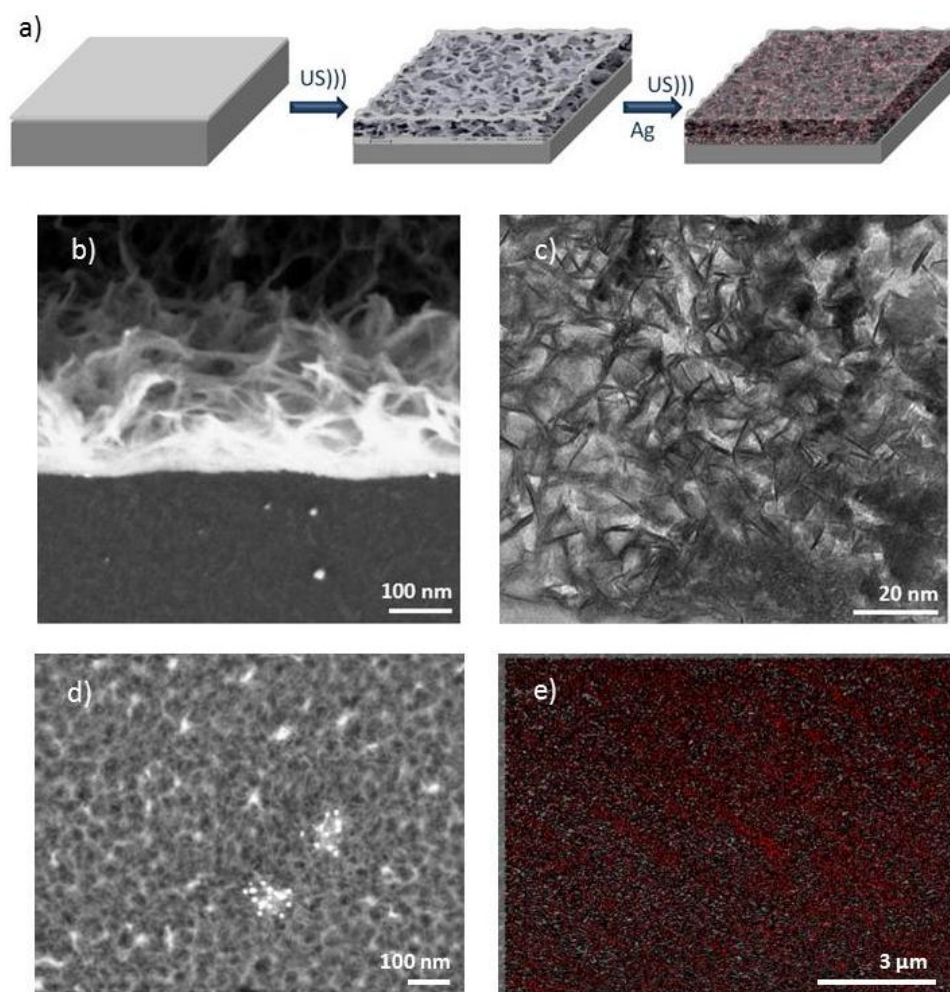
Fig. 6.1: a) Schematic reconstruction based on SEM/EDS measurements of the sonochemically formed porous aluminum layer and silver incorporation into sponge. b) SEM (side-view) and c) TEM images of 200-nm aluminum layer deposited on a glass substrate modified via ultrasonication (20 kHz, 57 W/cm^2) in aqueous solution after a 60-s modification. d) SEM (top-view) e) EDS mapping (aluminum (gray) and silver (red)) of aluminum based sponge after ultrasonic assisted silver incorporation.

Then, ultrasonically formed sponge-like silver/aluminum (Ag/Al) surfaces as well as Ag free surfaces were used for self-assembled immobilization of pH-responsive triblock terpolymer micelles. The self-cell release surface regulation and antibacterial properties were tested by using *Lactoccocus. Lactis 411* bacteria as a model system. These types of bacteria produce lactic acid in their life cycle and change the pH of their environment. To develop responsive surface coatings, we used a linear ABC triblock terpolymer consisting of polyb-utadiene (B), poly(methacrylic acid) (MAA), and quaternized poly(2-(dimethylamino)ethyl methacrylate) (Dq), $B_{800}MAA_{200}Dq_{285}$, (subscripts denoting the degrees of polymerization of

the corresponding blocks) which was recently designed by the Müller group.[28] For simplicity, the polymer will be denoted as BMAADq throughout the manuscript. In aqueous solutions, BMAADq self-assembles into core-shell-corona micelles with a hydrophobic B core, a pH-sensitive shell and a cationic Dq corona. The schematic representation of the obtained core-shell-corona micelles is shown in Figure 6.2.
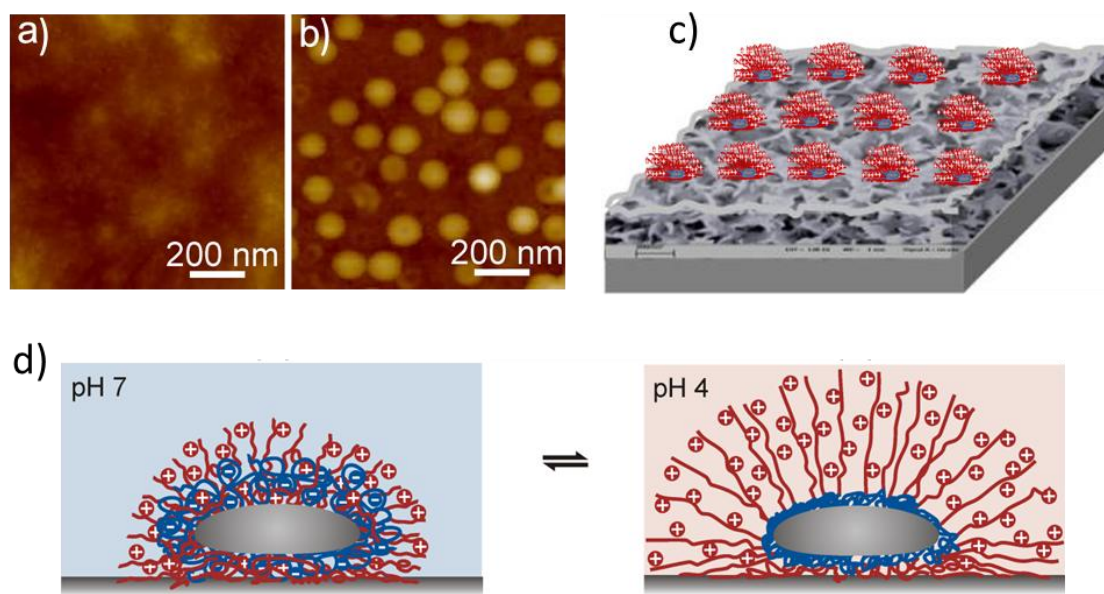

Fig. 6.2: Surface immobilization of pH-responsive triblock terpolymer micelles on a porous aluminum surface formed by ultrasonication: a, b) AFM images of a sponge-like Al surface before and after adsorption of BMAADq micelles, respectively (height image scale: 0–100 nm); c, d) Schematic representation of adsorbed micelles on the porous surface depicting their pH-dependent structure.

The terpolymer micelles show a rapid response to pH cycling.[28] The pH-responsive behaviour of the micelles can be controlled by the ionization degree of the MAA block ($pK_{a,apparent} \sim 5.5$). In the pH range between 7 and 4 the ionization degree, α, decreases from unity to ~ 0.[29] At pH 10 ($\alpha \sim 1$), the attraction between the negatively charged MAA and the positively charged Dq blocks induces the formation of an intramicellar interpolyelectrolyte complex (*im*-IPEC) shell. According to the degrees of polymerization ($DP_n(MAA) < DP_n(Dq)$), parts of the cationic Dq block remain uncomplexed forming a positively charged corona. At pH 4, the protonation of the MAA block ($\alpha \sim 0$) results in *im*-IPEC dissolution. As a consequence, the uncharged MAA block collapses onto the B core forming a new shell, and

the length and charge density of the cationic Dq corona increase. Accordingly, the charge density of the MAA block and the dissolution or regeneration of the *im*-IPEC shell can be adjusted by the pH of the solution. The length and charge density of the cationic Dq corona are regulated by the shell composition and therefore can be varied by pH. This short-term response to pH changes was shown to be completely reversible within several cycling steps.[28b]

Due to the cationic nature of the Dq corona, BMAADq micelles can be immobilized on negatively charged surfaces, while their core-shell-corona structure remains intact upon adsorption to a solid support.[28b] Therefore, a negatively charged Al sponge surface was used to immobilize the triblock terpolymer micelles by a simple dip coating method. To conclude on micelle adsorption onto the aluminium sponge (Figure 6.2) by atomic force microscopy (AFM), Figure 6.2b shows AFM height image of the dry micelles adsorbed from pH 10 buffer solution on an ultrasonically designed aluminum sponge as a monolayer. The surface adsorption of BMAADq micelles leads to regular arrays of particles with uniform size and spherical-cap shape. The adsorption is driven by the release of counter ions and hydration water.[30] The surface exclusion effect leads to formation of a laterally patterned monolayer of micelles, as often reported for the adsorption of charged colloidal particles.[31]

The cell adsorption on the metal/micelle surface is illustrated in the sketch (Figure 6.3, bottom). Indeed, as shown by the confocal fluorescence kinetic study (Figure 6.3, top), the number of adsorbed microorganisms drastic decreases already after 30 min of the experiments. After 5 hours we didn't observe any evidence of bacteria presence on the surface. This spectacular cell-cleaning surface effect is a pH-trigged desorption of the bacteria due to changes in morphology of the charged Dq corona. The lactic acid produced by *L. Lactis* loaded with Rh6G decreases the local pH of the metal/ micelle/ bacteria system together with having slightly positive charge. The decrease of the pH results in *im*-IPEC dissolution and therefore in switching of the surface properties.[28b] At pH 4 the length of the charged Dq corona increases and the adsorbed bacteria are detached from the surface and the positively charged micelles. Thus, we achieve pH-regulated self-cleaning of the metal/micelle network.
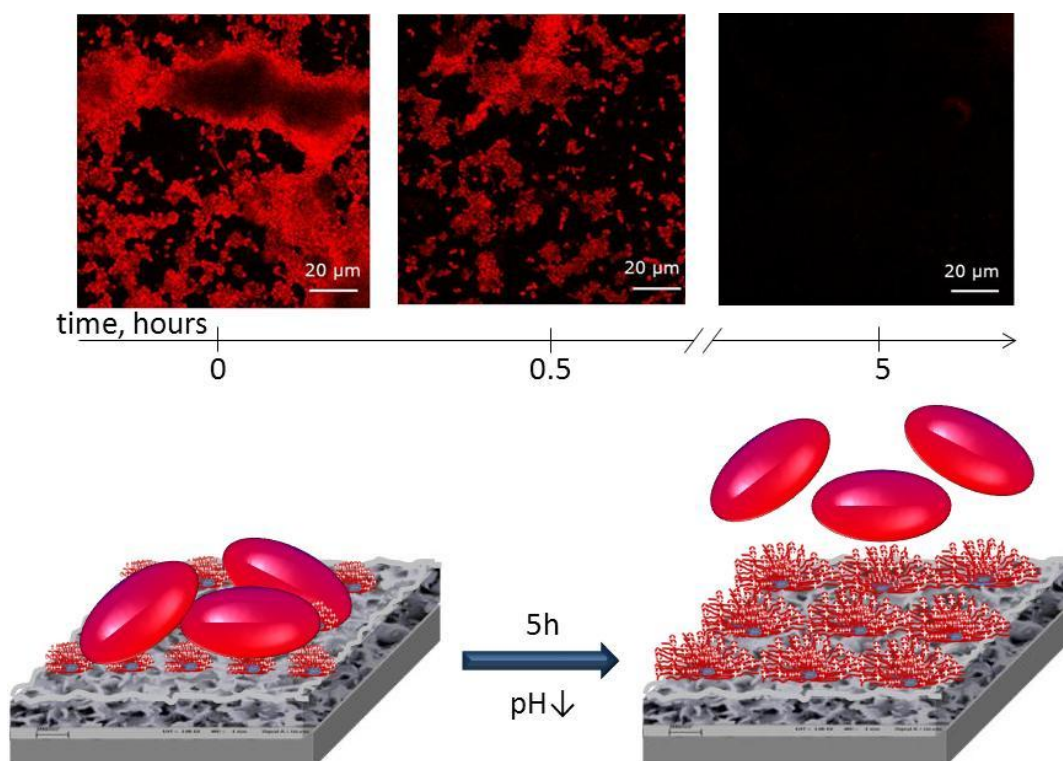
Fig. 6.3: Confocal kinetic study (fluorescent mode) and schematic illustration of pH trigged self-cleaning behavior on the porous Al surface covered with micelles. As model cells *Lactococcus Lactis 411* bacteria (loaded with Rh6G) were used.

The use of ultrasound for the formation of complex structures of Ag/Al sponges serves as the basis for the development of synergetic surfaces. The novelty of this work is the design of 3D architecture surfaces with both space- and time-dependent functionality (cell attraction, pH-triggered self-cleaning, antiseptic/disinfection). The different surface functionality and reactivity can be controlled by surface patterning. The combination of adhesion control through patterning and active component containing sponge use is shown in Figure 6.4. We patterned micelle lines on the ultrasonically formed Al and Ag/Al sponge-like surfaces. It is seen that after 5 hours of the experiment the bacteria are desorbed on the micelle patterns. Simultaneously the micelle-free porous surface provides high cell adhesion. The adsorbed bacteria are deactivated by Ag ultrasonically incorporated into the porous Al matrix in the case of the Ag/Al/micelle sponge-like surface. We cultivated the bacteria detached from the micelle patterns of porous surfaces (Figure 6.4d). Note that due to high initial bacteria concentration (5×10^4 CFU/mL) the suspension was diluted by a factor of 100 to calculate the CFU/mL in the case of the silver-free surface. In the control experiment with Ag-free Al sponges we observed an intense bacteria growth. After 24 hours of incubation of the bacteria

from the Ag/Al/micelle surface the 2×10^3 times decrease in survival factor from 80% to 0.05% and change of reduction factor from 1 to 2×10^3 was observed. The antimicrobial activity clearly indicates the antiseptic/disinfectant activity of the Ag/Al sponge surface.
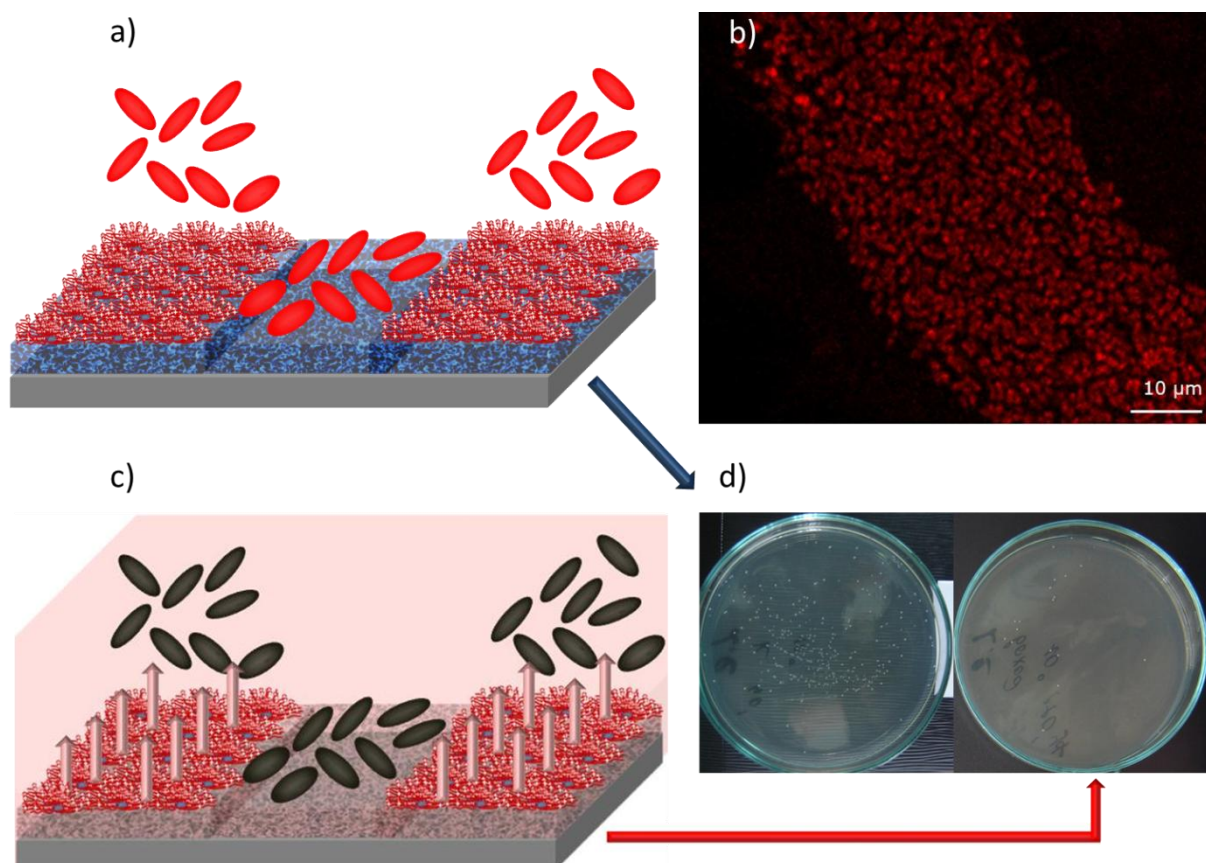

Fig. 6.4: a, b) Controllable bacteria adsorption on porous aluminium surfaces patterned with micelles: sketch and confocal fluorescence images, correspondingly. c) Synergetic surface activity: variation of cell adhesion through patterning with micelles and self-cleaning by antiseptic/ disinfectant properties of porous Ag/Al surface. d) Petri dish of *Lactococcus Lactis 411* after 24h incubation to analyse the inactivation behaviour of the Ag/Al/micelle surface (right, 20 CFU/mL) and the control Al/ micelle surface (left, 100-times diluted, ca. 400 x 100 CFU/mL). Initial bacteria concentration was 5×10^4 CFU/mL.

In the long run, we suggest a novel concept of protection of biocompatible surfaces. We present a nice way of functionalizing a metal surface with a soft matter layer. This is not always easy to achieve and there are specific applications where one has to work on metal substrates such as anti fouling systems,[32] implants, stem cell research, SERS[33] *etc*. We

described an effective sonochemical pathway of surface engineering providing lot of space for further optimization with an ultrasound assisted adsorption of temperature sensitive polymers in focus, some candidates are thermoresponsive poly(N-isopropylacrylamide) (PNIPAM)[34] and polyoxazolines[35] that change their morphology and reactivity in a narrow temperature region. These polymers can be extremely promising in the construction of 3-D temperature sensitive biosensors making use of the high surface area of metal sponges. For example, in our previous work on thermo-sensitive microgels,[34] we presented a switchable system, which, however, receives energy from an external source. However, in our particular case it is very important that the bacteria's metabolism basically acts as a source of chemical energy to trigger the response. Here, the bacteria themselves bring in the power and trigger the response. That's actually a nice way of designing "active" coatings.

6.2 Experimental Section

Materials: The triblock terpolymer $B_{800}MAA_{200}Dq_{285}$ (subscripts denoting the degrees of polymerization of the corresponding blocks, $M_n \sim 110\ 000$ g/mol, PDI = 1.10) was synthesized via sequential living anionic polymerization in THF followed by polymer-analogous modifications. Details about polymerization and characterization can be found elsewhere. (Reference 28a and b) Silver nitrate (99.9% AgNO3) was purchased from Sigma-Aldrich. All reactants were used without further purification. Milli-Q water (18.2 MΩ cm) was used in all aqueous solutions.

Preparation of mesoporous Al and Ag/Al plates: A glass substrate with an aluminum layer (thickness: 200 nm, vapor deposited, 5 mm^2 plate) was sonicated in 130 mL Milli-Q water for 60 s at 100% intensity with a Hielscher UIP1000hd (Germany) operated at 20 kHz with a maximal output power of 1000 W. The apparatus was equipped with a BS2d22 ultrasonic horn (head area of 3.2 cm^2) and with a booster (B2-1.2). The maximum intensity was calculated to 57 W·cm^{-2} at a mechanical amplitude of 81 μm. During sonication the samples were fixed in a home-made Teflon holder. The distance between Al-plate and ultrasonic horn was 1 cm. After replacing the water by 120 mL of an aqueous silver salt solution with the metal salt concentration of 2.5×10^{-5} M, the plates were sonicated at 50% intensity for additional 30 s.

Adsorption of BMAADq micelles on mesoporous metal plates: The triblock terpolymer micelles were adsorbed on freshly prepared substrates from a 0.45 g/L BMAADq in pH 10

buffer solution (AVS Titrinorm from VWR, ionic strength $\sim$ 0.05 M) via the dip coating method. After 15 minutes the plates were rinsed with milli-Q water (18.2 MΩ cm) and dried with a stream of nitrogen.

Micelle surface patterning: *S*elective adsorption of micelles onto the aluminum surface was controlled by a preformed Teflon mask. In particular, after ultrasonic modification of the aluminum surface, the mask protected plate in the special holder was dip coated into the micellar solution as described before.

Characterization Methods: Atomic force microscopy (AFM) images of dried samples were taken with a Dimension 3100 equipped with a NanoScope V controller (Veeco) operating in Tapping Mode using standard Si_3N_4 cantilevers (Olympus) with a typical spring constant of $\sim$42 N/m and a typical resonance frequency of 300 kHz (OMCL-AC160TS).

Scanning electron microscopy (SEM) measurements were conducted with a Gemini Leo 1550 instrument at an operation voltage of 3 keV. Samples were sputtered with gold. Microprobe analysis was performed using energy dispersive spectrometry (EDS) Model 6587, Pentafet Link, Oxford microanalysis group, UK.

Transmission electron microscopy (TEM) images were obtained on a Zeiss EM 912 Omega transmission electron microscope operating at 300 kV. The samples were ultramicrotomed (Leica EM FC6) and placed onto the copper grids coated with a carbon film.

Confocal Scanning Fluorescence Microscopy (CSFM). A Leica TCS SP confocal laser scanning microscope (Leica, Germany) with a 100$\times$ oil immersion objective (numerical aperture 1.4) was used.

The self-regulated bacterium adsorption properties of the samples were determined using gram-positive bacteria *Lactococcuslactis ssp. lactis 411* as the test cultures. The overnight cultures were cultivated in peptone-yeast MRS medium. Rhodamine 6G was added to the bacteria suspension to achieve a concentration of 10^{-7} M. After 30 min the bacteria were centrifuged and washed two times. Then the ultrasonically formed aluminum sponge modified with micelles was deposited on the bottom of flat sample cells, which were filled with 0.2 mL of the bacteria suspension. The adsorption equilibrium was typically attained in 5$-$10 min and the initial adsorption efficiency was measured with a confocal microscope. The same spot of the sample was controlled for the next six hours and imaged every 15-30 min. The standard deviations of three replicate experiments were within 7%. In the control test, in which the ultrasonic-engineered aluminum sponge was not additionally modified with micelles, no change in the bacteria adsorption was detected indicating no self-regulated bacteria release.

To evaluate the surface biocide activity, two parameters were calculated: (i) the survival ratio and (ii) the reduction factor. The survival ratio ($S = C/C_0 \cdot 100\%$, where C_0 is the initial number of colony-forming units (CFUs) and C the number of CFUs after desorption) provides information on the overall bactericidal efficiency of the system. The reduction factor (RF = Nc/N, where N and Nc are the numbers of CFUs remaining in suspension after contact with the silver-loaded and silver-free sponge, respectively) allows to determine the efficiency of inactivation.

Acknowledgements

References

1. a) S. Raghavan, C. S. Chen, *Adv. Mater.* **2004**, *16*, 1303; b) C. S. Chen, M. Mrksich, S. Huang, G. M. Whitesides, D. E. Ingberg, *Science* **1997**, *276*, 1425; c) T. Ekblad, L. Faxlv, O. Andersson, N. Wallmark, A. Larsson, T. L. Lindahl, B. Liedberg, *Adv. Funct. Mater.* **2010**, *20*, 2396.

2   a) J. Ziauddin, D. M. Sabatini, *Nature* **2001**, *411*, 107; b) J. El-Ali, P. K. Sorger, K. F. Jensen, *Nature* **2006**, *442*, 403; c) R. Langer, J. P. Vacanti, *Science* **1993**, *260*, 920.

3   a) M. Veiseh, H. Zareie, M. Zhang, *Langmuir* **2002**, *18*, 6671; b) H. Kim, R. E. Cohen, P. T. Hammond, D. J. Irvine, *Adv. Funct. Mater.* **2006**, *16*, 1313; c) T. H. Park, M. L. Shuler, *Biotechnol. Prog.* **2003**, *19*, 243.

4   a) N. Okochi, T. Okazaki, H. Hattori, *Langmuir* **2009**, *25*, 6947; b) M. Situmorang, J. J. Gooding, D. B. Hibbert, D. Barnett, *Electroanalysis* **2001**, *13*, 1469.

5   a) I. Banerjee, R. C. Pangule, R. S. Kane, *Adv. Mater.* **2011**, *23*, 690; b) C. Y. Flores, C. Diaz, A. Rubert, G. A. Benitez, M. S. Moreno, M. A. F. L. Mele, R. C. Salvarezza, P. L. Schilardi, C. Vericat, *J. Col. Interface Sci.* **2010**, *350*, 402.

6   a) V. A. Liu, S. N. Bhatia, *Biomedical Microdevices.* **2002**, *4*, 257; b) T. Y. Yu, C. K. Ober, *Biomacromolecules* **2003**, *4*, 1126; c) J. H. Ward, R. Bashir, N. A. Peppas, *J. Biomedical Mater. Res.* **2001**, *56*, 351.

7   K. Y. Suh, J. Seong, A. Khademhosseini, P. E. Laibinis, R. Langer, *Biomaterials* **2004**, *25*, 557.

8   E. Ostuni, R. S. Kane, C. S. Chen, D. E. Ingber, G. M. Whitesides, *Langmuir* **2000**, *16*, 7811.

9   W. Tan, T. A. Desai, *Biomed. Microdevices* **2003**, *5*, 235.

10 S. Takayama, J. C. McDonald, E. Ostuni, M. N. Liang, P. J. Kenis, R. F. Ismagilov, G. M. Whitesides, *Proc. Natl. Acad. Sci. USA* **1999**, *96*, 5545.

11 a) M. Nishizawa, K. Takoh, T. Matsue, *Langmuir* **2002**, *18*, 3645; b) H. Kaji, K. Tsukidate, T. Matsue, M. Nishizawa, *J. Am. Chem. Soc.* **2004**, *126*, 15026.

12 a) P. Roacha, T. Parker, N. Gadegaard, M. R. Alexander, *Surf. Sci. Reports* **2010**, *65*, 145; b) G. Decher, *Science* **1997**, *277*, 1232; c) M. Nolte, B. Schoeler, C. S. Peyratout, D. G. Kurth, A. Fery, *Adv. Mater.* **2005**, *17*, 1665; d) Y. Lvov, F. Caruso, *Anal. Chem.* **2001**, *73*, 4212; e) E. Kharlampieva, V. Kozlovskaya, S. A. Sukhishvili, *Adv. Mater.* **2009**, *21*, 3053.

13 a) R. Singhvi, A. Kumar, G. P. Lopez, G. N. Stephanopoulos, D. I. C. Wang, G. M. Whitesides, D. E. Ingber, *Science* **1994**, *264*, 696; b) M. D. Kurkuri, C. Driever, G. Johnson, G. McFarland, H. Thissen, N. H. Voelcker, *Biomacromol.* **2009**, *10*, 1163; c) M. C. Berg, S. Y. Yang, P. T. Hammond, M. F. Rubner, *Langmuir* **2004**, *20*, 1362.

14 a) K. Lewandowska, E. Pergament, N. Sukenik, L. A. Culp, *J. Biomed. Mater. Res.* **1992**, *26*, 1343; b) U. Hersel, C. Dahmen, H. Kessler, *Biomaterials.* **2003**, *24*, 4385; c) W. Feng, S. Zhu, K. Ishihara, J. L. Brash, *Langmuir* **2005**, *21*, 5980; d) Z. Zhang, S. Chen, Y. Chang, S. Jiang, *J. Phys. Chem. B* **2006**, *110*, 10799.

15 a) S.-H. Lee, J. J. Moon, J. L. West, *Biomaterials* **2008**, *29*, 2962; b) K. Rechendorff, M. B. Hovgaard, M. Foss, V. P. Zhdanov, F. Besenbacher, *Langmuir* **2006**, *22*, 10885.; c) Y. Dou, K. Lin, J. Chang, *Nanoscale.* **2011**, DOI: 10.1039/c1nr10028a; d) P. Roach, D. Farrar, C. C. Perry, *J. Am. Chem. Soc.* **2006**, *128*, 3939.

16 "The future of the Orthopedic Devices Market to 2012", Mike King, Oct. 12, **2008**, www.hipresurfacingnews.com.

17 a) D. V. Andreeva, *Int. J. Mat. Res.* **2011**, *102*, 597; b) D. V. Andreeva, D. V. Sviridov, A. Masic, H. Möhwald, E. V. Skorb, *SMALL.* **2011**, doi:10.1002 smll.201102365; c) E. V. Skorb, D. G. Shchukin, H. Möhwald, D. V. Andreeva, *Nanoscale* **2010**, *2*, 722; d) D. V. Andreeva, D. G. Shchukin, H. Möhwald, *Adv. Mater.* **2008**, *20*, 2789; e) J. Lu, K.-H- Zum Gahr, J. Schneider, *Wear* **2008**, *265*, 1680;

18 a) J. Schäferhans, S. Gomez-Guero, D. V. Andreeva, G. Rhotenberg, *Chem. Eur. J.* **2011**, *17*, 12254; b) Hielscher GmbH, http://www.hielscher.com/ultrasonics/industry.htm.

19 a) L. H. Thompson, L. K. Doraiswamy, *Ind. Eng. Chem. Res.* **1999**, *38*, 1215; b) K. S. Suslick, L. A. Crum, in *Encyclopedia of Acoustics*(Ed: M. J. Crocker), Wiley & Sons. Inc., N. Y. **1995**; c) J. H. Bang, K. S. Suslick, *Adv. Mater.* **2010**, *22*, 1059.

20 a) J. Banhart, *Prog. Mater. Sci.* **2001**, *46*, 559; b) G. J. Davies, S. J. Zhen, *J. Mater. Sci.* **1983**, *18*, 1899; c) H. Hakamada, M. Mabuchi, *Scr. Mater.* **2007**, *56*, 1003.

21 J. Erlebacher, M. J. Aziz, A. Karma, N. Dimitrov, K. Sieradzki, *Nature* **2001**, *410*, 450.

22 Y. Ding, J. Erlebacher, *J. Am. Chem. Soc.* **2003**, *125*, 7772.

23 *Preparation of Solid Catalysts,*(Eds: G. Ertl, H. Knözinger), Wiley-VCH, Weinheim, Germany **1997**.

24 a) E. V. Skorb, D. Fix, D. G. Shchukin, H. Möhwald, D. V. Sviridov, R. Mousa, N. Wanderka, J. Schäferhans, N. Pazos-Pérez, A. Fery, D. V. Andreeva, *Nanoscale* **2011**, *3*, 985; b) E. V. Skorb, H. Möhwald, T. Irrgang, A. Fery, D. V. Andreeva, *Chem. Comm.* **2010**, *46*, 7897; c) D. G. Shchukin, D.V. Andreeva, E. V. Skorb, H. Möhwald, in: *Supramolecular Chemistry of Hybrid Materials* (Ed: K. Rurack), Wiley-VCH, Weinheim, Germany **2010**.

25 a) Y. Sugimura, J. Meyer, M. Y. He, H. Bart-Smith, J. Grenstedt, A. G. Evans, *Acta Mater.* **1997**, *45*, 5245; b) O. Mizuno, T. Matsuura, S. Nakayama, K. Harad, A. Yamakawa, *SEI Tech. Rev.* **2003**, *55*, 95.

26 a) M. A. Margulis, Sonochemistry basis, High School, Moscow, **1984**; b) K. S. Suslick, G. J. Price, *Annu. Rev. Mater. Sci.* **1999**, *29*, 295.

27 a) E. V. Skorb, D. G. Shchukin, D. V. Andreeva, *Langmuir* **2010**, *26*, 16973; b) D. G. Shchukin, E. V. Skorb, V. Belova, H. Möhwald, *Adv. Mater.* **2011**, *23*, 1922; c) N. Pazos-Pérez, J. Schäferhans, E. V. Skorb, A. Fery, D. V. Andreeva, *Micropor. Mesopor. Mater.* **2011**, doi:10.1016/j.micromeso.2011.08.011.

28 a) E. Betthausen, M. Drechsler, M. Förtsch, F. H. Schacher, A. H. E. Müller, *Soft Matter.* **2011**, *7*, 8880; b) J. Gensel, E. Betthausen, C. Hasenöhrl, K. Trenkenschuh, M. Hund, F. Boulmedais, P. Schaaf, A. H. E. Müller, A. Fery, *Soft Matter.* **2011**, *23*, 11144.

29 a) H. Dautzenberg, W. Jaeger, J. Kötz, B. Philipp, C. Seidel, D. Stscherbina, in *Polyelectrolytes*, Carl Hanser Verlag, München, **1994**; b) I. Borukhov, D. Andelman, R. Borrega, M. Cloitre, L. Leibler, H. Orland, *J. Phys. Chem. B* **2000**, *104*, 11027; c) G. Battaglia, C. Fernyhough, A. J. Ryan, *Soft Matter* **2009**, *5*, 1674.

30 a) C. B. Bucur, Z. Sui, J. B. Schlenoff, *J. Am. Chem. Soc.* **2006**, *128*, 13690; b) J. B. Schlenoff, A. H. Rmaile, C. B. Bucur, *J. Am. Chem. Soc.* **2008**, *130*, 13589; c) P. Schaaf, J. Talbot, *J. Chem. Phys.* **1989**, *91*, 4401.

31 a) G. B. Webber, E. J. Wanless, S. P. Armes, F. L. Baines, S. Biggs, *Langmuir* **2001**, *17*, 5551; b) M. Borkovec, R. Pericet-Camara, B. P. Cahill, G. Papastavrou, *Chem. Comm.* **2007**, *266*; c) E. V. Skorb, D. Fix, D. V. Andreeva, D. G. Shchukin, H. Möhwald, *Adv. Funct. Mater.* **2009**, *19*, 2373; d) E. V. Skorb, D. G. Shchukin, H. Möhwald, D. V. Sviridov, *J. Mater. Chem.* **2009**, *19*, 4931; e) K. Sakai, E. G. Smith, G. B. Webber, M. Baker, E. J. Wanless, V. Bütün, S. P. Armes, S. Biggs, *Langmuir* **2006**, *22*, 8435.

32 a) D. V. Andreeva, E. V. Skorb, D. G. Shchukin, *Appl. Mater. Inter.* **2010**, *2*, 1954; b) E. V. Skorb, D. V. Sviridov, H. Möhwald, D. G. Shchukin, *Chem. Comm.* **2009**, *6041*; c) E. V. Skorb, A. Skirtach, D. V. Sviridov, D. G. Shchukin, H. Möhwald, *ACS Nano* **2009**, *3*, 1753.

33 N. Pazos-Perez, T. Borke, D. V. Andreeva, R. A. Alvarez-Puebla, *Nanoscale* **2011**, *3*, 3265.

34 a) S. Schmidt, M. Zeiser, T. Hellweg, C. Duschl, A. Fery, H. Möhwald, *Adv. Funct. Mater.* **2010**, *20*, 3235; b) R. Álvarez-Puebla, R. Contreras-Cáceres, I. Pastoriza-Santos, J. Pérez-Juste, L. M. Liz-Marzán, *Angew. Chem. Int. Ed.* **2009**, *48*, 138.

35 M. Meyer, M. Antonietti, H. Schlaad, *Soft. Matter.* **2007**, *3*, 430.

7 Reversible Swelling Transitions in Stimuli-Responsive Layer-by-Layer Films Containing Block Copolymer Micelles
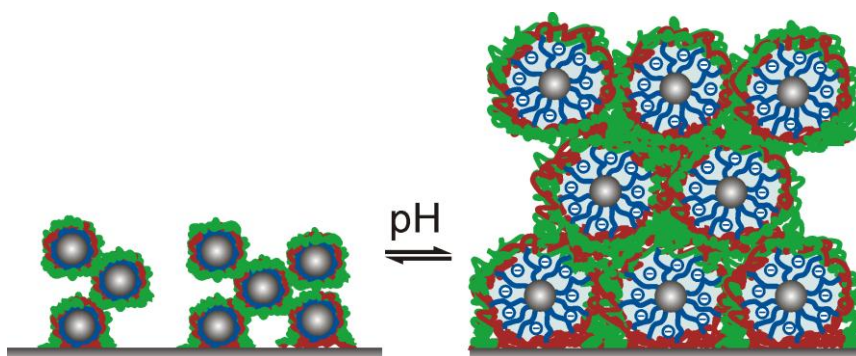
Julia Gensel,[a] Inna Dewald,[a] Johann Erath,[a] Eva Betthausen,[b] Axel. H. E. Müller[b] and Andreas Fery[a]*

[a] Department of Physical Chemistry II, University of Bayreuth, Universitätsstr. 30, 95440 Bayreuth, Germany

[b] Department of Macromolecular Chemistry II, University of Bayreuth, Universitätsstr. 30, 95440 Bayreuth, Germany

* e-mail: Andreas.Fery@uni-bayreuth.de

Abstract

We present a new nanoporous multilayer system with a reversible pH-triggered swelling transition. Using the layer-by-layer approach, pH-responsive block copolymer micelles with a hydrophobic core, a weak polyanion shell and a strong polycation corona formed from an ABC triblock terpolymer are included within multilayer films. The approach of complexing the strong polycationic corona with a strong polyanion leads to the creation of novel double-end-tethered polyelectrolyte brush structures confined between the hydrophobic micellar cores and the interpolyelectrolyte complexes.

The swelling degree, morphology as well as the mechanical properties of the coatings are reversibly tunable by the solution pH due to the ionization-induced swelling of the pH-sensitive polyelectrolyte-brush-like shell of the incorporated micelles resulting in large-scale volumetric changes of the film. Moreover, controlling the internal film architecture by the number of deposition steps allows tuning the properties of the porous multilayers such as the density of incorporated micelles, the porosity, and the equilibrium swelling degree to more than 1200%.

7.1 Introduction

The design of "smart" coatings, which can reversibly switch their physico-chemical characteristics in reaction to external stimuli is a very attractive research field regarding its diverse applications, *e.g.* in drug delivery and microfluidic systems, cell tissue engineering, as well as sensing, or actuation (see reviews 1-10). The adsorption of stimuli-responsive soft matter systems on a solid support is an effective and simple way to fabricate switchable surfaces. Coatings which respond to changes in pH or ionic strength, can be obtained by chemical grafting of polymer or polyelectrolyte brushes onto planar [11-14] or curved [15] surfaces. Alternatively, thin films of polymer networks can be used as smart coatings. In most of these cases hydrogel-like films can uptake large amounts of water, whereby their swelling degree (the ratio of swollen to dry volume), which can be controlled by external physical or chemical signals, determines their mechanical and optical properties, permeability, adhesion *etc*. Such a modulation of the mechanical properties of coatings can be used for example to control cell adhesion.[16]

Another elegant approach to design smart surfaces is the adsorption of block copolymer micelles. Several research groups have studied the stimuli-responsive behavior of an adsorbed monolayer of micelles.[17-21] Recently, we reported on the immobilization of micelles of a linear ABC triblock terpolymer consisting of polybutadiene (B), poly(methacrylic acid) (MAA), and quaternized poly(2-(dimethylamino)ethyl methacrylate) (Dq), BMAADq on silica.[22] We have found that by controlling the solution pH at the solid-liquid interface of the adsorbed micelles, it is possible to reversibly switch the micellar morphology and charge density of the corona. This pH-responsive behavior can be controlled by the ionization degree of the weak polyelectrolyte middle block (MAA) and is completely reversible on short time scale. More recently, we have successfully used these switchable coatings as active surfaces for bio-applications, in particular for controlled self-regulated bacteria release.[23] However, the long-term treatment at pH < p$K_{a,apparent}$ of MAA causes irreversible changes in the morphology of the immobilized BMAADq micelles.[22] In general, the instability of a monolayer of stimuli-responsive micelles is a challenging aspect[17, 19, 22, 24, 25] which is critical for many applications. One way to improve the resilience of such structures is the chemical cross-linking of the hydrophobic cores.[22] Sukhishvili and co-workers reported another facile way of stabilization against environmental influences for otherwise instable surface-attached micelles *via* self-assembly of the micelles with a polyelectrolyte layer using physical cross-linking.[24] They observed irreversible morphological changes and desorption of a significant fraction of temperature-responsive micelles of poly(*N*-vinylpyrrolidone)-*b*-poly(*N*-isopropylacrylamide) into the solution, while the same surface-adsorbed micelles covered with a top layer of poly(methacrylic acid) maintained their original structural integrity.

Besides the improved stability, this strategy allows coverage of any type of substrate and fine-tuning the thickness and nanostructure of the stimuli-responsive film *via* layer-by-layer (LbL) assembly of oppositely charged polymers.[26-28] In particular, Tan *et al.* reported that temperature-sensitive core–shell micelles of ABA triblock copolymers can be incorporated within the LbL films while retaining their stimuli-responsive properties.[29,30] The obtained films are generally very thin (10-100nm) enabling a rapid response to environmental changes as compared to bulk materials.

The incorporation of charged nanoparticles[31,32] as well as diblock copolymer micelles into multilayers with integrated stimuli-responsive properties has been previously reported for one-type-micellar[33-37] or micelle-micelle-systems.[38-40] These types of systems are particularly suitable for the fabrication of hydrogel-like films[35] for drug delivery,[24,34,36] coatings with tunable optical properties,[33,38] or antibacterial coatings.[41] Furthermore, LbL assembly of

micelles offers the advantage of fabricating porous thin films[38] without any additional post-treatment steps usually required for their preparation.[42] A special class of stimuli-responsive porous hydrogel-like thin films combines fast response and precise control over the pore closing/opening by an external signal.[7, 8]

Here, we study a new LbL system, consisting of ABC block terpolymer micelles with a hydrophobic polybutadiene (B) core, pH-sensitive poly(methacrylic acid) (MAA) shell, and a cationic corona of quaternized poly(2-(dimethylamino)ethyl methacrylate) (Dq) (BMAADq) and linear strong polyanion poly(sodium 4-styrenesulfonate) (PSS). Due to the pH-sensitive character of the incorporated micelles, the system allows the ionization degree of the weak polyelectrolyte block (MAA) to be varied by changing the pH. One remarkable feature of the system is that the pH-sensitive block is not a component of the multilayer complexes, but is covalently bound to the micellar core on the one side and to the multilayer-forming corona on the other side. This approach leads to the formation of a double-end-tethered weak polyelectrolyte brush-like shell. Hence, we investigated the effect of solution pH on the swelling behavior as well as on the mechanical properties of the hydrogel film. In addition, the influence of the swelling on the film porosity was studied.

7.2 Materials and methods

7.2.1 Materials

The triblock terpolymer consisting of polybutadiene (B), poly(methacrylic acid) (MAA), and quaternized poly(2-(dimethylamino)ethyl methacrylate) (Dq), B800MAA200Dq285 (subscripts denoting the degrees of polymerization of the respective blocks) with an M_n of ~ 110 000 g mol^{-1} and a PDI of 1.10 was synthesized via sequential living anionic polymerization followed by polymer-analogous modifications as described elsewhere.[43] In particular, the poly(2-(dimethylamino)ethyl methacrylate) block was exhaustively quaternized with dimethyl sulfate. After quaternization in a dioxane–water mixture (1 : 1, v/v), the BMAADq terpolymer was dialyzed against pH 10 buffer solution to obtain a micellar stock solution with a concentration of 0.5 g L^{-1}. From this stock solution changes in pH were performed by dialyzing against the corresponding buffer solutions (pH 4, VWR, AVS Titrinorm).[43] The obtained micelles have a spherical shape as confirmed by cryogenic TEM and DLS experiments.[43] The hydrodynamic radius R_h of the micelles in pH 4 buffer was

determined by DLS to 107 nm. According to the core radius obtained *via* cryo-TEM, the aggregation number, N_{agg}, of the BMAADq micelles can be calculated with eqn (7.1):

$$N_{agg} = \frac{m_{core}}{m_{PB}^{chain}} = \frac{4\pi N_A \rho_{PB} R_{core}^3}{3 M_{PB}^{chain}} \qquad (7.1)$$

where m_{core} is the mass of the micellar core; m_{PB}^{chain} is mass of an individual PB chain; N_A is the Avogadro constant; ρ_{PB} is the density of polybutadiene; R_{core} is the radius of the micellar core according to cryo-TEM and M_{PB}^{chain} is the molecular weight of an individual PB chain. At pH 4 the core radius is 32 nm, which yields an aggregation number of approximately 1800. Please note that this method is just a rough estimate and strongly depends on the quality of the cryo-TEM micrographs for the determination of the core interface. Poly(sodium 4-styrene sulfonate) (PSS, M_w = 70 000 g mol⁻¹) was purchased from Sigma-Aldrich. HCl and NaOH solution (0.1 mol L⁻¹, Grüssing) were used to adjust the pH of water.

7.2.2 Multilayer deposition

The LbL films were assembled on silicon wafers (CrysTec) from 0.45 g L⁻¹ polymer solutions *via* dip coating. The substrates were cleaned using the RCA technique[44] (sonication in a 1:1 mixture of water and 2-propanol for 15 min, followed by heating at 70 °C in a 5:1:1 mixture of water, 25% ammonia solution, and 30% hydrogen peroxide solution for 10 min). The freshly cleaned substrates were then dipped into a solution of BMAADq micelles in pH 4 buffer solution (VWR, AVS Titrinorm, ionic strength ~ 0.05 M) for 15 min before rinsing with water. Next, the substrates were dipped into an aqueous solution of PSS (adjusted to pH 4 with 0.1 M HCl) for 15 min. The films were dried in a stream of nitrogen before characterization.

7.2.3 Methods

Ellipsometry measurements in air were performed with a Sentech SE 850 spectroscopic ellipsometer at a constant incidence angle of 70°. A home build liquid cell[45] was used for *in situ* ellipsometry in water of a different pH at a constant incidence angle of 65°. Measurements were performed after a minimum equilibration time of 20 min.

Atomic force microscopy (AFM) images were taken with a commercial AFM (Dimension™ 3100 equipped with a NanoScope® V controller, both from Bruker AXS Inc.,

USA) operating in TappingMode™ using Si_3N_4 cantilevers from Olympus with a typical spring constant of ~ 42 N m^{-1} and a typical resonance frequency of 300 kHz (OMCL-AC160TS).

Scanning in fluid was performed with a direct driven TappingMode™ probe holder (DTFML-DD-HE, Bruker, AXS Inc., USA) using cantilevers with a spring constant of ~ 0.06 N m^{-1} and a resonance frequency of 12 - 24 kHz (Bruker, SNL-10).

Scanning electron microscopy (SEM) measurements were obtained on a Gemini Leo 1550 instrument operating at 3 keV. Samples were sputtered with a 1.3 nm thin platinum layer.

The colloidal probe atomic force microscopy (CP AFM) measurements were performed on an Asylum MFP 3D AFM (Mannheim, Germany) in a water droplet at the corresponding pH. Glass particles (Polysciences, Germany) were used as force sensors. The CPs, made of SiO_2, were glued with an epoxy resin (UHU schnellfest, Germany) to pre-calibrated cantilevers (force constant ~ 0.1 N m^{-1}, NSC 12, tipless, noAl, Micromash, Estonia) using a micromanipulator (MP-285, Shutter Instrument, USA) and an inverted optical microscope (Axiovert 200, Zeiss, Germany). Force constants of the cantilevers were determined by the thermal noise method introduced by Hutter and Bechhoefer.[46] For all the presented data, a cantilever with a force constant of 0.125 N m^{-1} and a CP with a radius of $R = 23$ μm was used. The optical lever sensitivity was always detected prior to recording the data by reference measurements on a hard glass substrate.

7.3 Results and discussion

7.3.1 Layer-by-layer assembly

To develop pH-responsive layer-by-layer hydrogel coatings, we used a linear ABC triblock terpolymer consisting of polybutadiene (B), poly(methacrylic acid) (MAA), and quaternized poly(2-(dimethylamino)ethyl methacrylate) (Dq), BMAADq. The molecular structure is given in Figure 7.1a. Details regarding the synthesis and characterization of the polymer can be found elsewhere.[43] In aqueous solution, BMAADq self-assembles into core-shell-corona micelles with a hydrophobic B core, a pH-sensitive MAA shell and a strong cationic Dq corona.

At low pH (pH < p$K_{a,app}$ of MAA ≈ 5.5 (ref. 47), the pH-sensitive MAA block is uncharged and does not form an IPEC, but rather phase separates from the corona as shown in Fig. 7.1b. At high pH, this block is negatively charged through the deprotonation of the carboxylic acid

groups leading to intramicellar interpolyelectrolyte complex (*im*-IPEC) formation with the cationic corona of Dq. Hence, the composition of the micellar shell as well as the charge density of the corona can be controlled by the solution pH (Fig. 7.1b).
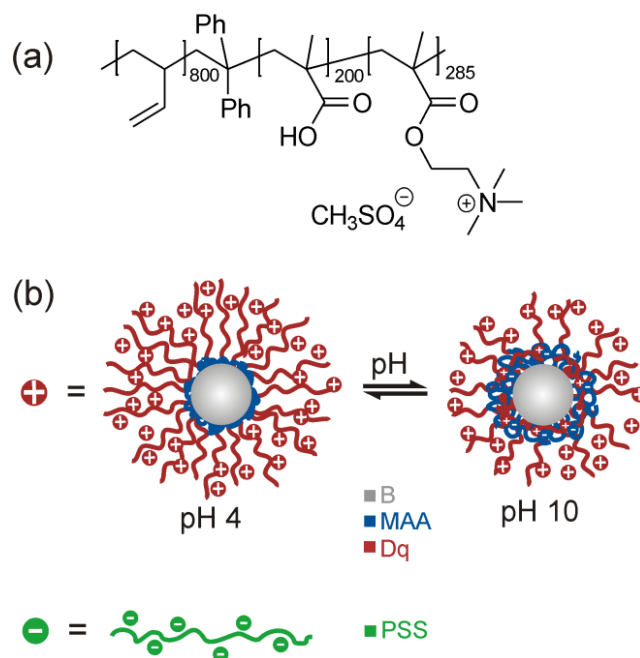

Fig. 7.1: Chemical structure of the BMAADq triblock terpolymer (a), schematic representation of the solution structure of positively charged BMAADq micelles at pH 4 and pH 10, and negatively charged PSS (b).

Due to the cationic character of the micelles, we chose anionic poly(sodium 4-styrene sulfonate) (PSS) as counterpart for the layer-by-layer assembly. PSS is known to form stable complexes/multilayers with strongly charged polycations (like Dq) because of its permanently high charge density.[48]

We prepared LbL films at pH 4. At this pH, the MAA shell is protonated and does not form an *im*-IPEC with the Dq corona. Therefore, all of the coronal chains are expected to form stable complexes with PSS. Consequently, the MAA block should form an uncharged shell around the B core at this pH. Figure 7.2a displays the ellipsometric dry film thickness plotted *versus* the number of triblock terpolymer/polyanion deposition steps, x. The film growth follows a square root dependency (Fig. 7.2b). This behavior indicates a diffusion-limited assembly process, which may originate from the diffusion of the micelles into the pores of the film: further deposited micelles do not adsorb on top of the film, but diffuse through the pores to fill them and thus increase the micelle density in the multilayers.
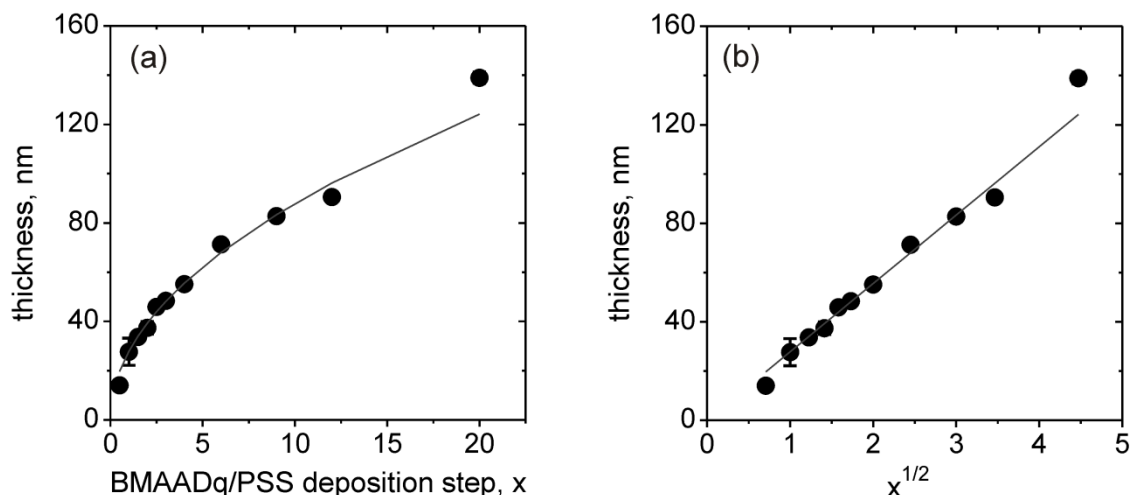
Fig. 7.2: Ellipsometric dry thickness *vs.* the number of BMAADq/PSS deposition steps, x (a) and *vs.* the square root of x (b). The lines are a square root fit and a linear fit to the data, respectively.

To obtain detailed structural information about the LbL multilayers, atomic force microscopy (AFM) and scanning electron microscopy (SEM) measurements were performed on dried samples. From the AFM height image of one bilayer of BMAADq/PSS (denoted as (BMAADq/PSS)$_1$) (Fig. 7.3a), the average diameter and the height of the spherical-cap-like structures (based on the average of at least 30 features) were estimated to be (125 ± 8) nm and (49 ± 5) nm, respectively. The dimensions obtained by AFM correspond to the topography image including the core, the shell, and the IPEC between the Dq corona and the extrinsic homopolymer PSS. In contrast, the SEM image of one bilayer in the dry state (Fig. 7.3c) shows the hydrophobic cores (bright) surrounded by a dark shell and the Dq/PSS IPEC indicating the retained core-shell-IPEC-structure upon incorporation of the micelles into multilayers. The diameter of the hydrophobic core is (71 ± 8) nm (based on the average of at least 30 micelles), which is comparable with the diameter of the cores in pH 4 buffer solution (~64 nm).[43] In our previous work, we have shown that the adsorption of BMAADq micelles onto a silica surface follows the random sequential adsorption (RSA) model with a maximum surface coverage of 0.54.[22] Therefore, micelles can only be randomly dispersed on the substrate for the first layer leading to a porous structure of the resulting LbL films (Fig. 7.3) The adsorption of the same micelles on the substrates covered with a layer of negatively charged PSS resulted in similar adsorption kinetics as well as the saturation value of ~0.5 (Fig. S1, SI). A further example is the random adsorption of the micelles studied on

ultrasonically formed mesoporous aluminum.[23] These examples confirm that the system studied here can be used to cover different substrates in a controlled and reproducible manner. Note that since this hit-stick RSA adsorption behavior is associated with the immobilization of micelles, rearrangements inside the film should not be possible. This is consistent with the work of Kabanov and co-workers: the high affinity of PSS to polycations imposes kinetic restrictions on the exchange reactions of PSS/Dq IPECs.[50] Therefore, to the best of our knowledge, the non-linear buildup and the reduction of porosity do not occur as a result of the rearrangement of micelles during the deposition.
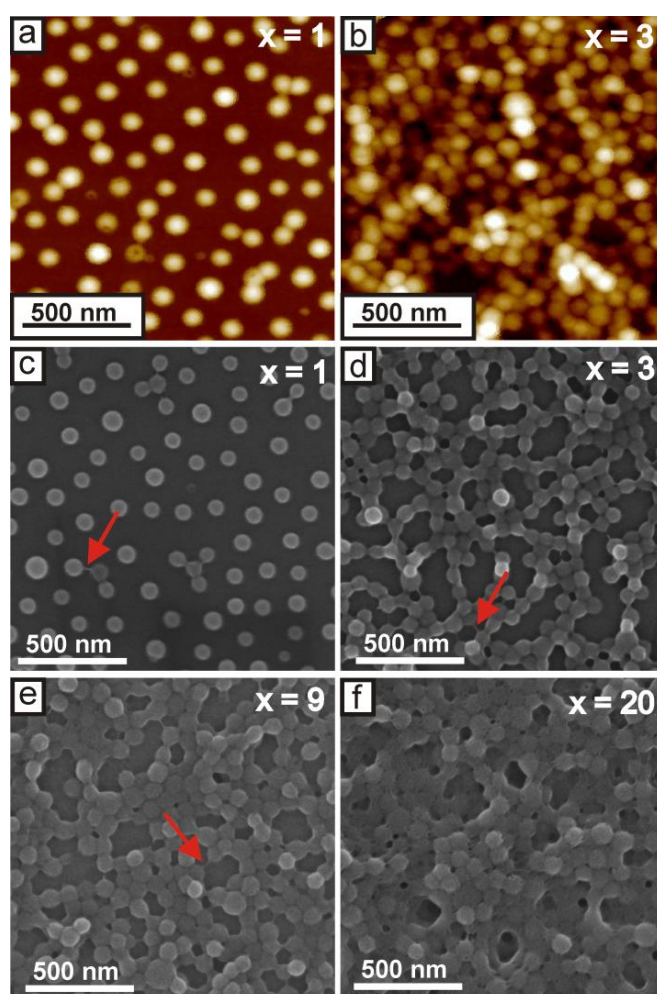

Fig. 7.3: 1.5 μm × 1.5 μm AFM height images (a, b) (color equates to z = 0 − 100 nm) and SEM images (c − f) of (BMAADq/PSS)$_x$ porous films. x is the number of build-up steps. Arrows indicate the formation of hydrophobic bridges.

The assumption of micelles filling the void space in the film instead of attaching on the top (resulting in a non-linear buildup behavior (Fig. 7.2)) is supported by a detailed study of the

nanostructure (Fig. 7.3). The AFM height and SEM images in Fig. 7.3 demonstrate a significant increase in the micelle density in the film and therefore a decreased porosity with increasing number of deposition steps.

The porosity (P) of the films was evaluated from refractive index measurements applying the mixing rule to the Lorentz-Lorenz equation[51]

$$\frac{n_x^2 - 1}{n_x^2 + 2} = P \frac{n_{air}^2 - 1}{n_{air}^2 + 2} + (1-P) \frac{n_f^2 - 1}{n_f^2 + 2} \tag{7.2}$$

where n_x, n_{air}, and n_f are the refractive indices of the porous film, air, and the dense film and P and (1-P) the volume fraction of the pores and of the dense film, respectively. With $n_{air} = 1$, the equation (7.1) can be simplified to

$$P = 1 - \frac{n_x^2 - 1}{n_f^2 - 1} \cdot \frac{n_f^2 + 2}{n_x^2 + 2} \tag{7.3}$$

Fig. 7.4 shows the refractive indices n_x of porous films measured by ellipsometry and the resulting porosity values obtained from (7.3), assuming that the refractive index of the dense film n_f=1.51 (estimated by ellipsometry of drop-coated PSS (n = 1.51) and BMAADq (n = 1.51) films).
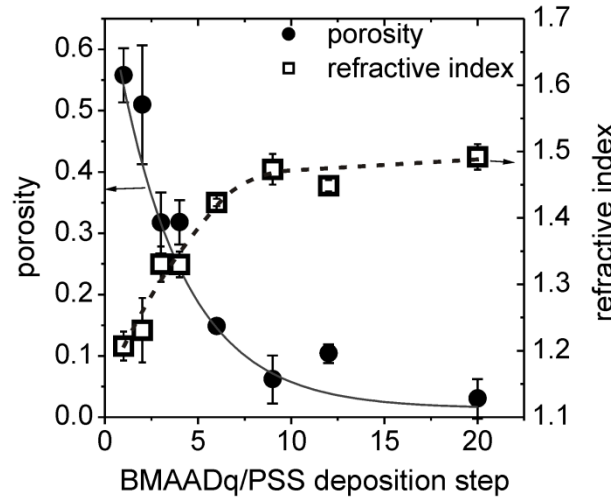

Fig. 7.4: Porosity (●) and refractive index (□) *vs.* the number of BMAADq/PSS deposition steps. The lines are guides to the eye.

The porosity of the multilayers can be easily tuned between ~50% and 0% by the number of deposition steps. Such interconnected micellar network formation can be explained by the generation of hydrophobic bridges during the assembly process as indicated by the arrows in the SEM-images (Fig. 7.3c-e). Hydrophobic bridges were also found in aqueous solutions of the same micelles[43] as well as of other block terpolymer micelles with a low glass transition temperature of the core-forming block.[52, 53] Still, mainly spherical particles are found in the multilayers indicating that the core-shell structure remains intact upon integration into multilayers.

7.3.2 Stimulus response

On the basis of the retained core-shell structure of the LbL-incorporated micelles and due to the pH-responsive character of the polyelectrolyte brush-like MAA shell, we investigated the swelling behavior of these films by *in-situ* ellipsometry. To confirm data obtained from ellipsometry, we additionally measured the height difference at the edge of a scratch by AFM in a liquid cell. Exemplarily, results for a three-bilayer-film (BMAADq/PSS)$_3$ at different pH between pH 4 and 12 are shown in Figure 7.5a. Films with differing number of bilayers follow the same trend with varying pH.

Swelling of the film is observed when the pH is increased to alkaline values with a transition at pH ~ 9.5. The increase in thickness corresponds to the deprotonation of the carboxylic groups of the MAA shell and can be tuned by the degree of dissociation α. In acidic solutions at α ~ 0, the film is in a contracted state. With increasing pH, α increases leading to a higher charge density and therefore increased repulsive interactions between the COO$^-$ groups. This results in a higher osmotic pressure of trapped counter ions, a stretching of the MAA chains and a swelling of the film.

The transition region at pH ~9.5 (corresponding to the pH at which $α$ ~0.5) is significantly higher than the apparent pK_a value of PMAA reported in the literature (p$K_{a,app}$ ~5.5 (ref. 47)) indicating that when confined into the micellar multilayer film, MAA becomes a weaker polyacid in comparison to its behavior in dilute solution. The shift in the apparent pK_a values of weak polyelectrolytes upon incorporation into multilayered films is also known from other work.[54-58] In contrast to our results, in the latter cases, the apparent pK_a values of incorporated weak polyacids and polybases were shifted by ~1 to 4 pH units to the acidic or alkaline values, respectively. The above cited results indicate that the polyacid becomes a stronger acid if it is the component of a polyelectrolyte multilayer film.
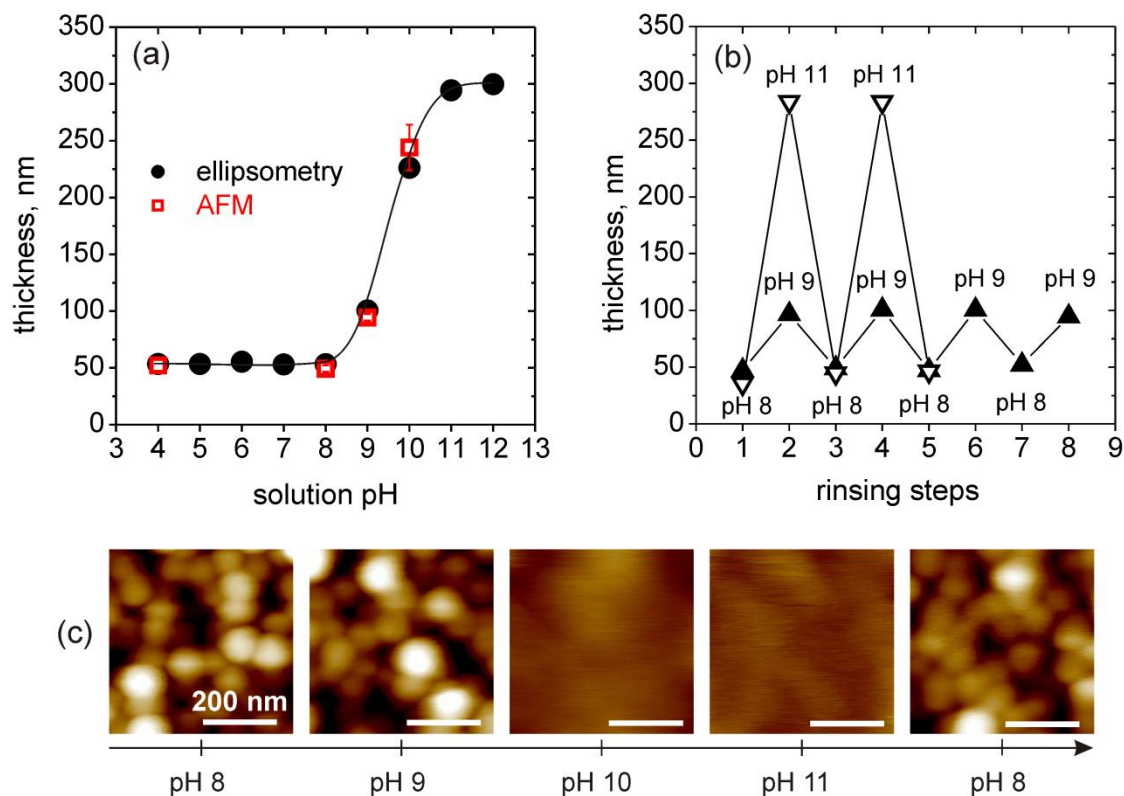
Fig. 7.5: *In situ* measurements of the ellipsometric thickness (●) and liquid cell AFM height difference at a scratch (□) of (BMAADq/PSS)$_3$ *vs.* the solution pH (a), *in situ* ellipsometry measurements of reversible pH-triggered swelling and contraction of (BMAADq/PSS)$_3$ film (b) and corresponding 500 nm × 500 nm AFM height images (color equates to z = 0 − 100 nm) in water at different pH values (c).

However, we observed an opposite effect, which originates from the fact that the MAA block is not a component of the multilayer complexes. In our system, the MAA block, which is covalently bound to the core-forming B block on the one side and to the Dq block (forming stable IPECs with PSS) on the other side, can be described as a spherical polyelectrolyte brush (around the micellar core), confined between electrostatically assembled layers. In fact, the shift to higher pH values agrees with experiments on polyelectrolyte brushes. The swelling transition of grafted PMAA brush layers with a high grafting density was found to be shifted to pH 9 as a result of the Coulombic repulsion of neighboring charges.[59] Currie *et al.* reported similar pK_a shifts of poly(acrylic acid) brushes that became more pronounced with increasing grafting density.[60] In potentiometric titrations of multi-arm star-shaped poly(acrylic acid) we also observed an increase in the p$K_{a,app}$ with increasing arm number.[61] These findings are additionally supported by theoretical predictions.[62]

The pH switch is fully reversible after several pH 8/pH 9 and pH 8/pH 11 cycling steps (Figure 7.5b). The MAA domains respond to pH switching by changing between high and low ionized states resulting in swelling and shrinking of the multilayers.

Although a single layer of micelles studied here shows irreversible morphological changes at pH 4 or lower,[22] micelles that are covered with a layer of PSS are very robust and stable after long-term treatment (in the order of several hours) at pH values between pH 4 and pH 12. This is due to the formation of a stable IPEC of PSS and the cationic corona of the micelles. A similar method for the stabilization against environmental influences for otherwise instable surface-attached micelles was reported by Sukhishvili and Zhu.[24] They observed that surface-adsorbed micelles covered with a top layer of poly(methacrylic acid) remained stable and maintained their original structural integrity, while the same uncovered micelles showed irreversible morphological changes and desorption into the solution.

The corresponding AFM images in water at different pH values are shown in Fig. 7.5c. At slightly alkaline pH (pH 8), the film maintains its porous micellar morphology with an average pore diameter of ~70 nm ranging from 30 to 160 nm. At higher pH (pH 9), the micellar diameter increases while the pore diameter decreases to a mean value of ~50 nm. Here, the pores range in diameter from 20 to 120 nm. At even higher pH (pH 10 and pH 11), the volume filling factor $V = V_{\mathrm{micelle}}/V_{\mathrm{total,\ film}}$ is changed significantly upon swelling. After decreasing the pH to 8, the film regained its original porous structure indicating the reversible morphology changes triggered by pH. On the basis of the ellipsometric and AFM studies, we propose a schematic illustration of the reversible pH-triggered swelling and contraction of BMAADq/PSS multilayers (Fig. 7.6).

As IPECs have an important and characteristic feature of competition (polyion exchange) and replacement (polyion substitution) reactions, the ionized MAA brush at pH 11 might compete with PSS in participating complexation with quaternized amine groups of the coronal chains. However, the rate and position of the equilibrium of these reactions is strongly dependent on the nature of the polyelectrolyte pair within a polyelectrolyte complex or multilayer (*e.g.* reviews 49, 50). A comparable polyion interchange reaction in polyelectrolyte multilayers (PSS or PMAA and a polycation containing quaternized amine groups) was studied by Jomaa and Schlenoff.[63] They demonstrated that PSS irreversibly replaced all PMAA chains that were already part of the multilayer film at alkaline pH, when PMAA groups are completely ionized. Exposure of the PSS-containing multilayers to an alkaline solution of PMAA yielded no incorporation of PMAA as this would result in the formation of the energetically less favorable complex. This is as well in line with earlier findings of

Kabanov and coworkers that in mixtures of polyanions, a polycation preferentially binds with sulfonate-containing polyanions.[49,50,64] PSS is one of the strongest competitors for associating with polycations, whereas PMAA is known to form weakly bound complexes.[49,63,65] Dubas and Schlenoff reported the difference in free energy of complexation of a quaternized amine group with an acrylic acid group and a sulfonate group to be 14.9 kJ mol^{-1}.[65] As a consequence of this strong binding of sulfonate-containing polyanions with polycations, the interpolyelectrolyte chain exchange is inhibited. Thus, for our system, the positively charged Dq corona will preferentially associate with PSS rather than PMAA, even at pH 11.
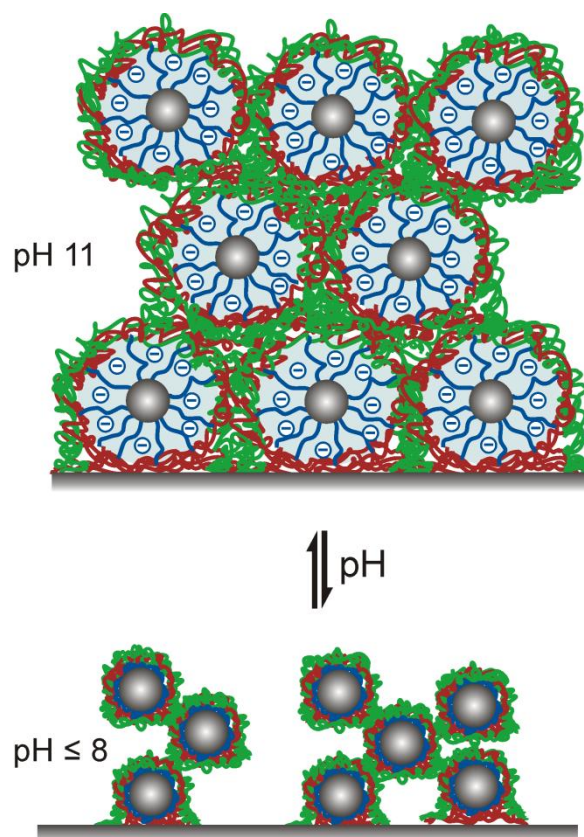

Fig. 7.6: Proposed schematic illustration of reversible pH-triggered swelling and contraction of BMAADq/PSS multilayers.

7.3.3 Mechanical characterization

As the BMAADq/PSS multilayers swell upon increasing the pH of the solution, we expect that the mechanical properties change with the degree of swelling. To study these changes we used the colloidal probe technique introduced by Butt[66] and Ducker.[67] Data were recorded by force-mapping measurements with an AFM. The detected force–distance curves were

transformed into force–indentation curves of the coatings by subtracting the effect of the cantilever deflection.

Fig. 7.7a shows the recorded force–indentation data for different swelling states of a (BMAADq/PSS)$_3$ multilayer. As upper force threshold we defined 20 nN which corresponds to deformations of around 80% of the film thickness. Measurements on the same spot of the sample show that the film is not plastically deformed (see Fig. S2 in the SI).

Since the adhesion in liquid is low and the films are not plastically deformed during the measurement, we used the linear elasticity theory to evaluate the mechanical properties of the system. The indentation of a sphere into a linear elastic infinite half space can be described by the Hertz model[68]

$$F = \frac{4}{3}\frac{E}{1-v^2}R^{1/2}\delta^{3/2} \qquad (7.4)$$

where F is the force applied by a spherical indenter (CP) with radius R, v is the Poisson ratio, E the Young's modulus, and δ the indentation of the film.

To avoid substrate effects, only data below 30 % of indentation were used for the Hertz analysis. However, the values should be treated only as a rough estimation because the Hertz model is not exactly suited for inhomogeneous systems as in our case. Still, our data is well represented by the Hertz model as shown by the comparison of force curves plotted in log-log scale together with the power function $F = \delta^{3/2}$, confirming the Hertzian power law (Fig. S3, SI).
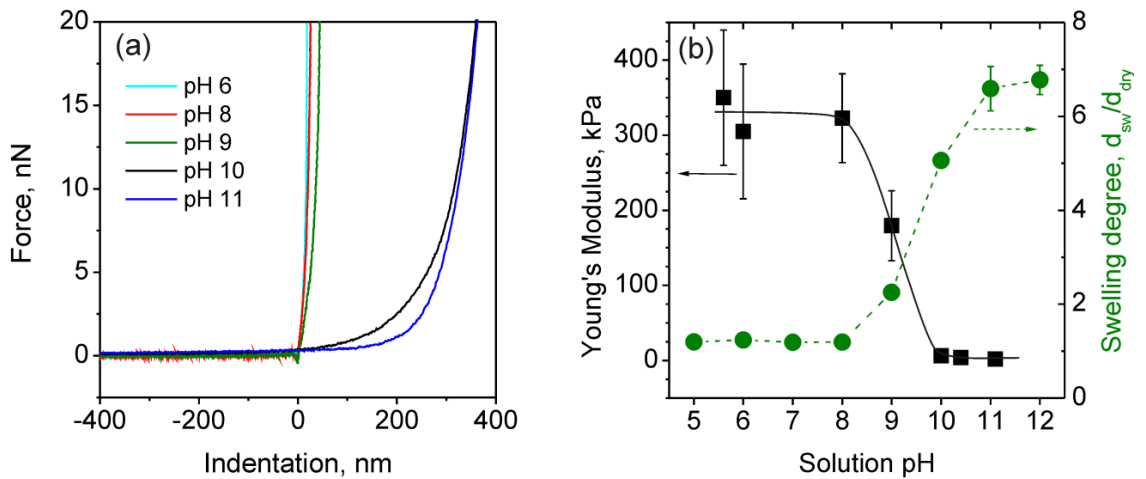

Fig. 7.7: Force–indentation data for different swelling states (a) and Young's modulus (■) and swelling degree (●) (determined by ellipsometric measurements) as a function of the solution pH for a (BMAADq/PSS)$_3$ film (b).

The Young's modulus was estimated using equation (7.4). Fig. 7.7b summarizes the obtained data of the Young's modulus and the swelling degree as a function of the solution pH. Each value for the Young's modulus contains at least 300 data points.

The swelling degree was estimated from the ellipsometric measurements as d_{sw}/d_{dry}, where d_{sw} and d_{dry} are the film thicknesses in the swollen and dry state, respectively. As can be clearly seen, the Young's modulus is inversely proportional to the degree of swelling. The modulus decreases with increasing pH (6 to 11) by at least 2 orders of magnitude from around 100 to 1 kPa. For the quenched state (pH ≤ 8), the modulus is nearly constant at around 300 kPa. Surface force spectroscopy studies performed by Tsukruk and co-workers have also shown a softening of pH-sensitive LbL capsules by 2 orders of magnitude (in the range of 0.1–1 MPa in the contracted and 10 kPa in the swollen state) within a narrow pH range.[69–71] Their results are comparable to our system: for the quenched state (pH ≤ 8), the modulus is nearly constant at around 300 kPa, which is typical for partially swollen hydrogel films[16] or LbL capsules.[69] The transition between the contracted and swollen states occurs at pH ~ 9 corresponding to the estimated apparent pK_a value of the MAA brush. At pH ≥ 10 (highly swollen state), the modulus converges the low kPa-range. This low kPa range of the Young's modulus is characteristic for highly swollen hydrogel materials.[69–72]

7.3.4 Effect of film thickness on swelling behavior

Due to significant differences in the density of the incorporated micelles and the porosity of the (BMAADq/PSS)$_x$ layers (Fig. 7.3), we studied the effect of film microstructure on the macroscopic swelling behavior. The swelling degree (the ratio of swollen to dry volume) of surface-attached films equals the linear degree of swelling[73] and can be calculated using ellipsometric thickness measurements. The equilibrium swelling degrees of the hydrogel-like films as a function of the dry thickness are summarized in Fig. 7.8a.

Ellipsometric measurements show that the swelling degree is strongly dependent on the LbL film thickness and therefore on the porosity of the multilayers, which can be tuned by the number of LbL deposition steps. The maximum swelling degree of ~ 12 is obtained for the thinnest films made by one deposition step. With increasing thickness (decreased porosity), the swelling degree drops to a value of 2 for the thickest film studied.
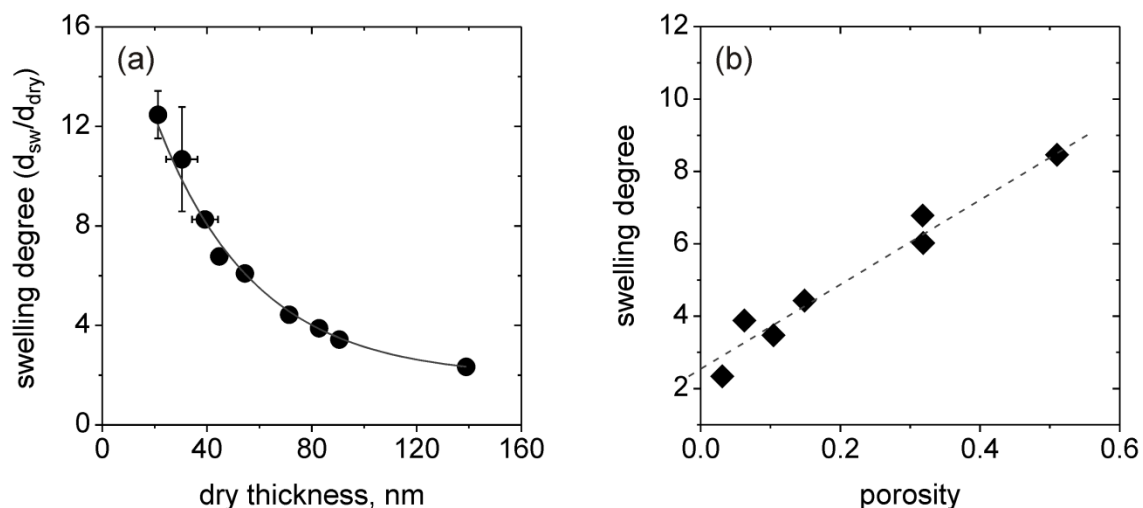
Fig. 7.8: Swelling degree *vs.* dry thickness determined by ellipsometric measurements (a) and swelling degree *vs.* porosity showing a linear dependency (b).

Taking the differences in the microstructure into account, the observed trend of decreased swelling degree with increasing dry thickness is reasonable. The equilibrium swelling degree is a balance between two opposing forces: on the one hand the electrostatic self-repulsion and osmotic pressure of the trapped counter ions, which favor swelling, and on the other hand the elastic free energy, which opposes swelling. Thus, with increasing dry thickness the decreasing void fraction confines the particle volume change to one dimension perpendicular to the substrate. Consequently, steric effects may lead to a dominating contribution of the stretching entropy resulting in decreased swelling.

Additionally, the solvent gradient induced by the accumulation of solvent at the outmost layers may impact the swelling behavior. A similar trend of decreased swelling degree with increasing thickness was found for block copolymer films[74] and for polyelectrolyte multilayers in saturated solvent vapor[75] and solvents.[76]

Recalculation of the data to the water content in a swollen film ($1 - d_{dry}/d_{sw}$) results in a linear decrease with increasing dry thickness for all films with more than one bilayer (Fig. S4, SI). The highly swollen films exhibit a maximum water content of ~90%. Interestingly, the plot of the swelling degree *versus* the porosity of the films yields a linear dependence (Fig. 7.8b), reconfirming the dominating elastic energy contribution with decreasing porosity. The non-zero intercept means that a close-packed film with a porosity of 0 would still swell by a factor of 2 due to the contribution of the PSS/Dq IPEC and the swelling of the MAA brush.

Note that in the case of zero porosity, only 1D swelling perpendicular to the substrate is possible.

7.4 Conclusions

Using the layer-by-layer technique, ABC block terpolymer micelles with a hydrophobic B core, a pH-sensitive MAA shell and a charged Dq corona were included within multilayer films with tailored porous nanostructure and integrated pH-responsive properties. The approach of ionic cross-linking of the cationic corona with a strong polyanion leads to the creation of a novel polyelectrolyte brush-like structure, which is double-end-tethered between the hydrophobic cores and the flexible IPECs of the Dq corona and PSS. The purpose of the latter is to prevent the dissolution of incorporated micelles providing the stability of the multilayers on the one hand. On the other hand, IPECs are penetrable for water and electrolytes enabling high pH-induced volumetric changes. The medium surrounding the $(BMAADq/PSS)_x$ multilayers strongly influences the ionization degree of the double-end-tethered MAA brush and therefore its degree of swelling and mechanical properties.

The film swelling degree and morphology, as well as the mechanical properties of the coatings are reversibly tunable by the solution pH. Furthermore, the swelling behavior and the water content in the hydrogel-like films can be tuned by the porosity of the multilayers, which can be adjusted by the number of micelles/PSS deposition steps to more than 1200% swelling degree and 90% water content in the swollen films. With increasing thickness (decreased porosity), the swelling degree drops since the contribution of the elastic energy dominates the osmotic pressure.

Surface-attached pH-responsive hydrogel-like LbL films can be assembled from weak polyelectrolytes.[77] Although these films are highly swellable, they are often unstable with respect to pH variations.[78] Other LbL-derived stimuli-responsive hydrogel-like systems, whose structure is stabilized by covalent cross-links often show considerably lower swelling degrees.[79] In our case, the stabilization results from the formation of IPECs, which are covalently bound to the pH-sensitive component. Thus, no stabilization by covalent bonding is needed to trap the PMAA chains and significantly higher swelling degrees are observed.

High swelling due to the separation of the binding and responsive components within the LbL films is also known for multilayers with other incorporated core–shell ABA triblock copolymer micelles with temperature-sensitive cores.[29,30] In this particular case, Tan *et al.*

reported on the temperature-driven swelling behavior of LbL films with swelling degrees ranging from 4 to 10.

Our results demonstrate that significant (2–12 fold), reversible, and controllable (by pH and bilayer number) swelling can be realized via the incorporation of core–shell–corona micelles into the LbL films. Here we take advantage of the separation of the functional components and the retained internal structure consisting of hydrophobic core, a pH-sensitive double-end-tethered polyelectrolyte brush shell and a binding corona.

Acknowledgments

References

1.   Y. Liu, L. Mu, B. H. Liu and J. L. Kong, *Chem.--Eur. J.*, 2005, **11**, 2622-2631.

2.   K. Glinel, C. Dejugnat, M. Prevot, B. Schöler, M. Schönhoff and R. V. Klitzing, *Colloids Surf. A*, 2007, **303**, 3-13.

3.   J. F. Mano, *Adv. Eng. Mater.*, 2008, **10**, 515-527.

4.   V. Kozlovskaya, E. Kharlampieva, I. Erel and S. A. Sukhishvili, *Soft Matter*, 2009, **5**, 4077-4087.

5.   P. M. Mendes, *Chem. Soc. Rev.*, 2008, **37**, 2512-2529.

6.   I. Tokarev and S. Minko, *Soft Matter*, 2009, **5**, 511-524.

7.   I. Tokarev and S. Minko, *Adv. Mater.*, 2010, **22**, 3446-3462.

8.   I. Tokarev and S. Minko, *Adv. Mater.*, 2009, **21**, 241-247.

9.   I. Tokarev, M. Motornov and S. Minko, *J. Mater. Chem.*, 2009, **19**, 6932-6948.

10. M. A. Cohen Stuart, W. T. S. Huck, J. Genzer, M. Müller, C. Ober, M. Stamm, G. B. Sukhorukov, I. Szleifer, V. V. Tsukruk, M. Urban, F. Winnik, S. Zauscher, I. Luzinov and S. Minko, *Nat. Mater.*, 2010, **9**, 101-113.

11. E. B. Zhulina, O. V. Borisov and T. M. Birshtein, *J. Phys. II*, 1992, **2**, 63-74.

12. S. Minko, *Polym. Rev.*, 2006, **46**, 397-420.

13. A. Synytska, M. Stamm, S. Diez and L. Ionov, *Langmuir*, 2007, **23**, 5205-5209.

14. P. Uhlmann, H. Merlitz, J. U. Sommer and M. Stamm, *Macromol. Rapid Commun.*, 2009, **30**, 732-740.

15. M. Ballauff, *Prog. Polym. Sci.*, 2007, **32**, 1135-1151.

16. S. Schmidt, M. Zeiser, T. Hellweg, C. Duschl, A. Fery and H. Möhwald, *Adv. Funct. Mater.*, 2010, **20**, 3235-3243.

17. G. B. Webber, E. J. Wanless, V. Bütün, S. P. Armes and S. Biggs, *Nano Lett.*, 2002, **2**, 1307-1313.

18. G. B. Webber, E. J. Wanless, S. P. Armes, Y. Q. Tang, Y. T. Li and S. Biggs, *Adv. Mater.*, 2004, **16**, 1794-1798.

19. G. B. Webber, E. J. Wanless, S. P. Armes and S. Biggs, *Faraday Discuss.*, 2005, **128**, 193-209.

20. K. Sakai, E. G. Smith, G. B. Webber, M. Baker, E. J. Wanless, V. Bütün, S. P. Armes and S. Biggs, *Langmuir*, 2006, **22**, 8435-8442.

21. K. Sakai, E. G. Smith, G. B. Webber, M. Baker, E. J. Wanless, V. Bütün, S. P. Armes and S. Biggs, *J. Colloid Interface Sci.*, 2007, **314**, 381-388.

22. J. Gensel, E. Betthausen, C. Hasenöhrl, K. Trenkenschuh, M. Hund, F. Boulmedais, P. Schaaf, A. H. E. Müller and A. Fery, *Soft Matter*, 2011, **23**, 11144-11153.

23. J. Gensel, T. Borke, N. Pazos Pérez, A. Fery, D. V. Andreeva, E. Betthausen, A. H. E. Müller, H. Möhwald and E. V. Skorb, *Adv. Mater.*, 2012, **24**, 985-989.

24. Z. C. Zhu and S. A. Sukhishvili, *ACS Nano*, 2009, **3**, 3595-3605.

25. B. Mahltig, P. Müller-Buschbaum, M. Wolkenhauer, O. Wunnicke, S. Wiegand, J.-F. Gohy, R. Jérôme and M. Stamm, *J. Colloid Interface Sci.*, 2001, **242**, 36-43.

26. G. Decher and J. D. Hong, *Ber. Bunsen-Ges. Phys. Chem.*, 1991, **95**, 1430-1434.

27. G. Decher and J. Schmitt, *Prog. Colloid Polym. Sci.*, 1992, **89**, 160-164.

28. G. Decher, *Science*, 1997, **277**, 1232-1237.

29. W. S. Tan, R. E. Cohen, M. F. Rubner and S. A. Sukhishvili, *Macromolecules*, 2010, **43**, 1950-1957.

30. W. S. Tan, Z. C. Zhu, S. A. Sukhishvili, M. F. Rubner and R. E. Cohen, *Macromolecules*, 2011, **44**, 7767-7774.

31. N. A. Kotov, I. Dekany and J. H. Fendler, *J. Phys. Chem.*, 1995, **99**, 13065-13069.

32. F. G. Aliev, M. A. Correa-Duarte, A. Mamedov, J. W. Ostrander, M. Giersig, L. M. Liz-Marzan and N. A. Kotov, *Adv. Mater.*, 1999, **11**, 1006-1010.

33. N. Ma, Y. P. Wang, Z. Q. Wang and X. Zhang, *Langmuir*, 2006, **22**, 3906-3909.

34. B. S. Kim, S. W. Park and P. T. Hammond, *ACS Nano*, 2008, **2**, 386-392.

35. K. Emoto, M. Iijima, Y. Nagasaki and K. Kataoka, *J. Am. Chem. Sos.*, 2000, **122**, 2653-2654.

36. T. Addison, O. J. Cayre, S. Biggs, S. P. Armes and D. York, *Langmuir*, 2008, **24**, 13328-13333.

37. Z. C. Zhu and S. A. Sukhishvili, *J. Mater. Chem.*, 2012, **22**, 7667-7671.

38. J. H. Cho, J. K. Hong, K. Char and F. Caruso, *J. Am. Chem. Soc.*, 2006, **128**, 9935-9942.

39. S. Biggs, K. Sakai, T. Addison, A. Schmid, S. P. Armes, M. Vamvakaki, V. Bütün and G. Webber, *Adv. Mater.*, 2007, **19**, 247-250.

40. T. Addison, O. J. Cayre, S. Biggs, S. P. Armes and D. York, *Langmuir*, 2010, **26**, 6281-6286.

41. P. M. Nguyen, N. S. Zacharia, E. Verploegen and P. T. Hammond, *Chem. Mater.*, 2007, **19**, 5524-5530.

42. D. A. Bernards and T. A. Desai, *Soft Matter*, 2010, **6**, 1621-1631.

43. E. Betthausen, M. Drechsler, M. Förtsch, F. H. Schacher and A. H. E. Müller, *Soft Matter*, 2011, **7**, 8880-8891.

44. W. Kern and D. A. Puotinen, *RCA Rev.*, 1970, **31**, 187-206.

45. H. Elbs and G. Krausch, *Polymer*, 2004, **45**, 7935-7942.

46. J. L. Hutter and J. Bechhoefer, *Rev. Sci. Instrum.*, 1993, **64**, 1868-1873.

47. H. Dautzenberg, W. Jaeger, J. Kötz, B. Philipp, C. Seidel and D. Stscherbina, *Polyelectrolytes*, Carl Hanser Verlag, München, 1994.

48. N. G. Hoogeveen, M. A. C. Stuart, G. J. Fleer and M. R. Bohmer, *Langmuir*, 1996, **12**, 3675-3681.

49. S. A. Sukhishvili, E. Kharlampieva and V. Izumrudov, *Macromolecules*, 2006, **39**, 8873-8881.

50. V. A. Kabanov, *Russ. Chem. Rev.*, 2005, **74**, 3-20.

51. M. Born and E. Wolf, *Principles of Optics*, Cambridge University Press, Cambridge, 1999.

52. A. Walther and A. H. E. Müller, *Chem. Commun.*, 2009, 1127-1129.

53. C. V. Synatschke, F. H. Schacher, M. Förtsch, M. Drechsler and A. H. E. Müller, *Soft Matter*, 2011, **7**, 1714-1725.

54. J. D. Mendelsohn, C. J. Barrett, V. V. Chan, A. J. Pal, A. M. Mayes and M. F. Rubner, *Langmuir*, 2000, **16**, 5017-5023.

55. T. Mauser, C. Dejugnat and G. B. Sukhorukov, *Macromol. Rapid Commun.*, 2004, **25**, 1781-1785.

56. H. H. Rmaile and J. B. Schlenoff, *Langmuir*, 2002, **18**, 8263-8265.

57. S. S. Shiratori and M. F. Rubner, *Macromolecules*, 2000, **33**, 4213-4219.

58. Z. J. Sui and J. B. Schlenoff, *Langmuir*, 2004, **20**, 6026-6031.

59. A. J. Parnell, S. J. Martin, C. C. Dang, M. Geoghegan, R. A. L. Jones, C. J. Crook, J. R. Howse and A. J. Ryan, *Polymer*, 2009, **50**, 1005-1014.

60. E. P. K. Currie, A. B. Sieval, G. J. Fleer and M. A. Cohen Stuart, *Langmuir*, 2000, **16**, 8324-8333.

61. F. A. Plamper, H. Becker, M. Lanzendörfer, M. Patel, A. Wittemann, M. Ballauff and A. H. E. Müller, *Macromol. Chem. Phys.*, 2005, **206**, 1813-1825.

62. E. B. Zhulina, T. M. Birshtein and O. V. Borisov, *Macromolecules*, 1995, **28**, 1491-1499.

63. H. W. Jomaa and J. B. Schlenoff, *Langmuir*, 2005, **21**, 8081-8084.

64. V. A. Kabanov, A. B. Zezin, V. A. Izumrudov, T. K. Bronich and K. N. Bakeev, *Makromol. Chem., Suppl.*, 1985, 137-155.

65. S. T. Dubas and J. B. Schlenoff, *Langmuir*, 2001, **17**, 7725-7727.

66. H. J. Butt, *Biophys. J.*, 1991, **60**, 1438-1444.

67. W. A. Ducker, T. J. Senden and R. M. Pashley, *Nature*, 1991, **353**, 239-241.

68. H. Hertz, *J. Reine Angew. Math.*, 1881, **92**, 156-171.

69. M. O. Lisunova, I. Drachuk, O. A. Shchepelina, K. D. Anderson and V. V. Tsukruk, *Langmuir*, 2011, **27**, 11157-11165.

70. O. Shchepelina, M. O. Lisunova, I. Drachuk and V. V. Tsukruk, *Chem. Mater.*, 2012, **24**, 1245-1254.

71. I. Drachuk, O. Shchepelina, M. Lisunova, S. Harbaugh, N. Kelley-Loughnane, M. Stone and V. V. Tsukruk, *ASC Nano*, 2012, **6**, 4266-4278.

72. C. Picart, B. Senger, K. Sengupta, F. Dubreuil and A. Fery, *Colloids Surf. A*, 2007, **303**, 30-36.

73. R. Toomey, D. Freidank and J. Rühe, *Macromolecules*, 2004, **37**, 882-887.

74. J. Gensel, C. Liedel, H. G. Schoberth and L. Tsarkova, *Soft Matter*, 2009, **5**, 2534-2537.

75. J. E. Wong, F. Rehfeldt, P. Hanni, M. Tanaka and R. V. Klitzing, *Macromolecules*, 2004, **37**, 7285-7289.

76. S. E. Burke and C. J. Barrett, *Biomacromolecules*, 2005, **6**, 1419-1428.

77. J. Hiller and M. F. Rubner, *Macromolecules*, 2003, **36**, 4078-4083.

78. S. T. Dubas and J. B. Schlenoff, *Macromolecules*, 2001, **34**, 3736-3740.

79. E. Kharlampieva, I. Erel-Unal and S. A. Sukhishvili, *Langmuir*, 2007, **23**, 175-181.
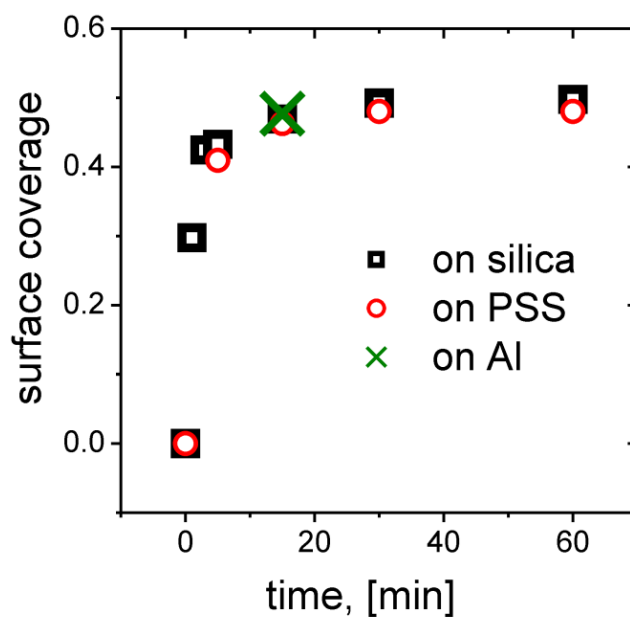
7.5 Supporting Information

Figure S1: Adsorption kinetics of BMAADq micelles onto different substrates studied by AFM.
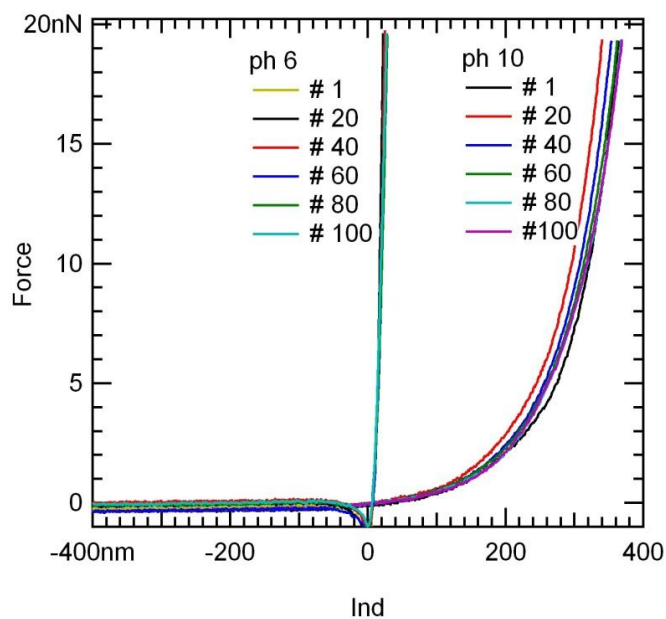

Figure S2: Force-indentation measurements on the same spot of the sample show that the film is not plastically deformed. Legend indicates the number of measurements.
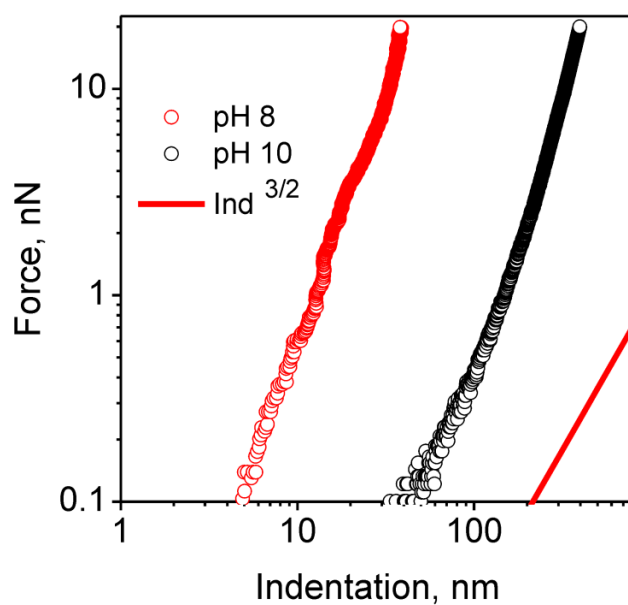
Figure S3: log-log plot of the force–indentation data for different swelling states of a (BMAADq/PSS)$_3$ film. The force is proportional to the 3/2 power of the indentation confirming the validity of the Hertzian model. For comparison, a line corresponding to the 3/2 power law relationship is plotted (solid line).
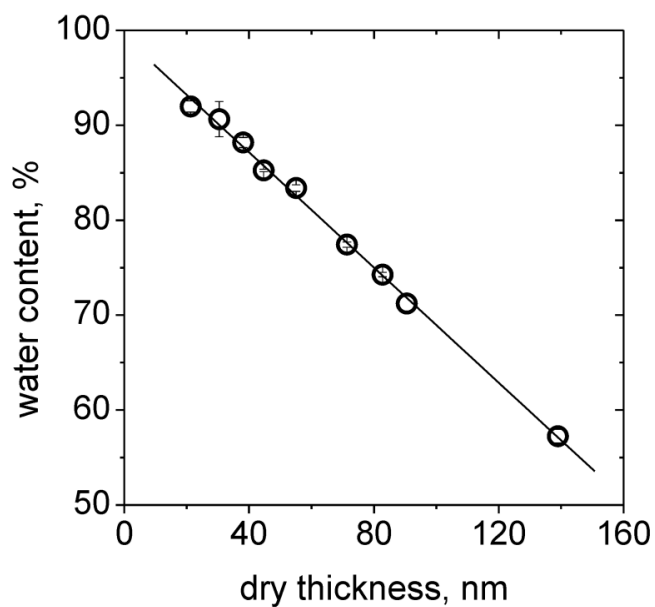

Figure S4: Water content *vs.* the dry thickness of (BMAADq/PSS)$_x$ films.

Danksagung

Ich möchte mich bei allen bedanken, die diese Arbeit ermöglicht und zu ihrem Gelingen beigetragen haben.

An erster Stelle danke ich meinem Betreuer Prof. Dr. Andreas Fery für das interessante Thema sowie für die lehrreiche Betreuung und die vielen Diskussionsrunden. Vor allem aber hat er mich stets motiviert und gefördert. Ich habe viel in dieser Zeit dazugelernt.

Mein Dank gilt allen Kollegen des Lehrstuhls Physikalische Chemie II für die ständige Hilfsbereitschaft und die beste Arbeitsatmosphäre. Liebe Sybille, danke dir für die Gemütlichkeit in der PC II! Danke auch dafür, dass du bei allen meinen Fragen immer mit Rat und Tat zur Seite standest.

Bei Prof. Dr. Axel Müller, Prof. Dr. Andre Laschewsky, Dr. Fouzia Boulmedais, Dr. Daria Andreeva, Dr. Nico Pazos Perez und Dr. Katja Skorb möchte ich mich für die erfolgreichen Kooperationsprojekte bedanken. Eva Betthausen danke ich für die „Mizellen, die mein wissenschaftliches Leben bereichert haben"!

Dank geht auch an Markus Hund für die vielen hilfreichen Tipps zum AFM. Carmen Kunert danke ich für die SEM-Messungen. Danke an Petra Zippelius für die *security* am Lehrstuhl. Dr. Wolfgang Häfner hatte immer eine passende Geschichte parat. Danke dafür!

Dank gilt auch Johann Erath für die *colloidal probe* AFM-Messungen und für den Versuch, mich in die *force*-Welt einzuführen. Volodymyr Kuznetsov, Pavel Cherepanov und Alexej Korovin danke ich für die spannenden wissenschaftlichen Diskussionen. Danke an Andrea Wolf und Katja Gräf für die tollen Mittwochs-Kaffeepausen. Christoph Hanske danke ich dafür, dass er meinen Rechner samt allen Daten vor den schrecklichen Viren gerettet und auch sonst immer meine Computer-Probleme gelöst hat. Danke auch an Chris Kuttner und Heiko Schoberth für die PC-Hilfe.

Ich danke Sina Rösler, Christoph Hasenöhrl, Anita Leha, Inna Dewald und Olga Isakin für die Möglichkeit, meine wissenschaftlichen Erfahrungen und Erkenntnisse weiterzugeben und für die tolle Zusammenarbeit.

Insbesondere möchte ich mich bei Katja Trenkenschuh bedanken. Ich bin sehr glücklich, dass du mich während meines Studiums und der PhD-Zeit immer begleitet hast. Danke für deine Witze, Motivation und Diskussionen, danke für deine Freundschaft!

Danke an Johann, Inna, Pavel, Katja und Andrea für das Korrekturlesen meiner Arbeit.

Tausend Dank an meine Familie für die Unterstützung und Liebe.

Erklärung

Die vorliegende Arbeit wurde von mir selbstständig verfasst und ich habe dabei keine anderen als die angegebenen Hilfsmittel und Quellen benutzt.

Ferner habe ich nicht versucht, anderweitig mit oder ohne Erfolg eine Dissertation einzureichen oder mich der Doktorprüfung zu unterziehen.

Bayreuth, den 07.03.2012

Julia Gensel